

**GRAFT COPOLYMERIZATION OF p-ACRYLOYLOXYBENZOIC ACID
AND p-METHACRYLOYLOXYBENZOIC ACID ONTO
ISOTACTIC POLYPROPYLENE**

**A THESIS SUBMITTED TO
THE GRADUATE SCHOOL OF NATURAL AND APPLIED SCIENCES
OF
MIDDLE EAST TECHNICAL UNIVERSITY**

BY

SEDAT ÇETİN

**IN PARTIAL FULFILLMENT OF THE REQUIREMENTS
FOR
THE DEGREE OF DOCTOR OF PHILOSOPHY
IN
CHEMISTRY**

JULY 2004

Approval of the graduate school of the Natural and Applied Sciences.

Prof. Dr. Canan Özgen
Director

I certify that this thesis satisfies all the requirements as a thesis for the degree of Doctor of Philosophy.

Prof. Dr. Hüseyin İşçi
Head of the Department

This is to certify that we have read this thesis and that in our opinion it is fully adequate, in scope and quality, as a thesis for the degree of Doctor of Philosophy.

Prof. Dr. Teoman Tinçer
Supervisor

Examining Committee Members

Prof. Dr. Kemal Alyürük	(METU, CHEM)	_____
Prof. Dr. Teoman Tinçer	(METU, CHEM)	_____
Prof. Dr. H. İbrahim Ünal	(GAZİ Ü, CHEM)	_____
Prof. Dr. Zuhale Küçükayavuz	(METU, CHEM)	_____
Prof. Dr. Ahmet Önal	(METU, CHEM)	_____

I hereby declare that all information in this document has been obtained and presented in accordance with academic rules and ethical conduct. I also declare that, as required by these rules and conduct, I have fully cited and referenced all material and results that are not original to this work.

Name, Last Name : Sedat Çetin

Signature:

ABSTRACT

GRAFT COPOLYMERIZATION OF *p*-ACRYLOYLOXYBENZOIC ACID AND *p*-METHACRYLOYLOXYBENZOIC ACID ONTO ISOTACTIC POLYPROPYLENE

Çetin, Sedat

Ph.D., Department of Chemistry

Supervisor: Prof. Dr. Teoman Tinçer

July 2004, 124 pages

The monomers, *p*-acryloyloxybenzoic acid (ABA) and *p*-methacryloyloxybenzoic acid (MBA) were synthesized by condensation reaction of corresponding acid chlorides with *p*-hydroxybenzoic acid in alkaline medium. The polymerization of the monomers were studied by several techniques. Polyacryloyloxybenzoic acid (PABA) was obtained by γ -radiation induced, solution and bulk melt polymerization by initiation of dicumyl peroxide (DCP). Polymethacryloyloxybenzoic acid (PMBA) could be obtained by only bulk melt polymerization.

The graft copolymerization of the monomers onto isotactic polypropylene, IPP, was successfully carried out only with bulk melt polymerization. The IPP used in the graft copolymerization was firstly subjected to γ -radiation to create active sites for grafting. The graft copolymerization of the monomers, ABA and MBA onto IPP were initiated by these active sites. The grafting was studied at constant concentration of the monomers in the reaction mixture (50%) and at different reaction temperatures (170, 185, 202, 215 and 225°C). The maximum grafting of PABA and PMBA were found to be 33.1% and 33.9% in the graft copolymers, respectively. The maximum grafting was reached in shorter times at higher temperatures, and it also increased with the increase of concentration of the monomers in the reaction medium. The graft copolymerization was also carried out

by using initiator, DCP at 170°C, however, the grafting extent was lower due to the homopolymerization of the monomers and the direct reactions between peroxides of initiator and peroxides on IPP.

The graft copolymers were characterized by several techniques, DSC, WAX, TG/IR, MS, SEM and mechanical testing. The formation of both crystalline forms of (α_1 and α_2) were observed in the products obtained at 170°C. The graft copolymerization of ABA did not have any significance on the formation of both forms of α form, while MBA lead to increase in α_2 form. The β crystalline modification formed in PABA-g-PP products obtained at 185°C and at higher temperature and also in the second run of DSC studies after fast cooling. β form was not observed in graft copolymers of PMBA

The decomposition mechanism of PABA, PMBA and the graft coproducts were studied by mass spectrometry and TG/IR. The polymers degraded predominantly by decomposition of side groups giving phenol, benzoic acid, hydroxybenzoic acid, carbondioxide and cyclodiene mainly.

The mechanical properties of the graft copolymers showed an improvement particularly in tensile strength and modulus. The maximum tensile strength and modulus of PABA-g-PP were found as 41.1 and 881 MPa, and the values of PMBA-g-PP were measured as 35.9 and 721 MPa, respectively. These values were 28.1 and 486 MPa for irradiated IPP and 33.9 and 632 MPa for virgin IPP, respectively. The copolymerization of ABA did not alter the impact properties of the graft copolymer, while a slight decrease was observed in PMBA-g-PP samples.

The tensile and impact fractured surface of the graft copolymers studied by scanning electron microscopy showed homogeneous structure. The brittle nature with some extent of ductility was seen in the samples.

Key words: Polypropylene, acryloyloxybenzoic acid, methacryloyloxybenzoic acid, polyacryloyloxybenzoic acid, polymethacryloyloxybenzoic acid, liquid crystalline polymers and graft copolymerization,

ÖZ

p-AKRİLOİLOKSİBENZOİK ASİT VE p-METAKRİLOİLOKSİBENZOİK ASİTİN İZOTAKTİK POLİPROPİLEN ÜZERİNE AŞI KOPOLİMERLEŞMESİ

Çetin, Sedat

Doktora, Kimya Bölümü

Tez Danışmanı: Prof. Dr. Teoman Tinçer

Temmuz 2004, 124 sayfa

p-Akriloyloksibenzoik asit (ABA) ve p-metakriloyloksibenzoik asit (MBA) monomerleri bazik ortamda asit klorürlerin p-hidroksibenzoik asit ile kondensasyon tepkimesiyle sentezlendi. Monomerlerin polimerleşmesi çeşitli yöntemlerle çalışıldı. Poliakriloyloksibenzoik asit (PABA) γ -radyasyonu başlatmasıyla, çözelti ve dikünil peroksit (DCP) başlatıcısının kullanıldığı kütleli polimerleşme ile elde edildi. Polimetakriloyloksibenzoik asit (PMBA) sadece kütleli polimerleşmeyle elde edilebildi.

Bu monomerlerin izotaktik polipropilen, IPP üzerine aşu kopolimerleşmesi sadece kütle polimerleşmesiyle başarılı oldu. Aşu kopolimerleşmesinde kullanılan IPP üzerinde aktif gruplar oluşturmak için önce γ -radyasyonuna tutuldu ve monomerlerin aşulanması bu aktif grupların tepkimesiyle gerçekleşti. Monomerlerin IPP üzerine takılma miktarları monomerlerin tepkime ortamındaki sabit derişiminde (%50) ve 170, 185, 202, 215 ve 225°C tepkime sıcaklıklarında çalışıldı. Aşu kopolimerlerinde maksimum takılma PABA'da %33,1 PMBA'da % 33,9 oldu ve bu maksimum değerlere yüksek sıcaklıklarda daha erken ulaşıldı. Takılma miktarı monomer derişimindeki artmayla arttı. Ayrıca aşu kopolimerleşmesi 170°C de DCP başlatıcısının kullanılmasıyla da gerçekleştirildi. Monomerlerin homopolimerleşmesi ve IPP üzerinde γ -radyasyonu ile oluşturulan peroksit ile DCP başlatıcısının peroksiti arasındaki direkt tepkimeden dolayı takılma miktarlarında azalma görüldü.

Üretilen aşu kopolimerleri çeşitli yöntemlerle karakterize edildi: DSC, WAX,

TG/IR, MS, SEM ve mekanik test. 170°C de elde edilen kopolimer ürünlerde α kristal formunun iki formu da (α_1 ve α_2) görüldü. ABA'nın kopolimerleşmesi α formunun iki formunun oluşumu üzerine bir etkisi olmazken, MBA α_2 formunun artmasına neden oldu. β kristal formu 185°C ve daha yüksek sıcaklıklarda elde edilen ürünlerde, ve özellikle hızlı soğutmalardan sonra gerçekleştirilen ikinci DSC ölçümlerinde oluştu. PMBA'nın kopolimerlerinde ise β oluşumu gözlenmedi.

PABA, PMBA ve elde edilen kopolimerlerin bozunma mekanizmaları kütle spektrometresi ile termogravimetri ve FTIR (TG/IR) sistemi ile çalışıldı. Bozunma genelde yan grupların başlıca fenol, benzoic asit, hidroksibenzoik asit, karbondioksit ve siklodiene parçalanmasıyla gerçekleşti.

Aşı kopolimerlerin mekanik özellikleri oda sıcaklığında çalışıldı. Özellikle gerilim direnci ve modulus değerlerinde gelişme görüldü. PABA-g-PP maksimum gerilim direnci ve modulus değeri 41,1 ve 881 MPa, PMBA-g-PP'nin maksimum gerilim direnci ve modulus değeri 35.9 ve 721 MPa olarak ölçüldü. Bu değerler ışınlanmış IPPde 28.1 ve 486 MPa ışınlanmamış IPP de 33.9 ve 632 MPa olarak belirlendi. ABAnın kopolimerleşmesi aşı kopolimerin çarpma direncine bir etkisi olmazken PMBA-g-PP örneklerinde azalma görüldü.

Gerilim ve çarpma etkisiyle kırılan yüzeylerin taramalı electron mikroskobu ile incelenmesinde tüm elde edilen aşı kopolimerlerin homojen bir yapı oluşturduğu gözlemlendi. Kırılgan ve az da olsa sünek yapı görüldü.

Anahtar Kelimeler: p-Akriiloiloksibenzoik asit, p-metakriiloiloksibenzoik asit, poliakriiloiloksibenzoik asit, polimetakriiloiloksibenzoik asit, polipropilen, sıvı kristalik polimerler ve aşı kopolimerleşmesi

To my family

ACKNOWLEDGEMENTS

I would like to express my deepest gratitude to my supervisor Prof. Dr. Teoman TİNÇER for his inspiration, endless support, guidance, encouragement and patience that helps me improve my polymer vision throughout the research.

I would like to thank also members of thesis supervising committee Prof. Dr. Kemal Alyürük and Assoc. Prof. Dr. Gülsü Akın Öktem for their cooperation and suggestions throughout this study.

I would like to extend my sincere tanks to Binnur Özkan, Semra Can and Hasan Çakmak for their help and valuable discussion.

I wish to express my sincere thaks to Elif Öztürk, Eylem Tarkın and Hüseyin Taş for their help in using vacuum line.

I am thankful to Cengiz Tan from Metallurgical and Materials Engineering for his helps about SEM, and also to Metin Yanık from our department for all glassware works.

I am grateful to all B36 earlier and newer members for their helps and support.

I want to thank all of the administrative staff of Chemistry Department of METU for their friendship.

TABLE OF CONTENTS

PLAGIARISM	iii
ABSTRACT	iv
ÖZ	vi
ACKNOWLEDGEMENT	ix
TABLE OF CONTENTS	x
LIST OF TABLES	xiii
LIST OF FIGURES	xiv
ABBREVIATIONS	xx
CHAPTER	
1. INTRODUCTION	1
1.1. General Review on PP, LCP and Their Blends	2
1.1.1. Polypropylene	2
1.1.2. Liquid Crystalline Polymers	3
1.1.3. Blends and Combining Thermoplastics with LCP's	4
1.2. Reinforcement of PP with LCP's	8
1.3. Liquid Crystals, Poly(acryloyloxybenzoic acid) and Poly(methacryloyloxybenzoic acid)	9
1.3.1. LCP	9
1.3.2. PABA and PMBA	11
1.4. Radiation Induced Grafting	14
1.4.1. Radiation Induced Graft Copolymerization	15
1.4.1.1. Direct Grafting to Polymer	16
1.4.1.2. Grafting on Radiation-Peroxidized Polymer	17
1.4.1.3. Grafting Initiated by Trapped Radicals	19
1.4.1.4. The Crosslinking of Different Polymers	19
1.5. Aim of the Work	20
2. EXPERIMENTAL	21
2.1. Chemicals and Materials Used	21
2.1.1. Solvents and Reagents	21

2.1.2. Preparation of Powder Isotactic Polypropylene	21
2.2. Synthesis of the Monomers	22
2.2.1. Synthesis of p-Acryloyloxybenzoic Acid	22
2.2.2. Synthesis of p-Methacryloyloxybenzoic Acid	23
2.3. Polymerization of the Monomers, ABA and MBA	23
2.3.1. γ -Irradiation Induced Polymerization	24
2.3.2. UV-Induced Polymerization	24
2.3.3. Bulk Polymerization of the Monomers	24
2.3.4. Solution Polymerization of the Monomers	25
2.4. Graft Copolymerization of the Monomers	26
2.4.1. γ -Irradiation and UV-Induced Graft Copolymerization of ABA onto PP	26
2.4.2. Thermally Induced Graft Copolymerization of ABA and MBA onto PP	26
2.5. Characterization and Instruments	27
2.5.1. FT-IR Measurements	27
2.5.2. NMR Measurements	27
2.5.3. Differential Scanning Calorimetry (DSC) Analysis	27
2.5.4. TG/IR Measurements	27
2.5.5. X-Ray Measurements	28
2.5.6. Mechanical Properties	28
2.5.7. Scanning Electron Microscope (SEM) Study	29
2.5.8. MS Measurements	29
3. RESULTS AND DISCUSSION	30
3.1. Characterizations	30
3.1.1. Characterization of Isotactic Polypropylene, IPP	30
3.1.2. Characterization of p-Acryloyloxybenzoic Acid	31
3.1.3. Characterization of p-Methacryloyloxybenzoic Acid	33
3.1.4. Characterization of Polyacryloyloxybenzoic Acid	35
3.1.5. Characterization of Polmethacryloyloxybenzoic Acid	37
3.2. Graft Copolymerization of ABA onto IPP	39
3.2.1. Characterization of PABA-g-PP	42

3.3. Graft Copolymerization of MBA onto IPP	43
3.3.1. Characterization of PMBA-g-PP	45
3.4. Characterization of PABA-g-PP by DSC and X-Ray	46
3.5. Characterization of PMBA-g-PP DSC and X-Ray	66
3.6. Characterization of Polymers by MS and TG/IR	75
3.6.1. MS Spectrometry	76
3.6.2. TG/IR Analysis	89
3.7. Mechanical Properties of the Polymers	99
3.8. SEM Analysis of the Polymers	106
4. CONCLUSION	116
REFERENCES	118
VITA	124

LIST OF TABLES

TABLE	PAGE
1. % PABA in products (temperature and time dependence of graft copolymerization of ABA onto PP)	40
2. The dependence of content of PABA grafted onto PP on concentration of ABA in reaction mixture	41
3. % PMBA in products (temperature and time dependence of graft copolymerization of MBA onto PP)	43
4. The dependence of content of PMBA grafted onto PP on the concentration of MBA in reaction mixture	44
5. DSC results with PABA percentages in products	49
6. DSC results with PABA percentages in products	56
7. DSC results with PABA percentages in products	59
8. DSC results with PMBA percentages in products	67
9. DSC results with PMBA percentages in products	68
10. The characteristics of the peaks present in the pyrolysis mass spectra corresponding to the degradation products of PABA produced by initiation of DCP recorded at 29.1 minutes (291°C) with the heating rate of 10°C/min	79
11. The peaks present in the pyrolysis mass spectra corresponding to the degradation products of PABA produced by γ -radiation recorded at 35.5 minutes (355°C) with the heating rate of 10°C/min	82
12. Ultimate strength, Young's modulus and impact strength of irradiated and non-irradiated PP	99
13. Ultimate tensile strength of PABA-g-PP with % PABA in samples	101
14. Young's modulus of PABA-g-PP with % PABA	101
15. Impact strength of PABA-g-PP with % PABA	103
16. Ultimate tensile strength of PMBA-g-PP with % PMBA	104
17. Young's modulus of PMBA-g-PP with % PMBA	104
18. Impact strength of PMBA-g-PP with % PMBA	105

LIST OF FIGURES

FIGURE	PAGE
1. The simplified reaction between p-hydroxybenzoic acid and acryloyl chloride	22
2. The simplified reaction between p-hydroxybenzoic acid and methacryloylchloride	23
3. FTIR spectrum of IPP irradiated by γ -radiation (10 kGy)	30
4. FTIR spectrum of acryloyloxybenzoic acid	31
5. $^1\text{H-NMR}$ spectrum of acryloyloxybenzoic acid	32
6. DSC thermogram of acryloyloxybenzoic acid	32
7. FTIR spectrum of methacryloyloxybenzoic acid	33
8. $^1\text{H-NMR}$ spectrum of MBA	34
9. DSC thermogram of methacryloyloxybenzoic acid	34
10. $^1\text{H-NMR}$ spectrum of PABA produced by γ -radiation	35
11. $^1\text{H-NMR}$ spectrum of PABA produced by initiation of DCP	36
12. FTIR spectrum of PABA produced by γ -radiation	36
13. DSC thermogram of PABA produced by γ -radiation	37
14. $^1\text{H-NMR}$ spectrum of PMBA	38
15. FTIR spectrum of PMBA	38
16. DSC thermogram of PMBA	39
17. The dependence of content of PABA grafted onto PP on reaction temperature and time	40
18. The dependence of content of PABA grafted onto PP on concentration of ABA in reaction mixture	41
19. FTIR spectrum of PABA-g-PP produced at 170°C for 40 minutes reaction time	42
20. The dependence of content of PMBA grafted onto PP on reaction temperature and time	44
21. The dependence of content of PMBA grafted onto PP on concentration of MBA in reaction mixture	45

22. FTIR spectrum of PMBA-g-PP produced at 170°C for 40 minutes reaction time	46
23. DSC thermogram of IPP (10 kGy irradiated).....	47
24. X-ray spectrum of irradiated IPP	47
25. DSC thermogram of PABA-g-PP produced at 170°C containing 16.3% PABA.....	49
26. DSC thermograms of PABA-g-PP produced at 170°C containing b) 21.9% PABA, and c) 28.9%	50
27. X-ray spectrum of PABA-g-PP (16.3% PABA)	51
28. DSC thermogram of PABA-g-PP produced at 185°C with the reaction time of 40 minutes (31.9% PABA)	52
29. DSC thermogram of PABA-g-PP produced at 202°C with the reaction time of 40 minutes (31.5% PABA)	53
30. Second run DSC thermogram of PABA-g-PP produced at 170°C with the reaction time of 15 minutes (20.2% PABA) taken after cooling with the rate of 20°C/min	53
31. Second run DSC thermogram of PABA-g-PP produced at 185°C with the reaction time of 40 minutes (31.9% PABA) after cooling with the rate of 20°C/min	54
32. X-ray spectrum of PABA-g-PP produced at 202°C with the reaction time of 30 minutes (32.2% PABA)	54
33. X-ray spectrum of PABA-g-PP produced at 185°C with the reaction time of 40 minutes (31.5% PABA) taken after heating the sample to 230°C and cooling to room temperature with the rate of 2°C/min	55
4. Second run DSC thermogram of PABA-g-PP produced at 170°C with the reaction time of 40 minutes (33.3% PABA) after cooling with the rate of 20°C/min ...	57
35. Second run DSC thermogram of PABA-g-PP produced at 170°C with the reaction time of 40 minutes (33.3% PABA) after cooling with the rate of 2°C/min)	58
36. X-ray spectrum of PABA-g-PP produced at 185°C with the reaction time of 40 minutes (31.5% PABA)	61

37. DSC thermogram of PABA-g-PP produced at 185°C with the reaction time of 15 minutes (31.7% PABA)	61
38. Second run DSC thermogram of PABA-g-PP produced at 202°C with the reaction time of 40 minutes (31.5% PABA) after cooling with the rate of 20°C/min)	63
39. Second run DSC thermogram of PABA-g-PP produced at 202°C with the reaction time of 40minutes (31.5% PABA) after cooling with the rate of 2°C/min)	63
40. X-ray spectrum of PABA-g-PP produced at 202°C with the reaction time of 30 minutes (32.2% PABA) taken after heating the sample to 230°C and cooling to room temperature with the rate of 2°C/min	64
41. DSC thermogram of IPP (heated to 170°C keeping the temperature constant for 30 minutes)	64
42. DSC thermogram of IPP (heated to 202°C keeping the temperature constant for 30 minutes)	65
43. DSC thermogram of PMBA-g-PP produced at 170°C with the reaction time 20 minutes (16.7% PMBA)	68
44. DSC thermogram of PMBA-g-PP produced at 170°C with the reaction time 30 minutes (18.8% PMBA)	69
45. DSC thermogram of PMBA-g-PP produced at 170°C with the reaction time of 50 minutes (17.9% PMBA)	69
46. X-ray spectrum of PMBA-g-PP produced at 170°C with the reaction time of 40 minutes	70
47. Second run DSC thermogram of PMBA-g-PP produced at 170°C with the reaction time of 15 minutes (10.2% PMBA)	71
48. DSC thermogram of PMBA-g-PP produced at 185°C with the reaction time of 10 minutes (12.28% PMBA)	72
49. X-ray spectrum of PMBA-g-PP produced at 185°C with the reaction time of 30 minutes (24.4% PMBA)	72
50. X-ray spectrum of PMBA-g-PP produced at 201°C with the reaction time of 40 minutes (23.08% PMBA), (heated to 230°C and cooled to room temperature with 2°C/min)	73

51. The total ion current of the pyrolysis of PABA produced by initiation of DCP at 202°C, with the heating rate of 10°C/min.	76
52. The mass spectra of PABA, produced by initiation of DCP at 202°C, taken at a) 29.1, and b) 41.5 minutes, with the heating rate of 10°C/min.	77
53. Degradation mechanism of PABA	78
54. The total ion current of the pyrolysis of PABA produced by γ -radiation, with the heating rate of 10°C/min.	80
55. The mass spectrum of PABA produced by γ -radiation taken at a) 24.4 (244°C), and b) 35.5 minutes (355°C)	81
56. The total ion current during the pyrolysis of PABA-g-PP (47.5% PABA), with the heating rate of 10°C/min	83
57. The mass spectra of PABA-g-PP (47.5% PABA) taken at a) 25.4 minutes (254°C), b) 41.8 minutes (418°C)	84
58. The total ion current of the pyrolysis of PMBA taken with the heating rate of between c) 19.7-22.7 minutes (394-454°C), and d) 24.9-29.5 minutes (498-590°C) with 10°C/min	85
59. Mass spectra of PMBA taken at a) 27.3 minutes (273°C), and b) 35.2 minutes (352°C) with the heating rate of 10°C/min.	86
60. The total ion current of PMBA-g-PP (27.3% PMBA) taken with the heating rate of 10°C/min.	87
61. Mass spectrum of PMBA-g-PP (27.3% PMBA) taken at 33.9 minutes (339°C) with the heating rate of 10°C/min.	87
62. Mass spectrum of PMBA-g-PP (27.3% PMBA) taken at 42.7 minutes (427°C) with the heating rate of 10°C/min.	88
63. TGA thermogram of PABA produced by DCP initiator taken with the heating rate of 20°C/min in N ₂	89
64. The FTIR spectra of the products formed at a) 12 minutes (240°C), and b) 14.4 minutes (288°C) during the heating of PABA with the rate of 20°C/min in nitrogen	90
65. The FTIR spectra of the products formed during the heating of PABA the rate of 20°C/min in nitrogen	91

66. TGA thermogram of PABA produced by DCP initiator taken with the heating rate of 20°C/min in air	92
67. The FTIR spectrum of the products formed during the heating of PABA at 12 minutes (240°C) with the rate of 20°C/min in air	92
68. The FTIR spectra of the products formed during the heating of PABA between b) 15.4-17.5 minutes (308-350°C), and c) 20.0-21.3 minutes (400-426°C) with the rate of 20°C/min in air	93
69. TGA thermogram of PMBA-g-PP (30.68% PMBA) taken with the heating rate of 20°C/min in nitrogen	95
70. FTIR spectrum of the products taken at 9.6 minutes (192°C) formed during the heating of PMBA-g-PP (30.68% PMBA) with the rate of 20°C/min in nitrogen	95
71. FTIR spectrum of the products formed during the heating of PMBA-g-PP (30.68% PMBA) taken at 19.8 minutes (396°C) with the rate of 20°C/min in nitrogen.....	96
72. TGA thermogram of PMBA-g-PP (30.7% PMBA) taken with the heating rate of 20°C/min in air	97
73. FTIR spectrum of the products formed during the heating of PMBA-g-PP (30.7% PMBA) taken at 11.6 minutes (232°C) and 14.9 minutes (298°C) with the rate of 20°C/min in air	97
74. FTIR spectrum of the products formed during the heating of PMBA-g-PP (30.7% PMBA) taken at 21.9 minutes (438°C) and 24.2 minutes (484°C) with the heating rate of 20°C/min in air	98
75. Stress-strain curves of PP, irradiated PP and PABA-g-PP with the content of 7.2 and 18.3% PABA	100
76. The dependence of ultimate tensile strength of PABA-g-PP on content of PABA	101
77. The dependence of Young's modulus of PABA-g-PP on content of PABA	102
78. The dependence of impact strength of PABA-g-PP on content of PABA	103
79. The dependence of ultimate tensile strength of PMBA-g-PP on content of PMBA.....	104

80. The dependence of Young's modulus of PMBA-g-PP on content of PMBA .	105
81. The dependence of impact strength of PMBA-g-PP on content of PABA	106
82. SEM photograph of PABA-g-PP (9.2% PABA), Tensile Test	107
83. SEM photograph of PABA-g-PP (9.2% PABA), Tensile Test	108
84. SEM photograph of PABA-g-PP (13.4% PABA), Tensile Test	108
85. SEM photograph of PABA-g-PP (18.3% PABA), Tensile Test	109
86. SEM photograph of PABA-g-PP (20.2% PABA), Tensile Test	109
87. SEM photograph of PABA-g-PP (32.1% PABA), Tensile Test	110
88. SEM photograph of PABA-g-PP (18.3% PABA), Slow Tensile Test	111
89. SEM photograph of PABA-g-PP (15.5% PABA), Slow Tensile Test	111
90. SEM photograph of PABA-g-PP (6.6% PABA), Impact Test	112
91. SEM photograph of PABA-g-PP (12.7% PABA), Impact Test	113
92. SEM photograph of PABA-g-PP (18.3% PABA), Impact Test	113
93. SEM photograph of PMBA-g-PP (5.8% PMBA), Impact Test	114
94. SEM photograph of PMBA-g-PP (5.8% PMBA), Impact Test	114
95. SEM photograph of PMBA-g-PP (10.5% PMBA), Impact Test	115

ABBREVIATIONS

IPP	: Isotactic Polypropylene
ABA	: p-Acryloyloxybenzoic Acid
MBA	: p-Methacryloyloxybenzoic Acid
PABA	: Polyacryloyloxybenzoic Acid
PMBA	: Polymethacryloyloxybenzoic Acid
PABA-g-PP	: Polyacryloyloxybenzoic Acid-graft- Polypropylene
PMBA-g-PP	: Polymethacryloyloxybenzoic Acid-graft-Polypropylene
DSC	: Differential Scanning Calorimetry
WAX	: Wide Angle X-Ray Diffraction
TG/IR	: Thermogravimetry/ Infrared Spectrometry
MS	: Mass Spectrometry

CHAPTER 1

INTRODUCTION

The modification of polyolefins, particularly polypropylene, by functionalizing to obtain engineering materials with superior properties, has been an area of interest shared with several workers in recent years. Functional and engineered polyolefins are becoming more and more commercially important and expanding their applications⁽¹⁻³⁾.

The modified properties of polymers by grafting or copolymerization result in increased intermolecular interactions and possible crosslinking of the macromolecules. The surface chemistry and physics of polymers can also be altered by several surface modifying techniques such as surface coating, degradation, hydrolysis, and radiation induced, photochemistry-induced, or catalytic-initiated graft copolymerization. On the other hand, modification of polymers through graft copolymerization presents an effective approach to produce functional polyolefins. The graft copolymerization may introduce some desirable properties into the polymer without a change in the architecture of the polymer backbone and thus gives rise to commercial importance for polymer applications. Grafting improves adhesion, tensile strength, abrasion resistance and enhances thermal and photochemical stability, and it improves compatibility for required engineered polyolefin composites.

1.1. General Review on PP, LCP and Their Blends

1.1.1. Polypropylene

Polypropylene (PP) is known to exhibit different tacticities and several polymorphic forms which affect its overall performance. Because of ease of

processing, recyclability and ability to be modified, its low cost, low density, and growing commercial importance, PP has occupied a considerable and important position among the synthetic polymers. However, the use of PP is limited in several industrially important fields particularly lack of chemical functionalities, sensitivity to photo or thermal oxidation, its low surface energy, difficulty in dyeing, extremely poor hygroscopicity, low strength and modulus, low melting and sticking temperature, inadequate compatibility with other synthetic polymers, and virtually no adhesion to metal and glass. To improve this commodity polymer via the chemical modification of PP by introduction of functional groups into macromolecules has been the area of interest as a route by copolymerization of propylene with polar monomers or by grafting or graft copolymerization of functional compounds to the PP backbone, and reinforcement of PP by fibers, and it meant its importance is still in progress today.

PP chains are made up of carbon-carbon or propylene repeating units. The individual chains are entangled in stable form in the solid state. Carbon bond is very strong in nature, however this strength is not realized in the polymer because of the random entanglement of the coils. During crystallization polymers can organize into regular structures reducing the degree of molecular randomization, and thus the strength and modulus of polymers can be improved. The basic units of semicrystalline polymer morphology consist of chain-folded lamellae radiating outward from a nucleation site to form a spherulite. When orientation is achieved below melting point of the semicrystalline polymer extended chain crystals that have fewer chain folds and defects are obtained whereby the strength and modulus is improved in the orientation direction. When the crystal segments are lengthened this results in a stronger and stiffer fibres. The molecules in the extended chain conformation are locked, and a fully aligned polymer has a very high strength and modulus.

Isotactic polypropylene (IPP) crystallizes in at least three different crystalline modifications, α (or monoclinic), β (or hexagonal) and γ (triclinic), all containing 3_1 helices with the same value of the chain axis but different modes of the packing of the chains⁽⁴⁻⁷⁾. The α form is the most important and conventional one. It is produced

by industry in large amounts and the most extensively studied primary crystalline phase. It is the most stable form and can be easily obtained by crystallization from the melt or from solution. β form is occasionally found in commercial PP, usually at low levels⁽⁷⁾. It can be only partially formed in samples mixed with other crystal forms. The crystals formed rich or pure in β form were reported to be prepared through rapid quenching⁽⁷⁾, zone solidification^(14,15), crystallization in a temperature gradient⁽¹⁶⁻¹⁸⁾ or use of selective nucleating agent⁽¹⁹⁾. γ form can be observed in low molecular weight isotactic polypropylene⁽⁸⁾ or in the crystals obtained at higher pressure than 200 MPa^(9,10-12). On the other hand, one may find coexistence of the α and γ forms in the crystals⁽¹³⁾.

1.1.2. Liquid Crystalline Polymers

Liquid crystal polymers (LCP) are composed of long chain rod-like molecules, and the polymers that form liquid crystal organization in solution are called as lyotropic LCPs while those that form from melt are termed as thermotropic LCPs. The molecules of the liquid crystalline polymer exist as associated in an ordered fashion and form elongated domains⁽²⁰⁾. Within the domain the stiff molecules are found to be parallel with each other. This organized structure yields anisotropy both in the fluid and solid states. When an external force is applied, the order will increase to a high level, and since long relaxation times are associated with orientation decay of LCPs, the order may be retained upon coagulation or solidification in lyotropic or thermotropic LCPs, respectively^(21,22). By achieving a high state of orientation and extension in these extended rigid-chain molecules during processing, highly crystalline products with high modulus and high strength are obtained^(22,23). The moduli and strengths of these chain-extended liquid crystalline polymers are considerably higher than those of the chain-folded semicrystalline commodity polymers. The organized structure of liquid crystalline polymers also gives rise to have significantly increased crystalline melting temperatures with respect to the other polymers at the same conditions.

The orientability of a LCP in the fluid state is the basic factor that affects its

properties and distribution in the solid state⁽²²⁾. That's why it is so important to apprehend the processing-orientation relationship to utilize and control the LCP's properties in an optimal manner. Lewis and Fellers⁽²⁴⁾ reviewed the effect of processing conditions of polymer liquid crystals on their properties. It was pointed out that elongational flow is very effective in orientation enhancement, while no conclusive results could be made with respect to shear flow as the case of the effect of flow rate in the different polymers studied⁽²⁴⁾.

1.1.3. Blends and Combining Thermoplastics with LCP's

The common objective of polymeric material research is the improvement of physical properties. It is well known that the mechanical properties of polymers can be greatly affected by the inclusion or addition of filler materials, particularly, the strength and modulus enhanced by the reinforcing fillers.

Another popular approach is that two polymers are combined in the blend to achieve favorable properties. Because of the relative simplicity in blending commercial polymers, compared to rather complex and costly way of getting new polymers by the synthesis, and if the process is successful, polymer blends present an attractive favorable route to new polymeric materials. However, immiscibility at the molecular level gives rise to multiphase characteristics because of thermodynamic reasons. Yet, heterogeneous blends are generally preferred over miscible ones since one can take advantage of the useful properties of each blend component, but also find synergism, which results in unusual characteristics of the plastic material.

One relatively new type of blend is formed from thermotropic liquid crystalline polymers (LCPs) and thermoplastic (TP) matrices. It was reported that LCPs exhibit very high mechanical properties as a result of their stiff molecular backbones⁽²⁵⁾, their relative ease to orient and their ability to retain this orientation for up to several minutes in the melt state^(26,27). In the reinforcement of TP matrices with LCPs the creation of LCP fibrils by using appropriate processing conditions forms the basic of the processes, and these fibrils reinforce the matrix in an

analogous manner to fibre-reinforced composites. Because of this similarity LCP-reinforced TP are often termed *in situ* composites⁽²⁸⁾. The advantage of these materials is that the properties comparable to those of composite of short glass fibers are attained with improved processibility and favorable dispersion of the reinforcing phase with respect to conventional composite materials. The poor interfacial adhesion between the dispersed microfibrillar liquid crystalline polymer phase and the thermoplastic matrix phase is the most important shortcoming.

Several factors affect the ability of LCPs to reinforce thermoplastics. O'Donnel and Baird⁽²⁸⁾ reviewed these factors considering and discussing the effect of flow field, processing temperature, concentration and dispersion of LCP, miscibility of the components and use of interfacially active component in the blend.

The uniaxial extensional flow field is very effective in bringing about molecular orientation within neat LCPs^(22,29-32) as the influence of the flow field on orientation and mechanical properties of neat LCPs. Ide and Ophir⁽²⁹⁾ illustrated that both the orientation and moduli of LCP samples were significantly improved by drawing the extrudate with varying the draw ratio.

The dispersion of the LCP plays an important role in the properties of a polymer blend beside the effect of the type of flow on orientation. In the blends the fibrils with high aspect ratios are formed through the deformation of the LCP phase in an extensional flow field such as uniaxial extensional flow, and these fibrils can reinforce the TP matrix resulting in high mechanical properties⁽³³⁻³⁷⁾. However, the fibrils, after forming, must be solidified before interfacial instabilities occur, which would lead to break-up of the fibres into droplets^(38,39), or before undergoing relaxation, which would cause a significant loss in their molecular orientation^(26,27).

The concentration of a LCP within a matrix and the flow geometry have also been shown to be critical factors in creation of a fibrous morphology⁽³⁴⁻³⁶⁾. Blizard and Baird⁽³⁶⁾ demonstrated this point with blends of an LCP based on Poly(ethylene terephthalate)/p-hydroxybenzoic acid (PET/PHB) with polycarbonate (PC) or nylon-6,6 matrices. Blends with 10 wt% LCP extruded through a capillary die with a small L/D ratio were found to have a droplet morphology. However, the fibrils were obtained when the concentration reached 30% LCP. It can be stated that the

existence of extensional flows and higher concentrations are important factors that can lead to the creation of a reinforcing morphology⁽²⁸⁾.

In order to achieve a reinforcing morphology, one of the factors is the processing temperature of the blend to be suitably adjusted. Typically, LCPs are processed above 300°C while thermoplastics are processed usually well below this temperature. Despite this temperature difference, a fibrous morphology with enhanced mechanical properties can often be created within any TP/LCP blends. On the other hand, while high temperatures are generally required to process TP/LCP blends, temperatures much higher than the melting point of the LCP may lead to a reduction in the mechanical properties of the blend. The improved properties at a lower processing temperature may be the result of at least two factors. One is that at the lower temperature the conditions needed to deform smaller LCP droplets might be provided. The second factor is that the lower temperature may result in improved retention of molecular orientation or may permit solidification of the elongated LCP structures before interfacial tension can cause break-up or retraction of the elongated structures⁽²⁸⁾.

The degree of miscibility in a blend is one of the key factors that affects the ability of LCPs to reinforce TPs. Immiscible blends are generally preferred over miscible when the useful properties of each blend component are taken as an advantage. However, the immiscible blends often have poor mechanical properties, with regard to their components, and unstable morphology. Unfavorable interactions at the molecular level lead to large interfacial tension in the melt and make it difficult to disperse the component during mixing⁽⁴⁰⁾. For several TP/LCP blends studied by Zhuang et al.⁽⁴¹⁾, it was found that partially miscible systems exhibited the highest strengths while totally immiscible systems displayed strengths that did not differ significantly from the strength of the matrix.

Most polymer pairs are immiscible. Thermodynamic theories assume that a negative value of the Gibbs free energy change is required for miscibility. In thermodynamic terms the equation is $\Delta G_m = \Delta H_m - T\Delta S_m \leq 0$, where ΔG_m is the Gibbs molar free energy, and ΔH_m and ΔS_m are the molar enthalpy and entropy of mixing, respectively. In most cases ΔH_m is positive, which does not favor mixing, and ΔS_m is

positive, which favors mixing. Whether or not a blend components are miscible, depends on the contributions from enthalpy and entropy factor, where in the case of positive enthalpy of mixing the homogeneous mixing at the molecular level depends on the entropy increase, $T \Delta S_m$ term must be large enough to overcome the hindrance of the enthalpy factor. However, the entropy increase in the polymer mixing generally is too small to supply the necessary requirement for homogeneous mixing⁽⁴²⁾, because of the dominating enthalpy contribution most polymer blends are immiscible. The investigations have shown that the enthalpy of mixing can be reduced or made negative with the help of specific interactions, such as hydrogen bond^(43,44), dipole-dipole⁽⁴⁵⁾, ion-dipole⁽⁴⁶⁾, and ion-ion⁽⁴⁷⁾ interactions. These interactions can serve as physical crosslinks at the interphase leading to reduced interfacial energy and improved interfacial adhesion⁽⁴²⁾.

In order to improve the properties of blends composed of less suitable polymers, a third interfacially active component might be used. The process of bringing about enhanced properties by the addition of a minor third component is termed compatibilization^(48,49). Without compatibilizer, the blend components would exhibit poor adhesion and large phase sizes, and the blend would exhibit poor mechanical properties.

The compatibilizer may be a copolymer consisting of two blocks that are similar to the polymers in the blend, blocks capable of creating specific interactions with the polymers, or a functionalization of one of the polymers so that it is capable of undergoing a graft reaction with the dissimilar polymer. It is well known that among compatibilizing agents block or graft copolymers, made up of segments whose chemical structure and solubility parameters are similar to those of the polymers being blended, appear best suited to the scope⁽⁵⁰⁾. These compatibilizers can migrate to the interphase and reduce the interfacial energy between matrix and dispersed phase, thus causing a reduction of the minor phase dimensions and a stabilization of polymer blend morphology. A common point in the studies of compatibilizers is that successful compatibilization can be characterized by three features: reduced interfacial tension, finer dispersions and increased adhesion. In addition, successful compatibilization results in mechanical property improvements.

In particular, the impact strength and toughness of TP blends are markedly improved⁽²⁸⁾.

1.2. Reinforcement of PP with LCP's

Blends of PP with several LCPs have been studied by several workers⁽⁵¹⁻⁵⁵⁾. These blends show some improvements in modulus, the similar or even lower tensile strength has been obtained in the absence of appropriate compatibilizers despite nonpolar nature of PP to more polar LCPs.

For this reason, in recent years the studies have been directed towards the preparation and characterization of PP/LCP blends containing different compatibilizers. The effect of maleic anhydride grafted PP (MAP) on the mechanical properties and morphology of the PP/LCP blends were reported in several articles^(28, 56,57). It was found that the addition of MAP to the PP phase leads to significant increase in the mechanical properties of PP/LCP blends. The reinforcing LCP fibrils were found to be much more finely dispersed in the matrix, and the reduced interfacial tension and increased adhesion indicated that MAP compatibilized the PP/LCP blends. The interactions such as hydrogen bonding was believed to be responsible for the compatibilizing effect of MAP, instead of reaction with LCP.

Maleic anhydride (MAH) is a highly reactive monomer used frequently for radically initiated functionalization of PP. MAH molecules grafted onto PP not only increase the polarity, but also react with groups, such as $-NH_2$, $-OH$, and $-COOH$, of other polymers thus forming chemical links between components⁽⁵⁸⁾. On the other hand, a compatibilizer creates a droplet morphology resulting in lower tensile properties. In the reinforcement of TP with LCP the compatibilizer must not cause the loss of fibrous morphology, and it must improve the adhesion between phases⁽²⁸⁾.

Miller and coworkers⁽⁵⁹⁻⁶¹⁾ have used an acrylic acid-functionalized PP (PPAA) and a PPAA-based graft copolymer for the compatibilization of PP/LCP blends and the improvements in interfacial adhesion and thus in fibre properties, thermal stability and crystallinity of the blend products have been obtained. The

improvements have been attributed to the promotion of specific interactions between the blend components.

Miettinen et al.⁽⁶²⁾ have used a reactive terpolymer containing an epoxy end-group as a compatibilizer for PP/LCP blends. It was proposed that the carboxyl end groups of the polyesters react with the epoxy group of the compatibilizer. The addition of compatibilizer leads to a smaller size of the dispersed domains, thereby causing them to adhere better in the matrix. In another study, Chiou et al.⁽⁶³⁾ used a reactive compatibilizer based on the ethylene- glycidyl methacrylate copolymer (EGMA) for the PP/LCP blends. The compatibilized PP/LCP blends showed finer dispersed LCP domains but lower PP crystallinity. It was suggested that the epoxy functional groups of the EGMA copolymer can react with the carboxylic acid and/or the hydroxyl end groups of the liquid crystalline copolyester.

1.3. Liquid Crystals, Poly(Acryloyloxybenzoic Acid) and Poly(Methacryloyloxybenzoic Acid)

1.3.1. LCP

Liquid crystal polymers (LCP) are composed of assemblies of rigid and rodlike long molecular chains. The smaller groups that make the material capable of forming liquid crystal phase are called mesogens which are responsible for forming anisotropic liquid phase, and these groups can be composed of segments from the backbone of the polymer, segments from the side chain, or segments from both the backbone and side chain.

There are three basic types of liquid crystalline (LC) compounds identified as a function of the arrangement of the molecules according to the classification proposed by Friedel⁽⁶⁴⁾. These are nematic, smectic and cholesteric.

The nematic liquid crystalline form involves long range orientational order along a certain direction with an unordered arrangement of the centers of gravity of the molecules. The rod-like molecules are aligned along a direction, and the

orientations are distributed uniformly about the direction, with no greater the symmetry of the system.

In the smectic liquid crystals the molecules are aligned in one preferred direction with the ordering in a three dimensional layered fashion, in ordered and unordered layers. The long axes of the molecules in each layer can be positioned both perpendicular to the plane of the layer and at a slight angle, which makes the formation of different polymorphous modifications possible within the limits of the smectic mesophase (smectic A, B, C, D, E, F, etc.)⁽⁶⁵⁾.

In the cholesteric type of liquid crystals, the molecules are assembled in layers in which their arrangement is similar to the arrangement in the nematic phase, but each layer is rotated by a certain angle with respect to the preceding layer so that some helical twisting of the molecules occurs on the whole, describing a helix with pitch. The twist in a cholesteric phase arises spontaneously when the mesogenic molecules have optically active chiral nature^(65,66).

The so-called comb-shaped polymers, macromolecules which contain relatively long side branches spaced comparatively closely along the main chain, occupy a special position among the large number of polymers sometimes used in unusual areas. They differ from ordinary branched polymers due to the fact that they have many side chains: each monomeric unit can contain such a chain and this quantitative difference results in the appearance of a new set of qualitative properties which are absent in linear or weakly branched polymers. One of the most important properties of comb-shaped polymers with mesogenic groups in the chains of theoretical and practical interest is their capacity to form a liquid crystalline phase. The key to make side-chain liquid crystalline polymers is the incorporation of a flexible connecting link between the mesogenic group and its attachment point to the backbone. The rigid groups are sufficiently decoupled from the perturbing influence of the backbone to pack as a mesophase⁽⁶⁵⁾

1.3.2. PABA and PMBA

A vinyl monomer, p-methacryloyloxybenzoic acid (MBA) has been polymerized by free radical initiation in the nematic and smectic state through its inclusion into the lattice of two mesomorphic solvents, p-heptyloxybenzoic acid (HBA) and p-cetyloxybenzoic acid (CBA), respectively, by Blumstein and Kitagawa⁽⁶⁷⁾ and the influence of polymerization conditions of the population of isotactic, syndiotactic and heterotactic triads was studied. The increase in the percentage of isotactic component obtained in the nematic and the smectic state was explained on the basis of the steric organization of the monomer in the mesophase.

In another study, in the polymerization of p-methacryloyloxybenzoic acid, by Blumstein et al.⁽⁶⁸⁾ it was found that organization of the monomer within a mesophase solvent has a considerable influence on the kinetics of polymerization, the molecular weight and also an influence on the microtacticity of the polymer. In another study carried out by Blumstein et al.⁽⁶⁹⁾ MBA was polymerized in the isotropic bulk, in a nematic solvent, and also in isotropic solvents. When polymerized in bulk, the polymer displayed pronounced crystallinity. A mesomorphic smectic superstructure appeared in films of the polymer cast from dimethylformamide, regardless of method of polymerization, although none of the PMBA's studied are stereoregular. It was concluded that neither the presence of a mesomorphic matrix nor large amounts of crosslinking agent are necessary for the development and locking in of mesomorphic superstructure in polymers⁽⁶⁹⁾.

The crystallinity and order in atactic poly(acryloyloxybenzoic acid) (PABA) and poly(methacryloyloxybenzoic acid) (PMBA) were studied in the later work of Blumstein et al.⁽⁷⁰⁾. It was also reported that the family of p-n-alkoxybenzoic acids displays nematic and/or smectic liquid crystalline organization, beginning with the n-propoxy homologue. On the other hand, neither of the monomers, ABA and MBA displays mesomorphic behavior. Both give a sharp transition from crystal to isotropic melt. Rapid polymerization of the melt can be observed⁽⁷⁰⁾. The polymers PABA and PMBA were obtained by heating the corresponding monomers at or above the melting points and by solution polymerization in dimethylformamide.

Two crystal forms have been reported for PABA⁽⁷⁰⁾ ; One of these (form I) with a higher degree of crystallinity which may reach 40% and a higher crystallite perfection has a monoclinic structure, and the other (form II), obtained on rapid polymerization of the monomer at or above its melting point, was identified as smectic E_t. Form I can be obtained either on casting of a film of form II from DMF or on slower polymerization in thin layer of the molten monomer. It was reported that bulk polymerization by heating on a hot stage leads to an isotropic p-acryloyloxybenzoic acid (ABA) melt which forms a mobile, nematic schlieren texture out of which spherulites grow as the polymerization to PABA progresses. The development of spherulitic structures is more pronounced for poly(acryloyloxybenzoic acid) than for the poly(methacryloyloxybenzoic acid).

The development of crystallinity in both polymers depends strongly on the preparation conditions⁽⁷⁰⁾. On fast polymerization PMBA displays no crystallinity and gives x-ray pattern characteristic of smectic layered arrangements of macromolecules. The macromolecule of PABA with its more flexible backbone can form a three-dimensional lattice more easily than the PMBA macromolecule which is crowded by the presence of α -methyl groups along its backbone. The developed crystallinity and the organization of side groups proceeded beyond the formation of a long range lamellar (smectic) order in these atactic polymers were endowed with the hydrogen bonded benzoic acid moieties.

In order to investigate the influence of hydrogen bonding on the development of order in PABA some of the PABA samples were partially methylated. It was observed that hydrogen bonding plays an important part in the development of order in PMBA and PABA. The completely methylated polymers are *amorphous* glasses. They display neither birefringence nor crystallinity on annealing and their x-ray diffraction patterns are typical of amorphous compounds. Linear dimerization through hydrogen bonding is recognized as responsible for the mesomorphic behavior of p-n-alkoxybenzoic acids⁽⁷⁰⁾.

The phase transitions of PABA were studied by Menczel and Wunderlich⁽⁷¹⁾ and it was reported that PABA may exhibit, beside the reported smectic E_t form⁽⁷⁰⁾, another highly mobile mesophase state which is probably nematic. It is produced by

melting of crystal forms I and II, by Blumstein et al.⁽⁷⁰⁾ or out of amorphous PABA above the glass transition. Amorphous PABA was prepared by quick thermal polymerization. Sometimes partially crystalline polymers were obtained even by this method. It has been assumed that the partially crystalline samples arose probably whenever the monomer was not sufficiently dried before polymerization. In this case a small amount of oligomer of poly(p-oxybenzoate) is formed, which is liquid crystalline or crystalline depending on its molecular weight. As the acryl-polymerization proceeds, poly(p-oxybenzoate) crystals may act as seeds for crystallization of PABA. On the other hand amorphous PABA showed a strong heating rate dependent heat capacity increase⁽⁷¹⁾. The glass transition is followed at higher temperature by an exotherm. Optical microscopy showed that the sample in this temperature region is becoming birefringent, but no endotherm was observed in the melting of PABA. It was then concluded that the observed exotherm corresponded to the amorphous to mesophase transition, and a strong heating rate dependence of the glass transition, however, that amorphous PABA has a normal hysteresis behaviour⁽⁷¹⁾.

Blumstein et al.⁽⁷⁰⁾ reported the melting point of PABA as 252°C. Menczel and Wunderlich⁽⁷¹⁾ used optical microscopy and DSC measurements combined with thermogravimetric analysis in order to investigate the melting point. Optical microscopy showed that the polymer melts approximately at 252°C. This is not, however, a crystal to isotropic transition; but a mobile, liquid crystal phase which is observed beyond melting. From the texture under the microscope it was classified as a nematic phase. Certain amount of decomposition also occurs during the melting⁽⁷⁰⁾. Thermogravimetry showed 19% and 7% weight loss at the temperature at about the end of the melting endotherm for modifications I and II, respectively.

Furthermore, the polymerization of p-acryloyloxybenzoic acid was investigated to resolve the questions such as the nucleation of the mesophase and transformation of the mesophase into solid by parallel use of optical microscopy and quantitative thermal analysis by Menczel et al.⁽⁷²⁾. The search led to, however, the discovery of a much more complicated reaction instead of simple vinyl polymerization. It was assumed that the observed mesophase is not connected with

p-acryloyloxybenzoic acid or poly(acryloyloxybenzoic acid). The polymer is not involved in mesophase formation, but seems to cause solidification of the spherulites, *schlieren* texture, and isomorphous material. After melting of ABA, which leads to an isotropic phase, acidolysis produces acrylic acid and oligomers of poly(p-oxybenzoate), POB, and the oligomers of POB are the root of the mesophase formation. Polymerization of ABA without oligoester formation gives no intermediate mesophase.

As far as we know, there exists only one research on the blends of PABA and PMBA with a thermoplastic material. The thermal behaviour of PABA/nylon 6 (PA6) blends were investigated by Sainath et al ⁽⁷³⁾, it was reported that melting point of PA6 was depressed with increasing PABA content and it was suggested with wide angle X-ray analysis that crystallinity of PA6 was decreased with increasing PABA content.

1.4. Radiation Induced Grafting

Polymers with two chemically different repeating units are called copolymers. In an ordinary or random copolymer the monomer residues are located randomly along its chains, and they are produced by simultaneous polymerization of a mixture of two or more comonomers. There exists basically three types of linear copolymers:

- | | |
|------------------------------|-----------------------|
| 1) A-A-B-A-B-A-B-B-B-A-B-A-A | Random Copolymer |
| 2) A-B-A-B-A-B-A-B-A-B-A-B-A | Alternating Copolymer |
| 3) A-A-A-A-B-B-B-B-B-A-A-A-A | Block Copolymer |

what obtained with a chemical catalyst acting as initiator. Among the methods, radiation grafting is one of the most promising methods because of several advantages; A variety of the radiation doses produces different initiation rates, hence different products. The effect of temperature, which is relatively unimportant for radiation initiation, can be better assessed, controlled and utilized on propagation rate. The lack of any chemical initiator results in the product not contaminated by any side products brought about by the initiators. High penetration of energetic radiation into the polymer matrix, rapid and also uniformly distributed active sites for initiating grafting throughout the matrix are some of the other major advantages in radiation^(75,76).

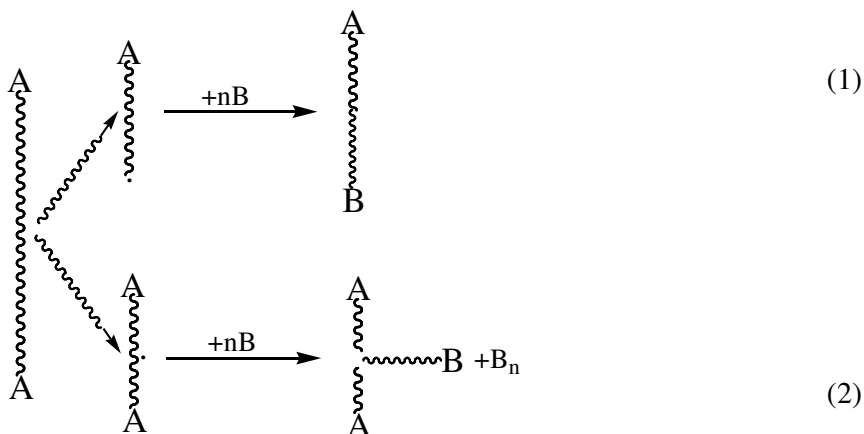
Several methods are available to produce graft copolymer by ionizing irradiation (mostly γ -ray), and these methods have been described by Chapiro in detail⁽⁷⁷⁾:

- a) The direct grafting of a monomer to a polymer
- b) Grafting on radiation-peroxidized polymers.
- c) Grafting initiated by trapped radicals.
- d) Inter-crosslinking of two different polymers.

methods (b) and (c) can also be called as pre-irradiation method. In all cases the initial radiation event leads to the same result, i.e., the formation of polymeric free radicals in a polymer A_m . These radicals (to a certain extent some ions) are thereafter used in different ways to achieve grafting⁽⁷⁷⁾.

1.4.1.1. Direct Grafting to Polymer

In direct grafting, if a polymer A_m is irradiated while in contact of a monomer B, the polymeric radicals generated from polymer A_m are directly used to initiate the polymerization of monomer B, and the resulting product is a graft or a block copolymer. This reaction can be written schematically as,



Here $\text{A}\text{---}\cdot$ and $\cdot\text{---}\text{A}$ are macro free radicals derived from A_m . Reaction (1) is expected to occur if A_m is a polymer of degrading type through chain scission resulting in a product of a block copolymer. On the other hand, if A_m cross-links under irradiation, reaction (2) is more likely to occur and this process leads to the formation of an equal number of graft copolymer and homopolymer molecules. In addition, the monomer B is also radiolized in this process:

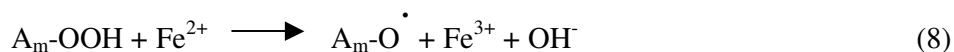


This reaction is another source of homopolymer B_n .

1.4.1.2. Grafting on Radiation-Peroxidized Polymer

Irradiation of a polymer A_m in the presence of oxygen leads to the formation of a peroxidized polymer $\text{A}_m(\text{O}_2)$. This can be used in a subsequent reaction for initiating the polymerization of a monomer, which leads to the formation of graft copolymers A_mB_n . When peroxidized polymer is placed in monomer B and then heated, the peroxide groups break down and can link to monomer B, which then propagates as in normal polymerization. Two different situations may arise in such systems, depending on whether diperoxidizes or hydroperoxidizes are formed in the irradiated polymer.

It appears that the thermal dissociation of hydroperoxide gives rise to an equivalent number of graft copolymer and homopolymers. In this case the formation of homopolymer, which results from the initiation of the polymerization by OH radicals, can be reduced by decomposing the hydroperoxides at low temperatures by a redox system, according to the following reaction :



1.4.1.3. Grafting Initiated by Trapped Radicals

The presence of trapped radicals has been detected in many irradiated polymers. If an irradiated polymer is brought into contact with a monomer, it leads almost to a graft copolymer. It is clear that the yield of grafting depends directly on the efficiency of radical trapping. On the other hand, oxygen is known to destroy trapped radicals since it converts radicals into peroxidic radicals, which can abstract hydrogens from surrounding polymer molecules. Thus, much higher yields are obtained if irradiation is carried out in the absence of oxygen. In addition, since the lifetime of trapped radicals is limited, highest yields are achieved if the grafting step is carried out within a short time after irradiation. Consequently, the main disadvantage is that only a small fraction of the radicals formed in the radiolysis remain trapped after irradiation.

1.4.1.4. The Intercrosslinking of Different Polymers

Very simple method of radiation grafting is based on the crosslinking of an intimate mixture of two polymers A_m and B_n . To encourage the combination of polymeric radicals A_m^\bullet and B_n^\bullet formed during radiolysis, the polymer molecules must be in very close contact. This can be achieved either by mixing both polymers mechanically at ordinary temperatures, or better on hot rolls. Alternatively, grafting

reaction can be carried out in solution. However, it should be noted that one major problem connected with this method is the fact that most polymers are incompatible; consequently it may be difficult to prepare the intimate mixture of polymers.

1.5. Aim of the Work

The objective of this study is to investigate the polymerization of p-acryloyloxybenzoic acid and p-methacryloyloxybenzoic acid and to carry out graft copolymerization of the monomers onto isotactic polypropylene. The monomers which do not form mesophases, result in mesomorphic polymers when polymerized. It is known that the mesomorphic polymers exist as associated in an ordered fashion with high state of orientation and extension on the molecular level. By the presumed properties of the polymers, obtained by polymerization of the monomers, the improvement in properties of the PP was mainly aimed by graft copolymerization. It was planned to get an improvement in processability and dispersion of the reinforcing liquid crystalline polymer phase in the graft copolymers.

CHAPTER 2

EXPERIMENTAL

2.1. Chemicals and Materials Used

2.1.1. Solvents and Reagents

Dimethyl sulfoxide, xylene and methanol (Riedel-de Haen A.G.) and dimethylformamide and acetone (Merck A.G.) were used without any purification. Technical grade ethanol was used without any purification.

Acryloyl chloride (Aldrich A.G.), methacryloyl chloride (Acros Organic A.G.), p-hydroxybenzoic acid (Aldrich A.G.) were the main chemicals for the preparation of p-acryloyloxybenzoic acid and p-methacryloyloxybenzoic acid monomer. The initiators, dicumyl peroxide (DCP) and benzoyl peroxide (BPO) (Merck A.G.) were used as received.

2.1.2. Preparation of Powder Isotactic Polypropylene

Isotactic polypropylene (IPP), coded as MH 418, was supplied by PETKİM, Turkish Petrochemical Industry

IPP was dissolved in boiling xylene (138-139°C) and precipitated by adding technical ethanol. The precipitate was collected, dried in vacuum at room temperature, and ground by cooling in liquid nitrogen. The powder IPP was subjected to 10 kGy γ -irradiation under open atmosphere to create active sites, -COOH groups, on it. This irradiated powder IPP was used in the graft copolymerization experiments.

2.2. Synthesis of the Monomers

2.2.1. Synthesis of p-Acryloyloxybenzoic Acid

p-Acryloyloxybenzoic acid, ABA, was synthesized by condensation of acryloyl chloride with p-hydroxybenzoic acid in alkaline medium (Figure 2.1) as described by Blumstein and Kitagawa⁽⁶⁷⁾. 3.6 g (0.026 mol) p-hydroxybenzoic acid was added to a solution of 3 g (0.054 mol) KOH in 50 mL of distilled water in a flask equipped with a magnetic stirrer. The solution was cooled to 0-5°C, and then 2.35 g (0.026 mol) acryloyl chloride was added dropwise by stirring about 20 min. The stirring then continued at room temperature for another 30 min. A precipitate formed after cool 3M HCl addition was filtered and washed with water. Then, ABA was purified by repeated recrystallization from acetone. The yield was 58 wt%. We could not reach the yield reported in literature, 75 %⁽⁷³⁾.

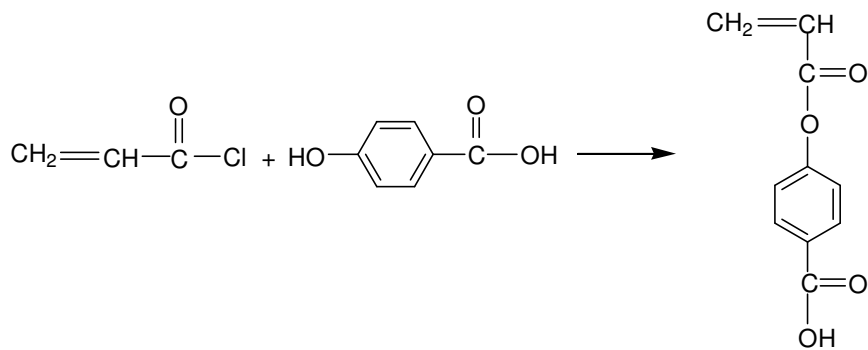


Figure 2.1. The simplified reaction between p-hydroxybenzoic acid and acryloyl chloride.

2.2.2. Synthesis of p-Methacryloyloxybenzoic Acid

p-Methacryloyloxybenzoic (MBA) acid was also synthesized by condensation of methacryloyl chloride with p-hydroxybenzoic acid in alkaline medium as in the synthesis of p-acryloyloxybenzoic acid with the the same amounts and same procedure, Figure 2.3. The yield was 50 wt% in good agreement with the literature⁽⁶⁷⁾.

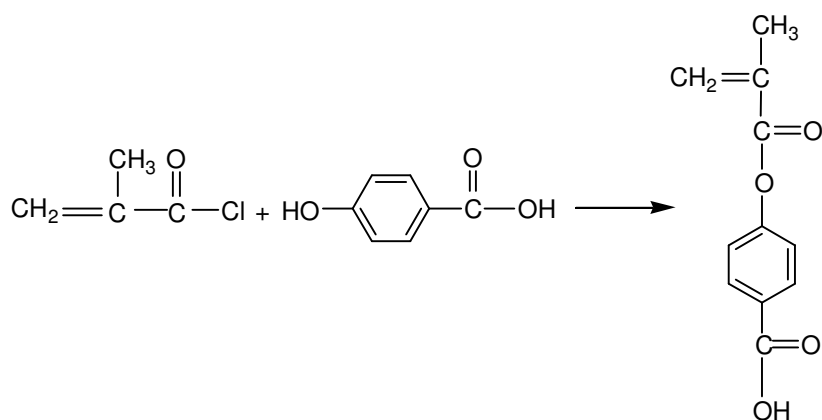


Figure 2.3. The simplified reaction between p-hydroxybenzoic acid and methacryloyl chloride.

2.3. Polymerization of the Monomers, ABA and MBA

There exists only few reports (see Introduction part page 10-14) which was all about bulk melt polymerization at high temperature. By means of these experiments the best way of grafting of both monomers were successfully revealed.

2.3.1. γ -Irradiation Induced Polymerization

γ -Irradiation induced polymerization of ABA and MBA were also carried out by cobalt-60 γ -radiation source. The tubes containing methanol solution of the monomers were evacuated, sealed and subjected to 10 kGy, 20 kGy and 30 kGy. The precipitate formed in the tube of ABA was collected, washed with methanol and dried in vacuum oven. The process was repeated in the presence of air and in solid state with the monomer ABA. The polymerization was successful only in methanol solution of ABA in vacuum. The maximum conversion was 87.3 % and this conversion was reached in early irradiation doses.

The above process was repeated by using dimethyl sulfoxide, DMSO, instead of methanol. Again the polymerization was successful with ABA. The product was precipitated by adding water, and treated with boiling methanol for 3 days to remove DMSO which is very difficult to remove from the product by vacuum drying. The polymer was dried in vacuum at 50-60°C for a week. MBA did not give any γ -radiation induced polymerization reaction in any condition.

2.3.2. UV-Induced Polymerization

The attempt of UV-induced polymerization of ABA was carried out in methanol solution of ABA in open atmosphere under UV-radiation for 4, 10 and 24 h., but the polymerization was not successful. Hence, MBA was not tried since MBA was also rather reluctant for polymerization even in γ radiation source.

2.3.3. Bulk Polymerization of The Monomers

The bulk melt polymerization of the monomers was studied without initiators due to the high melting point of the monomers, as reported in the literature⁽⁷⁰⁾. The polymerization of ABA and MBA were carried out by heating the samples to 215°C

and 190°C, respectively, and keeping the temperature constant for 3 h. The products were washed with methanol to remove monomer remaining and methanol soluble part. But, only the polymer PMBA could be obtained with conversion of 45,2 %, however, an undefined product was obtained with ABA probably due to degradation.

The mixture of ABA and dicumyl peroxide (DCP, 2% with respect to weight of monomer) was heated to 200°C in vacuum keeping the temperature constant for 40 minutes. The product, PABA, was washed with methanol repeatedly and dried in vacuum. The polymer yield was above 95%.

The polymerization of MBA was tried in the presence of DCP (2,5%) at 185°C, as the preceding process, however, was not successful.

2.3.4. Solution Polymerization of The Monomers

Dimethyl formamide (DMF) solution of ABA containing 1,5% (with respect to weight of ABA) benzoyl peroxide (BPO) was heated to 90°C in vacuum keeping the temperature constant for 40 minutes. The product was precipitated by adding water, washed with methanol to remove monomer remained unpolymerized and methanol soluble products, and dried in vacuum at 50°C. The polymer yield was above 81%.

The process was repeated with MBA using 2,5% BPO, however, no polymer was obtained.

The solution polymerization of ABA was also repeated with DMSO and methanol as in the preceding conditions. However, the polymerization was failure.

2.4. Graft Copolymerization of the Monomers

2.4.1. γ -Irradiation and UV-Induced Graft Copolymerization of ABA onto PP

γ -Irradiation induced graft copolymerization of ABA onto IPP was attempted as in the polymerization of the monomer. Methanol solution of ABA was mixed with powder IPP, and the flask containing the mixture was evacuated, sealed and subjected to 10 kGy radiation. But no grafting was obtained. The procedure was repeated in open atmosphere by using UV-radiation for 10 h instead of γ -irradiation, but, again no grafting was observed.

2.4.2. Thermally Induced Graft Copolymerization of ABA and MBA onto PP

The polymer IPP and monomer (ABA or MBA) were mixed in desired proportions in mortar with hand grinding extensively, and the mixture was transferred to the reaction flask. The flask, then, heated up to the desired temperatures keeping the temperature constant for a certain reaction time period. At the end of the reaction time the flask was cooled at room temperature and opened. The reaction products were first washed with methanol to remove soluble products, especially monomer. Then homopolymers (polyacryloyloxybenzoic acid and methacryloyloxybenzoic acid) were removed by DMSO washing. Finally, the grafted PP was rewashed extensively with methanol several times to ensure the removal of DMSO. The graft copolymerized IPP sample, then, was dried in vacuum at room temperature for 4-5 hours. The amount of grafting was determined gravimetrically and expressed as a percentage of grafted polymer by weight in the products.

2.5. Characterizations and Instruments

2.5.1. FT-IR Measurements

FT-IR characterization of IPP, monomers and the products, PABA-g-PP and PMBA-g-PP, were done with a Nicolet DX 510 FTIR spectrometer. FT-IR spectra of the samples were obtained from KBr pellets prepared from approximately 3 mg sample in 100 mg spectroscopic grade KBr.

2.5.2. NMR Measurements

ABA, MBA, PABA and PMBA were characterized by using a Bruker-Spectrospin Avance DPX 400 Ultra-shield ¹H-NMR spectrometer with a frequency of 400 MHz.

2.5.3. Differential Scanning Calorimetry (DSC) Analysis

DSC analyses of the monomers and the products were carried out with a TA-DSC 910S Differential Scanning Calorimeter, under nitrogen atmosphere, with a heating rate of 20°C/min, and sample size was varied between 5-10 mg. The glass transition temperature (T_g) and melting points (T_m) were determined from the obtained thermograms.

2.5.4. TG/IR Measurements

The TG/IR analysis of PABA and PMBA-g-PP samples were carried out by a TG/IR system, which combined with a Perkin Elmer Pyris 1 TGA

Thermogravimetric Analyzer and a Perkin Elmer Spectrum One FT-IR Spectrometer (Central Research Laboratory, METU). Sample of about 10 mg were pyrolysed in the TG analyzer, and the evolved gases were led to the Perkin Elmer Spectrum One FT-IR Spectrometer directly through a connected heated gas line to obtain FT-IR spectra. The thermogravimetry test were performed in the air and nitrogen atmosphere in the temperature range from 25 to 600°C at a heating rate of 20°C/min.

Other thermogravimetric analysis of PP, PABA and PABA-g-PP samples were carried out by a DuPont 2000 thermogravimetric analyzer in the air and nitrogen atmosphere with a heating rate of 20°C/min.

2.5.5. X-Ray Measurements

The x-ray diffraction patterns of IPP and PABA-g-PP samples were obtained by using a RIGAKU D-MAX 2000 Powder Diffractometer in Ankara University Central Research Labs. Monochromator-resolved $\text{CuK}\alpha$ radiation was employed. The profiles were measured by a scintillation counter system 0.5° receiving slit using a step scanning method (0.02° steps every 1s).

2.5.6. Mechanical Properties

Tensile properties of IPP, PABA-g-PP and PMBA-g-PP samples were determined by Instron Tensile Testing Machine (Model TM 1102) at room temperature. The test samples were prepared by micro-injection molding at 200°C with the thickness of 0.12, the width of 0.69 and the length of 3 cm. The injection temperature is well below the degradation temperature of PABA-g-PP and PMBA-g-PP. Crosshead speed and gauge length in testing were 5 cm/min and 1 cm, respectively.

The stress-strain values were computed from the load (F)-elongation values measured during the tests by the following relations:

$$\sigma = (F/A_0)$$

Where σ (Mpa) is the tensile stress, F is the load (tensile force) applied, and A_0 is the original (undeformed) cross-sectional area of the gauge region of the specimen. Strain, ϵ , is defined as

$$\epsilon = (\Delta L/L_0)$$

where L_0 is the initial gauge length, and ΔL is the change in the gauge length due to deformation. The tensile modulus (Young's Modulus), E, which is the initial slope of the stress-strain curve, is also calculated as

$$E = \sigma/\epsilon$$

The impact strength of the test samples were determined by Coesfeld Material Test Pendulum Impact Tester at room temperature. The samples were prepared as they were prepared for tensile tests.

2.5.7. Scanning Electron Microscope (SEM) Study

Morphological properties of tensile and impact fractured surfaces were studied by using scanning electron microscope, JEOL, JSM-6400.

2.5.8. MS Measurements

MS analysis of PABA, PABA-g-PP and PMBA-g-PP samples was carried out by a Hewlett-Packard 5973 Mass Spectrometer equipped with metallized gold quadrupole mass filter and coupled with Direct Insertion Probe. The samples were heated at a rate of 10°C/min between room temperature and 450°C. The mass data recorded under electron impact ionization energy of 70 eV at a scan rate of 2 scan/s and in the mass range of 16-600 amu.

CHAPTER 3

RESULTS AND DISCUSSION

3.1. Characterizations

3.1.1. Characterization of Isotactic Polypropylene, IPP

FT-IR spectrum of 10 kGy irradiated IPP was given in Figure 3.1. The absorption bands of stretching vibrations of CH₃ group were at 2961 and 2875 cm⁻¹, and CH₂ group at 2921 and 2838 cm⁻¹. The absorption bands due to bending vibrations of CH₃ and CH₂ groups were observed at 1378 and 1460 cm⁻¹, respectively. The bending vibrations of C-C and C-H groups were observed between 1166 and 841 cm⁻¹. The active sites, hydroperoxygroups, COOH on irradiated IPP was observed at about 3340 cm⁻¹ due to the O-H stretching vibrations.

DSC melting point of both irradiated and nonirradiated PP was found 162,7°C in N₂ indicated no change in the crystal structure upon irradiation.

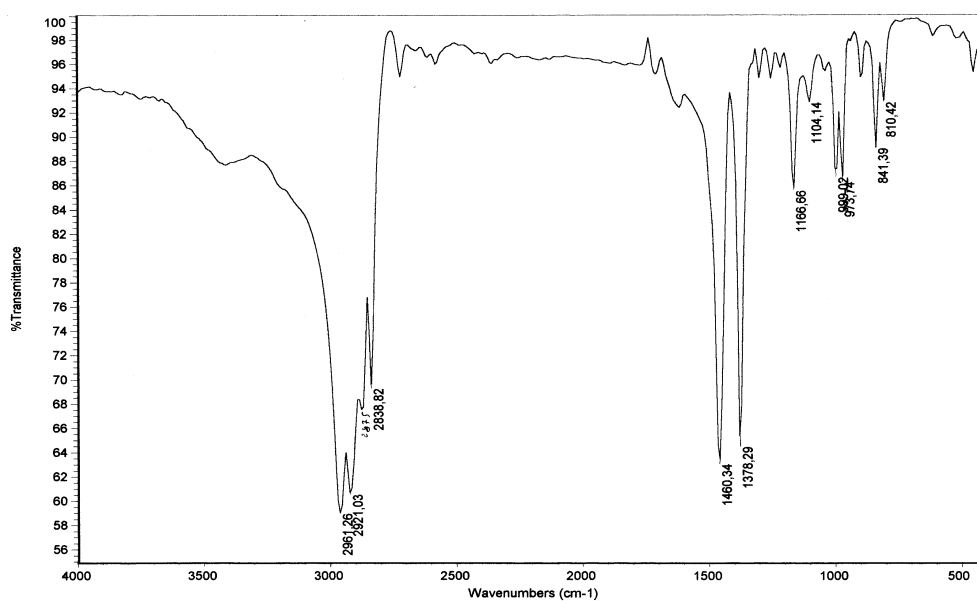


Figure 3.1. FTIR spectrum of IPP irradiated by γ -radiation (10 kGy)

3.1.2. Characterization of p-Acryloyloxybenzoic Acid

The FTIR spectrum of monomer ABA, Figure 3.2 shows broad bands between 3200-2500 cm^{-1} due to the carboxylic acid O-H and C-H stretching vibrations. The strong band at 1742 cm^{-1} is characteristic of C=O stretching vibrations of ester group. A strong band at 1688 cm^{-1} is due to C=O stretching vibrations of aryl carboxylic acids. The bands at 1600 and 1500 cm^{-1} are assigned to C=C stretching vibrations of aromatic compounds. The four bands at 800, 909, 939 and 987 cm^{-1} are due to vinylic C-H out-of-plane bending vibrations.

The $^1\text{H-NMR}$ spectrum of ABA, shows a quartet at δ 6.3 and doublets at δ 6.0 and δ 6.6 corresponding to three protons of $\text{CH}_2=\text{CH}-$, and two doublets at δ 7.1 and δ 8.1 corresponding to four protons of the C_6H_4- group, given in Figure 3.3.

DSC melting point of ABA was 199-200 $^\circ\text{C}$ in N_2 atmosphere with heating rate of 5 $^\circ\text{C}/\text{min}$, in good agreement with the literature⁽⁷⁰⁾, Figure 3.4.

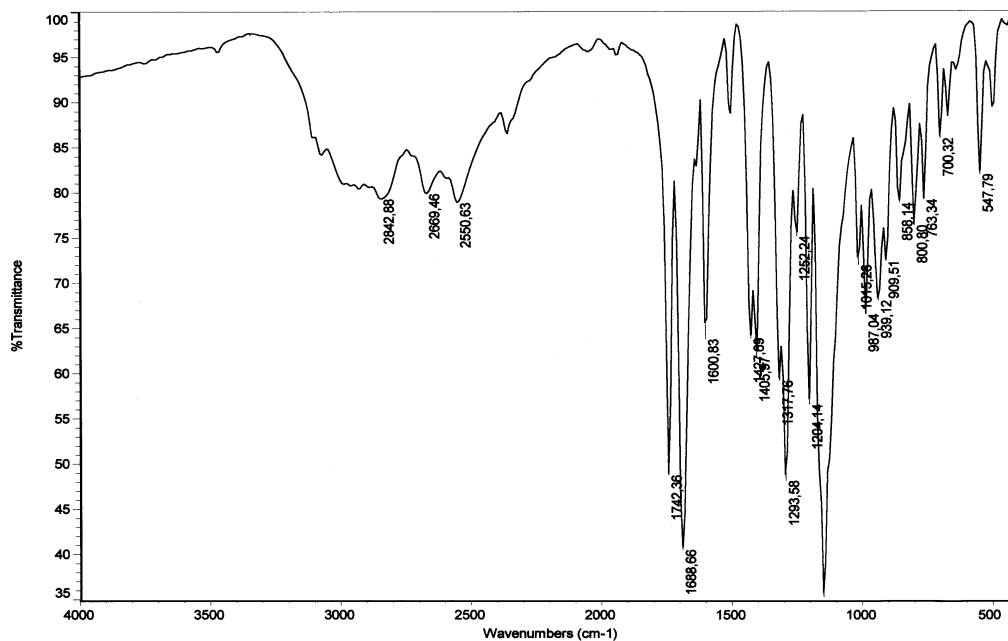


Figure 3.2. FTIR spectrum of acryloyloxybenzoic acid

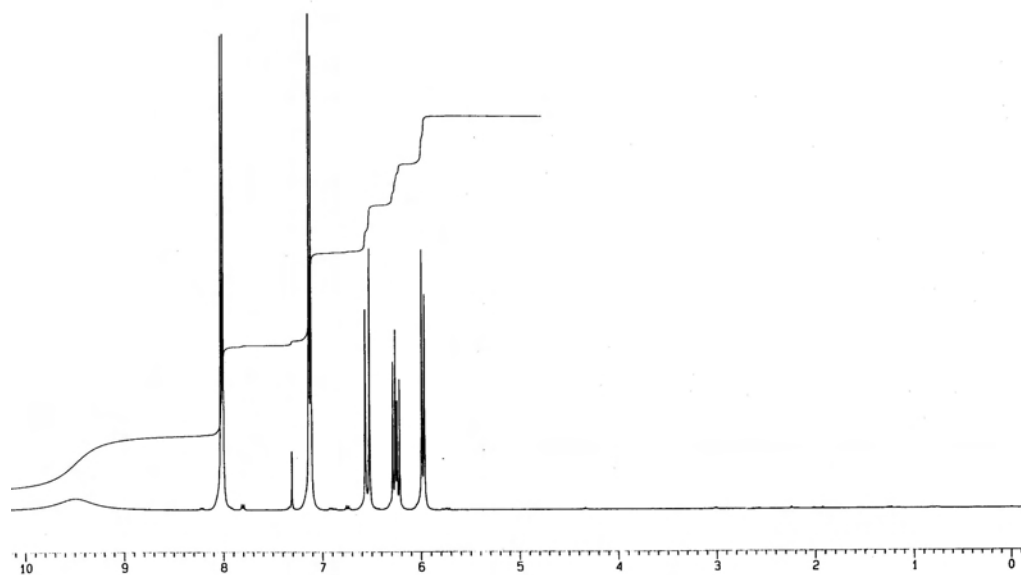


Figure 3.3. $^1\text{H-NMR}$ spectrum of acryloyloxybenzoic acid

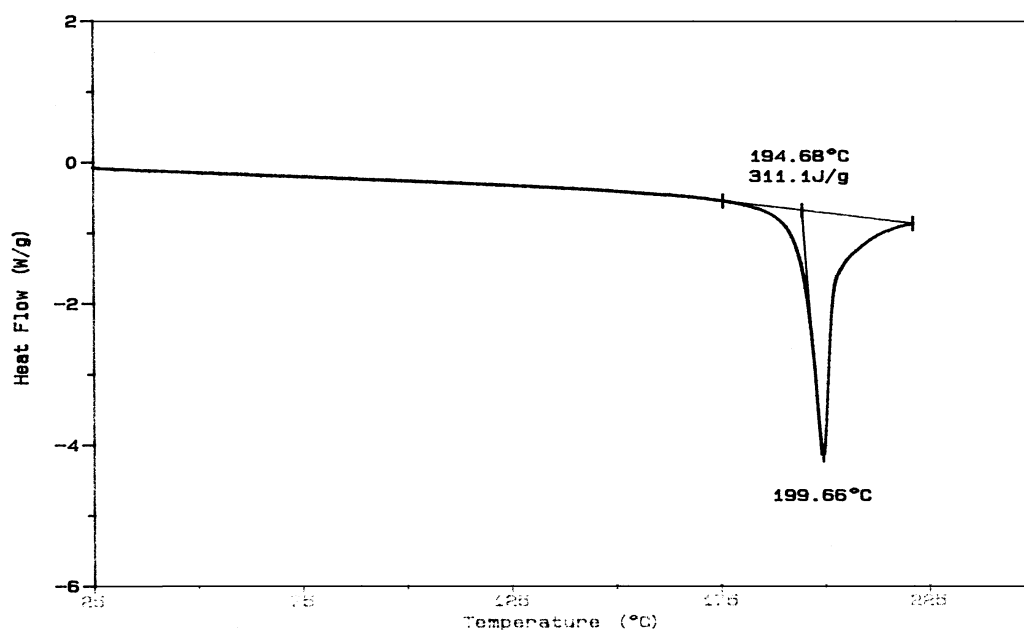


Figure 3.4. DSC thermogram of acryloyloxybenzoic acid

3.1.3. Characterization of p-Methacryloyloxybenzoic Acid

The FTIR spectrum of methacryloyloxybenzoic acid, MBA showed an almost similar spectrum to ABA. The broad bands between 3200-2500- cm^{-1} are due to the carboxylic acid O-H and C-H stretching vibrations. A strong band at 1733 cm^{-1} is characteristic of C=O stretching vibrations of ester group. The strong band at 1682 cm^{-1} was assigned to C=O stretching vibrations of aryl carboxylic acids, the bands at 1605 and 1508 cm^{-1} to C=C stretching vibrations of aromatic compounds. The bands at 806, 944 and 999 cm^{-1} are vinylic C-H out-of-plane bending vibrations, Figure 3.5.

The $^1\text{H-NMR}$ spectrum of MBA shown in Figure 3.6 consists of a singlet at δ 2.1 corresponding to three protons of the CH_3 group, two singlets at δ 5.8 and δ 6.4 corresponding to vinylic protons trans and cis to ester, and two doublets at δ 7.1 and δ 8.1 corresponding to four protons of the C_6H_4 - group..

DSC melting point of MBA was found to be 183.1 $^\circ\text{C}$ in N_2 atmosphere with heating rate of 20 $^\circ\text{C}/\text{min}$ in consistent with the literature⁽⁷⁰⁾, Figure 3.7.

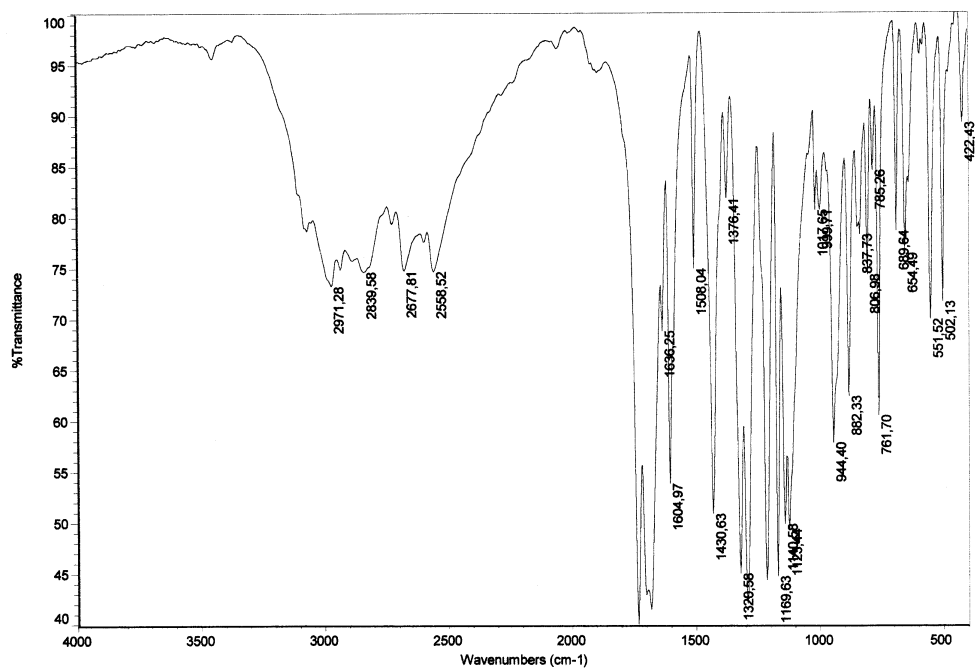


Figure 3.5. FTIR spectrum of methacryloyloxybenzoic acid

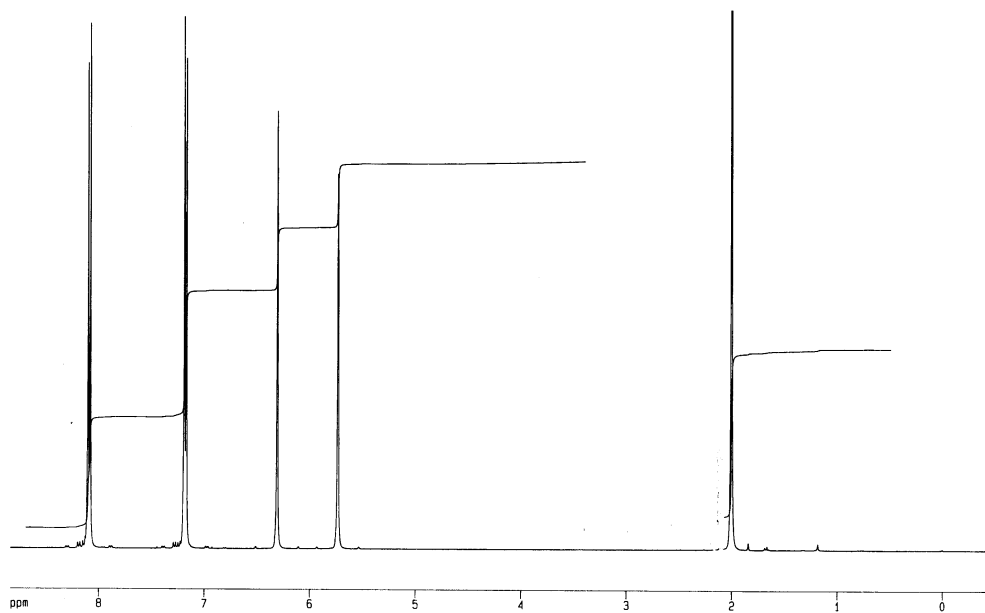


Figure 3.6. ^1H -NMR spectrum of MBA

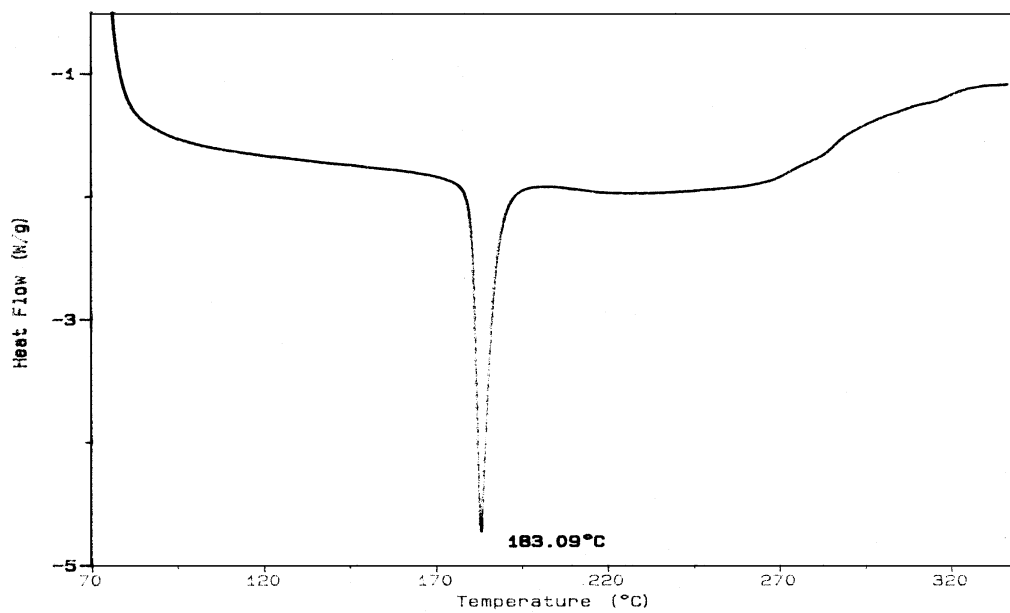


Figure 3.7. DSC thermogram of methacryloyloxybenzoic acid

3.1.4. Characterization of Polyacryloyloxybenzoic Acid, PABA

The $^1\text{H-NMR}$ spectrum of PABA indicates CH_2 protons at δ 2.1, CH protons at δ 3.0, carboxylic OH proton at δ 12.9 and four protons of the C_6H_4 - group at δ 7.1 and δ 7.8. The quartet at δ 6.3 and doublets at δ 6.0 and δ 6.6 corresponding to three protons of vinylic group of ABA disappeared in the $^1\text{H-NMR}$ spectrum of PABA. The peaks observed at δ 3.3 and δ 2.4 are due to protons of DMSO and H_2O . The $^1\text{H-NMR}$ spectra of PABA produced by γ -radiation and DCP are given in Figure 3.8 and 3.9, respectively.

The FTIR spectrum of PABA shows a strong band at 1757 cm^{-1} characteristic of $\text{C}=\text{O}$ stretching vibrations of ester group, a strong band at 1700 cm^{-1} due to $\text{C}=\text{O}$ stretching vibrations of aryl carboxylic acids, a band at 1604 and 1506 cm^{-1} due to $\text{C}=\text{C}$ stretching vibrations of aromatic compounds. The four bands at 800 , 909 , 939 and 987 cm^{-1} observed in the spectrum of ABA due to vinylic C-H out-of-plane bending vibrations disappeared in the spectrum of PABA, Figure 3.10.

Film of PABA was prepared from solution in DMSO cast on PTFE and dried in vacuum. The glass transition temperature and melting point were found as 134°C and 288°C from DSC in N_2 atmosphere with heating rate of $20^\circ\text{C}/\text{min}$, Figure 3.11.

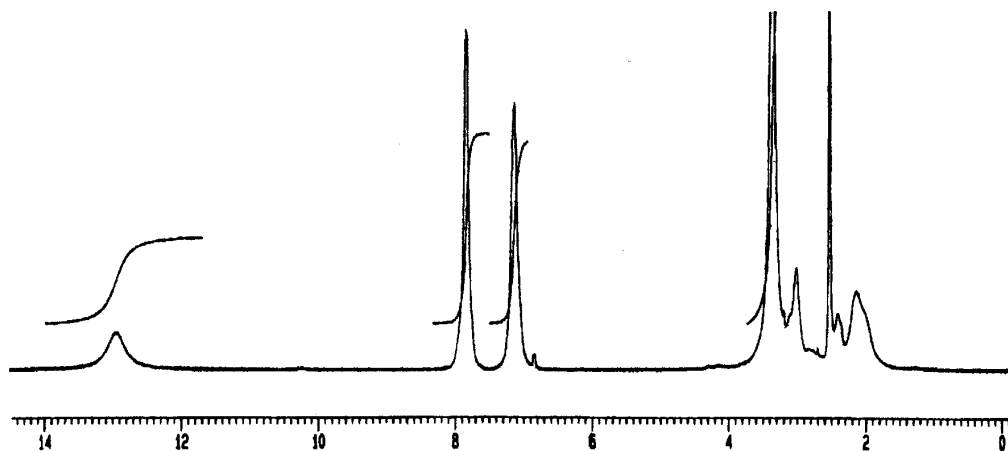


Figure 3.8. $^1\text{H-NMR}$ spectrum of PABA produced by γ -radiation

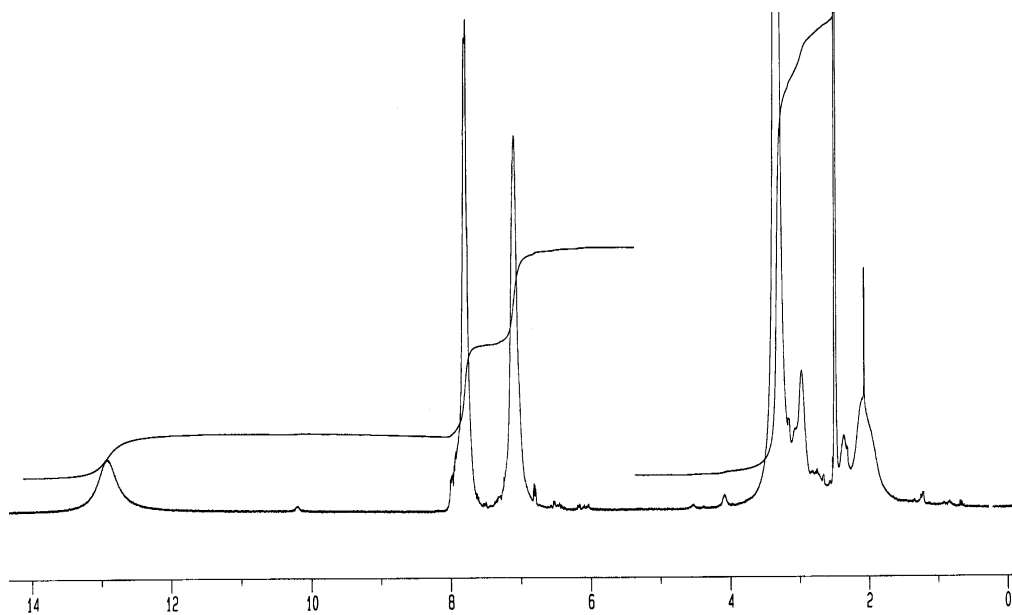


Figure 3.9. ^1H -NMR spectrum of PABA produced by initiation of DCP

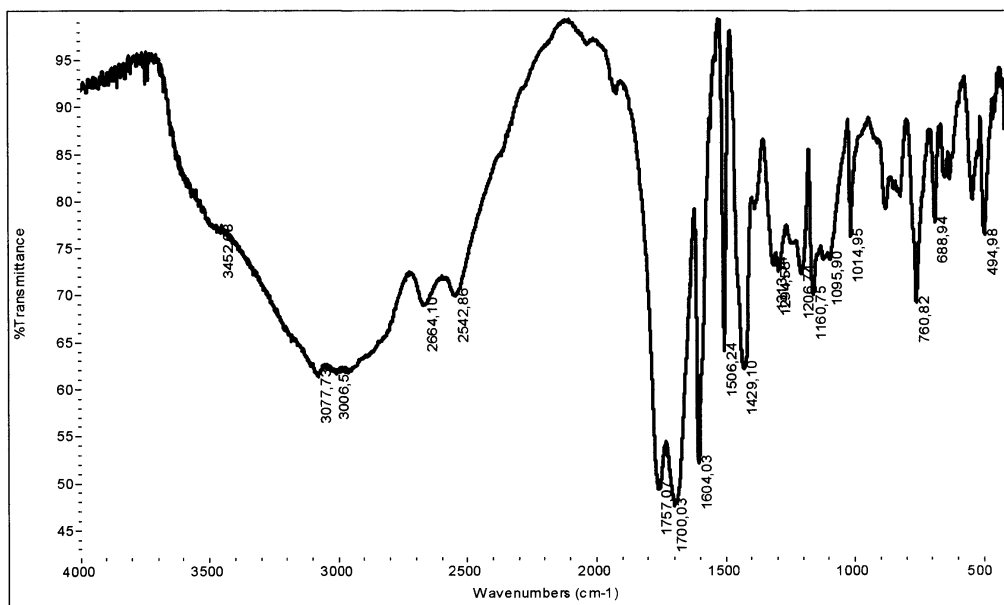


Figure 3.10. FTIR spectrum of PABA produced by γ -radiation

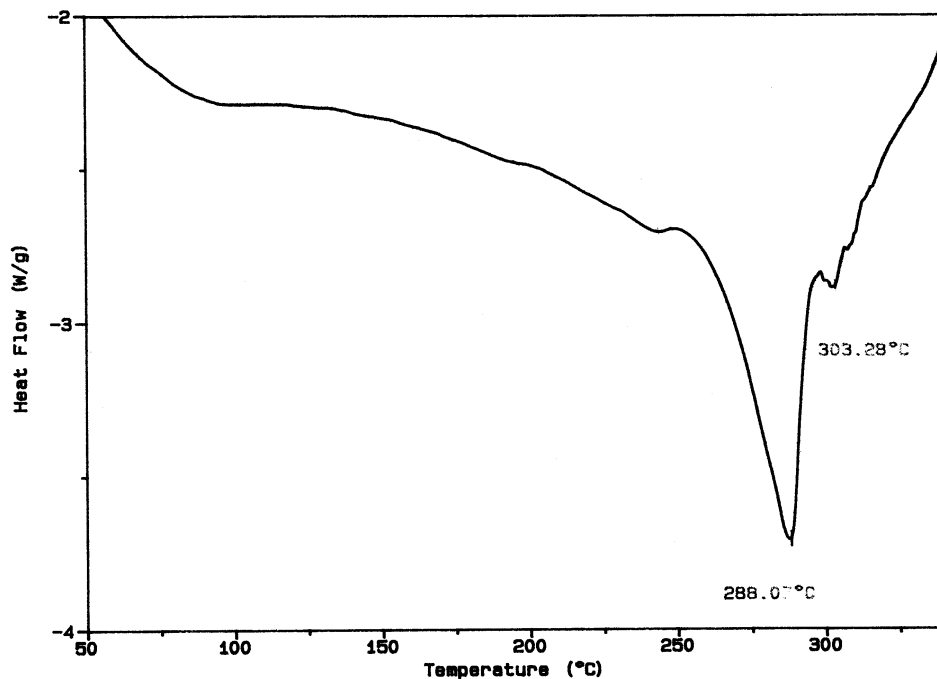


Figure 3.11. DSC thermogram of PABA produced by γ -radiation

3.1.5. Characterization of Polymethacryloyloxybenzoic Acid, PMBA

The $^1\text{H-NMR}$ spectrum of thermally polymerized PMBA indicates CH_2 protons at δ 1.3, CH_3 protons at δ 1.4, carboxylic OH proton at δ 13 and four protons of the C_6H_4 - group at δ 7.2 and δ 7.8. Two singlets at δ 5.8 and δ 6.4 corresponding to vinylic protons trans and cis to ester observed in MBA disappeared in $^1\text{H-NMR}$ spectrum of PMBA. The peaks observed at δ 3.3 and δ 2.5 are due to protons of DMSO and H_2O , Figure 3.12.

The FTIR spectrum of PMBA shows a strong band at 1751 cm^{-1} characteristic of $\text{C}=\text{O}$ stretching vibrations of ester group, a strong band at 1700 cm^{-1} due to $\text{C}=\text{O}$ stretching vibrations of aryl carboxylic acids. The bands at 1604 and 1506 cm^{-1} were assigned to $\text{C}=\text{C}$ stretching vibrations of aromatic compounds. The bands at 806 , 944 and 999 cm^{-1} observed for MBA due to vinylic C-H out-of-plane bending vibrations disappeared in the spectrum of PMBA, Figure 3.13.

Melting point was found as 284°C from DSC in N₂ atmosphere with heating rate of 20°C/min, Figure 3.14.

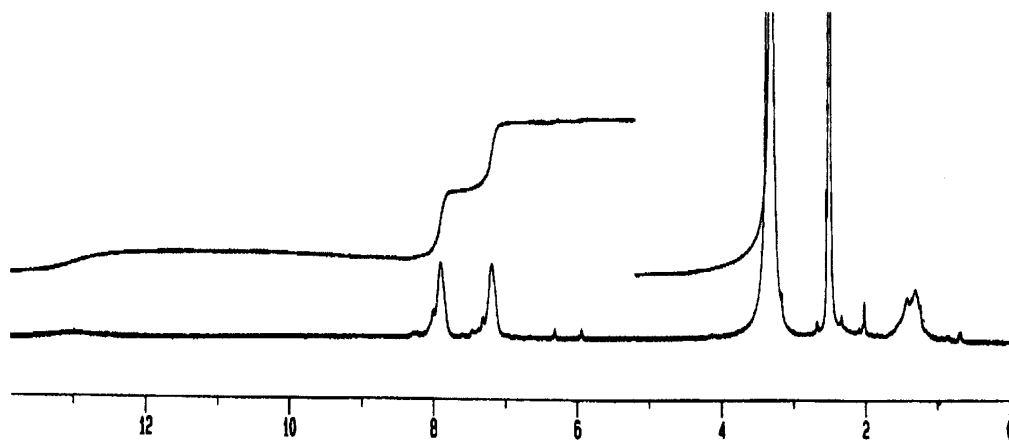


Figure 3.12. ¹H-NMR spectrum of PMBA

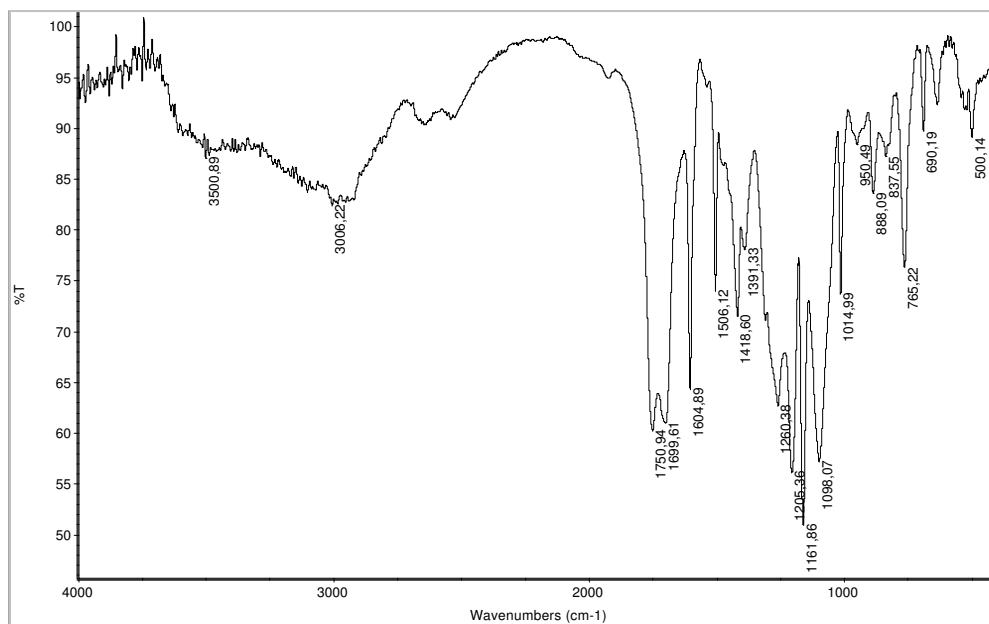


Figure 3.13. FTIR spectrum of PMBA

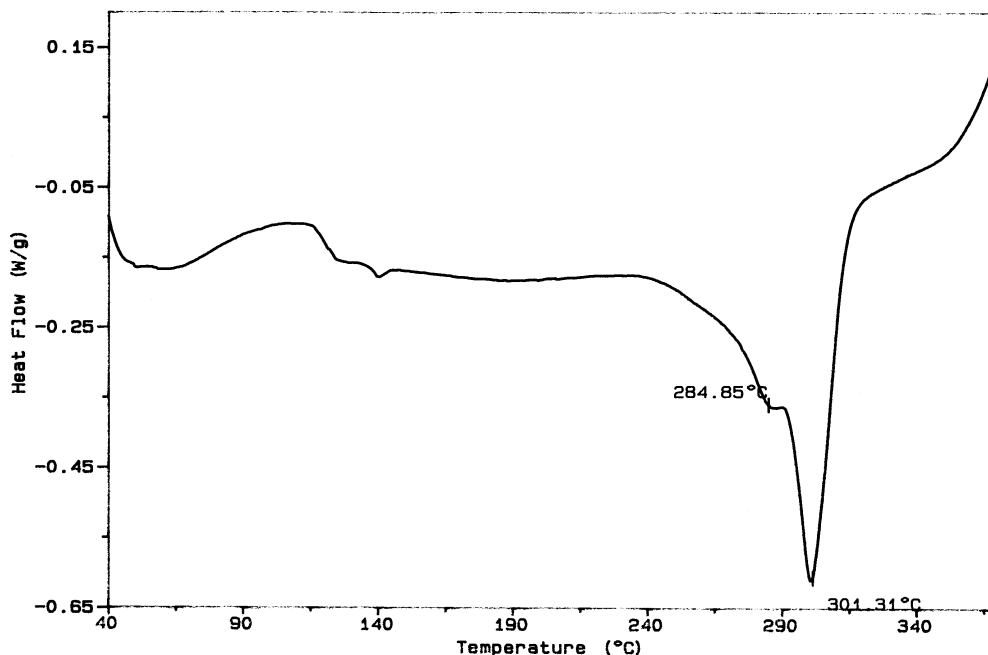


Figure 3.14. DSC thermogram of PMBA

3.2. Graft Copolymerization of ABA onto IPP

Thermally induced graft copolymerization of ABA onto PP was studied in detail. The dependence of content of PABA grafting on reaction temperature and reaction time period was examined at constant concentration of ABA (50 wt.% of mixture), Figure 3.15 and Table 3.1. The extent of grafting reached a maximum value in a shorter time with increasing temperature; for example in 30 minutes at 170°C while in 15 minutes at 202°C reaction temperature. There were almost no changes in the degree of grafting for longer times. This indicated the graft copolymerization reaction proceeds with time and reaches a plateau value after 30 minutes. However, the amount of grafting at high temperatures (185 and 202°C) reaches the maximum (average: 31,9 %) at early times of the reactions. It is important to note that 185°C and higher temperatures are well above the melting point of PP. The molten PP having higher chain mobility induces faster grafting in a shorter time compared to the grafting process at lower temperature (170°C).

Therefore, regarding a controlled degree of grafting, however, one can prefer an experiment at low temperature (170°C) which is a little above the melting point of PP (163°C).

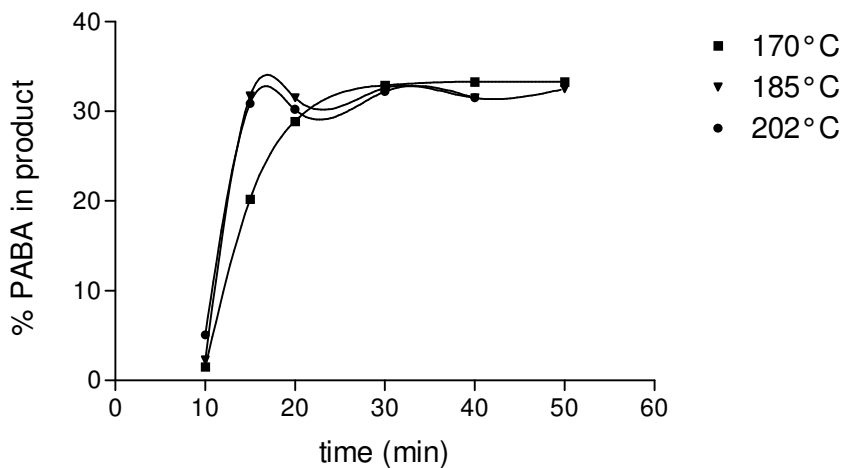


Figure 3.15. The dependence of content of PABA grafted onto PP on reaction temperature and time

Table 3.1. % PABA in products (temperature and time dependence of graft copolymerization of ABA onto PP)

	10 min	15 min	20 min	30 min	40 min	50 min
170°C	1.5	20.2	28.9	32.9	33.3	33.3
185°C	2.3	31.7	31.5	32.6	31.5	32.5
202°C	5.1	30.9	30.2	32.2	31.5	
215°C				30.9		
225°C				31.3		

The graft copolymerization was also carried out in the presence of dicumyl peroxide at 170°C for 40 minutes, and a product with the degree of grafting of 23,8 % PABA was obtained. The decrease observed in the amount of grafting is probably due to the direct reactions between the peroxides formed on the PP with γ -irradiation and dicumyl peroxide, in addition homopolymerization of ABA initiated by dicumyl peroxide.

The variation of grafting upon changing the mixing ratio of irradiated PP and monomer ABA was also studied at 170°C for 40 minutes reaction time. It was observed that the amount of grafting increased with increasing concentration of ABA in reaction medium, Table 3.2 and Figure 3.16.

Table 3.2. The dependence of content of PABA grafted onto PP on concentration of ABA in reaction mixture

% ABA in rxn. mixture	15	25	33	50	66	75
% PABA in products	7.13	16.3	21.6	33.3	43.3	57.0

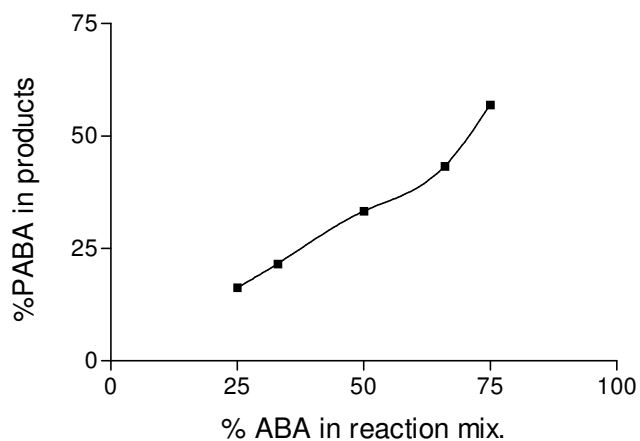


Figure 3.16. The dependence of content of PABA grafted onto PP on concentration of ABA in reaction mixture

3.2.1. Characterization of PABA-g-PP

FTIR analysis of the products confirmed the graft copolymerization of ABA onto PP. The characteristic absorption bands of PABA due to aromatic, carbonyl and carboxylic groups and of the aliphatic groups due to PP and main chain of PABA were also observed in the FTIR spectra of the graft coproducts. No absorption bands at 800, 909, 939 and 987 cm^{-1} were seen in the spectra, of which monomer ABA had, Figure 17.

Because of insolubility of the graft coproducts, PABA-g-PP in any solvent NMR analysis could not be carried out.

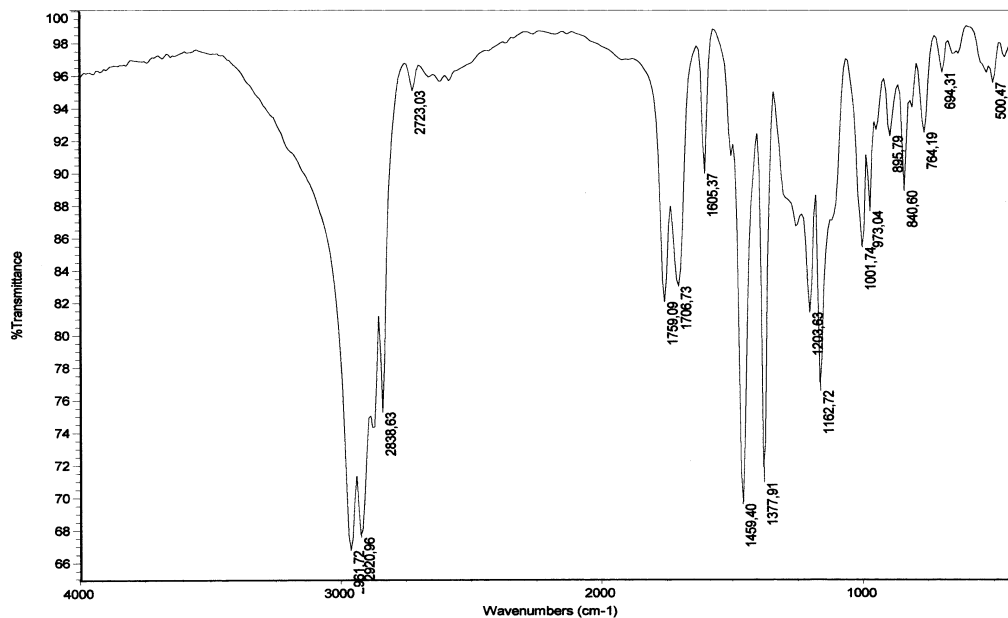


Figure 3.17. FTIR spectrum of PABA-g-PP produced at 170°C for 40 minutes reaction time

3.3. Graft Copolymerization of MBA onto IPP

The dependence of content of PMBA grafted on reaction temperature and reaction time period was examined at constant concentration of MBA (50 wt.% of mixture), Table 3.3. The content of PMBA grafted on PP increased with time up to 40 minutes at 170°C, 20 minutes at 185 and 15 minutes at 202 °C. There were almost no changes in the degree of grafting indicating the completion of the graft copolymerization reactions after longer reaction times. The effect of temperature is that the higher mobility of molten PP chains lead higher grafting at high temperatures (185 and 202°C) to reach the maximum (average: 24,3 %) at early times of the reactions, Figure 3.18.

Table 3.3. % PMBA in products (temperature and time dependence of graft copolymerization of MBA onto PP)

	10 min	15 min	20 min	30 min	40 min	50 min
170°C	3.2	11.5	15.8	20.8	22.5	25.8
185°C	15.0	20.6	24.7	25.6	24.2	25.3
202°C	21.6	22.7	24.1	25.4	24.3	24.8
215°C				27.3		
225°C				33.9		

The graft copolymerization was also tried in the presence of dicumyl peroxide at 170°C for 40 minutes, and a product with the degree of grafting of 20.5 % PMBA was obtained. The amount of grafting decreased probably owing to the direct reactions between the peroxides formed on the PP with γ -irradiation and dicumyl peroxide, and also homopolymerization of MBA initiated by dicumyl peroxide instead of grafting gives rise to a decrease in the degree of grafting.

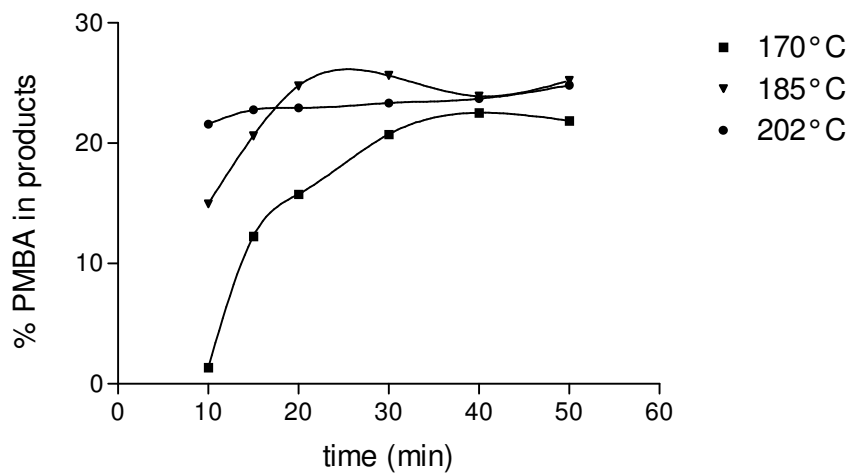


Figure 3.18. The dependence of content of PMBA grafted onto PP on reaction temperature and time

The variation of grafting upon changing the mixing ratio of irradiated PP and monomer MBA was also studied at 170°C for 40 minutes reaction time. It was observed that the amount of grafting increased with increasing concentration of MBA in reaction medium, Table 3.4 and Figure 3.19.

Table 3.4. The dependence of content of PMBA grafted onto PP on the concentration of MBA in reaction mixture

% MBA in rxn. mixture	25	33	50	66	75
% PMBA in products	14.6	18.2	25.2	29.6	30.7

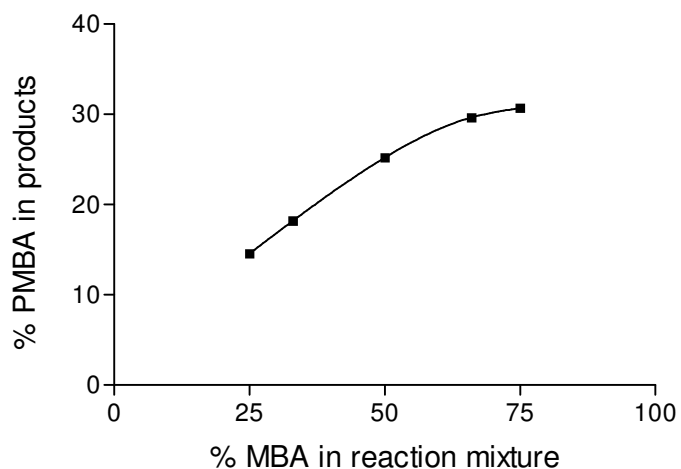


Figure 3.19. The dependence of content of PMBA grafted onto PP on concentration of MBA in reaction mixture

3.3.1. Characterization of PMBA-g-PP

The graft copolymerization of MBA onto PP was also confirmed by FTIR analysis. The characteristic absorption bands of PMBA due to aromatic, carbonyl and carboxylic groups and of the aliphatic groups due to PP and main chain of PABA were also observed in the FTIR spectra. The bands at 800, 909, 939 and 987 cm^{-1} observed in the spectrum of MBA due to vinylic group were also disappeared in the spectra of graft copolymers as it was observed in polymerization of MBA, Figure 3.20.

Similar to PABA-g-PP samples because of insolubility of the graft coproducts, PMBA-g-PP in any solvent NMR analysis could not be carried out.

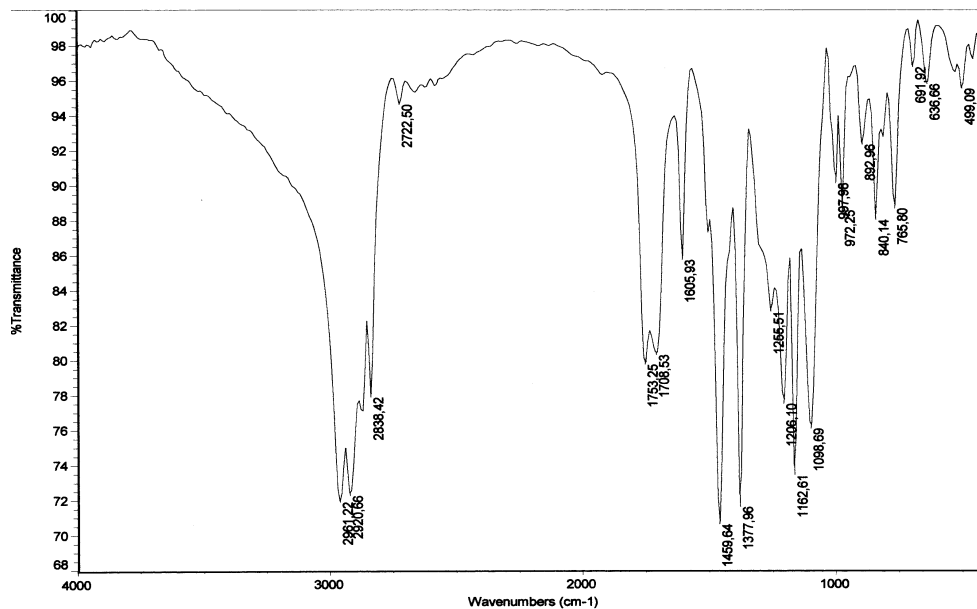


Figure 3.20. FTIR spectrum of PMBA-g-PP produced at 170°C for 40 minutes reaction time

3.4. Characterization of PABA-g-PP by DSC and X-Ray

In order to find out the effect of graft copolymerization of ABA onto IPP on the thermal and crystallization behavior of the graft coproducts PABA-g-PP samples were analyzed by differential scanning calorimetry, DSC and by wide angle x-ray diffraction, WAX. The isotactic polypropylene used in the graft copolymerization experiments was in the α form (monoclinic), determined by WAX experiments which showed five reflections at spacing of 6.33, 5.26, 4.79, 4.23 and 4.08 Å, with the melting point of 162.85°C, Figure 3.21 and 3.22. This agrees well with the other works^(4,78).

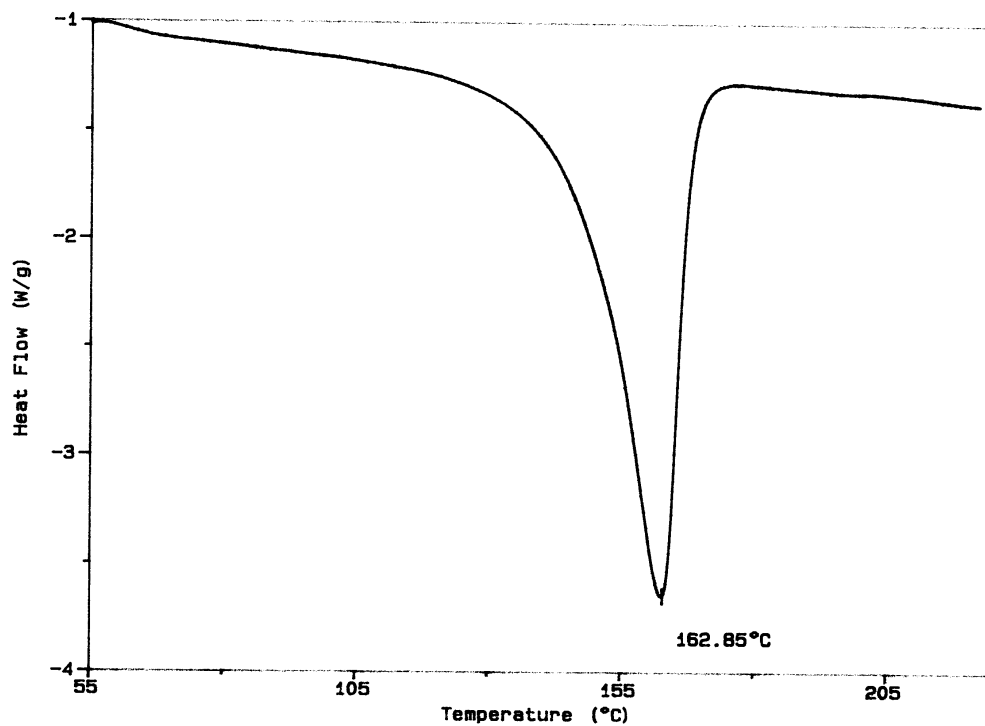


Figure 3.21. DSC thermogram of IPP (10 kGy irradiated)

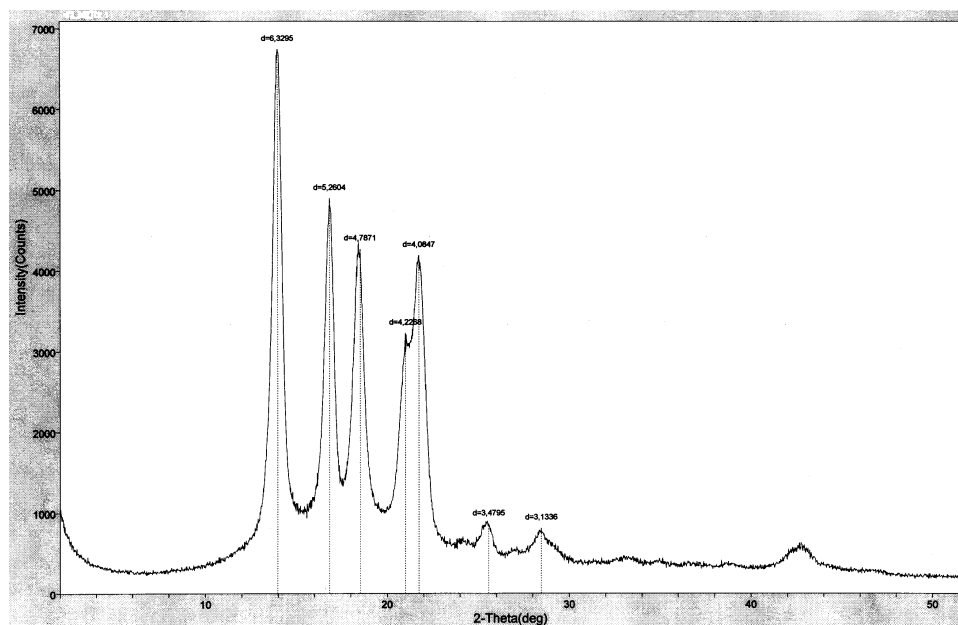


Figure 3.22. X-ray spectrum of irradiated IPP

It was reported that isotactic polypropylene, even if it shows the presence of only the α form by x-ray diffraction, may exhibit two melting endotherms in DSC⁽⁷⁹⁾. The crystalline structure of the α form may show various degrees of disorder in the up and down positioning of the chains as a consequence of different thermal and mechanical histories of the samples, while the unit cell and the ordered disposition in it remain substantially unchanged⁽⁶⁾. Two limiting structures were postulated for the α form⁽⁷⁹⁾: a disordered limiting structure (α_1) with a random distribution of up and down chains in each site of the unit cell, the corresponding crystallographic symmetry being $C2/c$ ⁽⁸⁰⁾ and an ordered limiting structure (α_2) having crystallographic symmetry $P2_1/c$ ⁽⁸⁰⁾, with a well-defined disposition of up and down helices in the unit cell. Guerra et al.⁽⁷⁹⁾ observed that when isotactic PP samples were annealed for 5 minutes above 160°C DSC scans begin to show occurrence of a double peak. Analogous phenomena were also described by Pae and Sauer⁽⁸¹⁾. With sufficiently long annealing times it was obtained DSC curves showing only one melting endotherm, probably completing the crystallization at temperatures above 160°C. They concluded, for the two melting endothermic peaks which are observed at low heating rates with DSC on disordered samples of isotactic PP (α form), that the first peak is related to the melting of crystals having a structure nearer to that of the α_1 modification and the second one is related to the melting of crystals having a structure nearer to that of the α_2 modification⁽⁷⁹⁾.

In the first run of DSC studies of PABA-g-PP samples, the similar double melting peak corresponding to the two limiting structures of α form were observed in low percent of PABA (16.3 and 21.9 % PABA) obtained at 170°C with the reaction time of 40 minutes, Table 3.5 and also in the product obtained with the reaction time of 20 minutes (28.9 % PABA), Figure 3.23.a, b and c and 3.24, as only the x-ray diffraction pattern of α form was observed despite occurrence of double melting peaks in the thermograms of the products. The first melting peak was at about 160°C, probably corresponding to the disordered limiting structure (α_1 form), and the second melting peak was observed at and above 171°C, probably having ordered limiting structure (α_2 form). In the other products obtained at 170°C the observed single melting points at about and below 160°C correspond to α_1 modification.

Table 3.5. DSC results with PABA percentages in products (1st run:30-230°C with 20°C/min; cooling with 2°C/min; 2nd run: 30-350°C with 20°C/min), (Italic numbers show % PABA in products, the stars with superscript, * and **, show melting points of PP in first and second runs)

% ABA in rxn. mixture	25	33	50	66	75
% PABA in grafting at 170°C for 40 minutes rxn time	<i>16.3</i>	<i>21.9</i>	<i>33.3</i>	<i>39.1</i>	<i>57.0</i>
	160.7*	159.4 ¹ *	156.8*	157.2*	157.4*
	174.6*	174.0*			
	132.8**	158.7**	152.2**	156.2**	156.9**

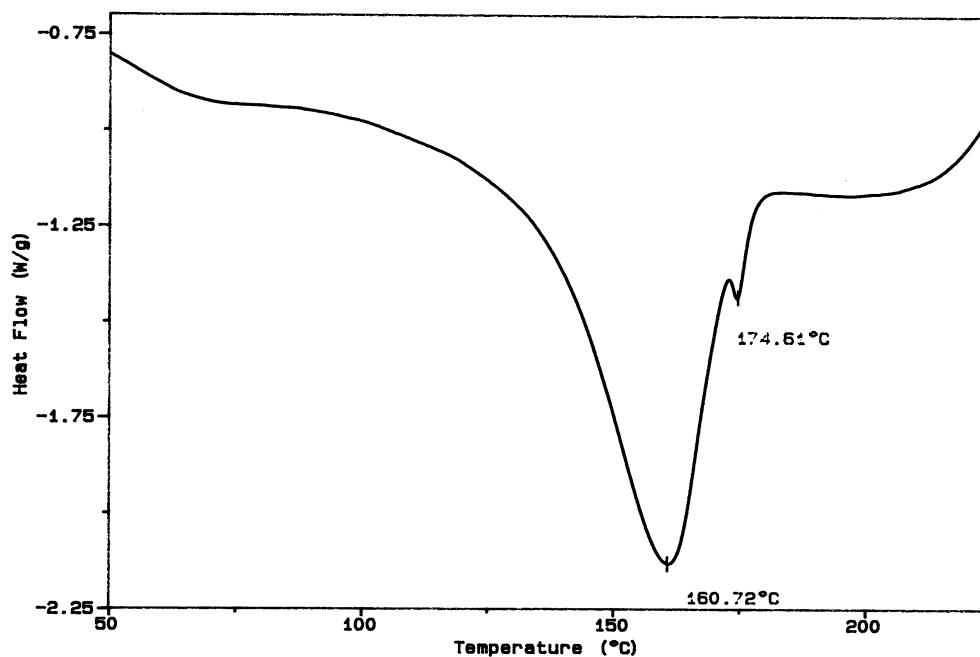
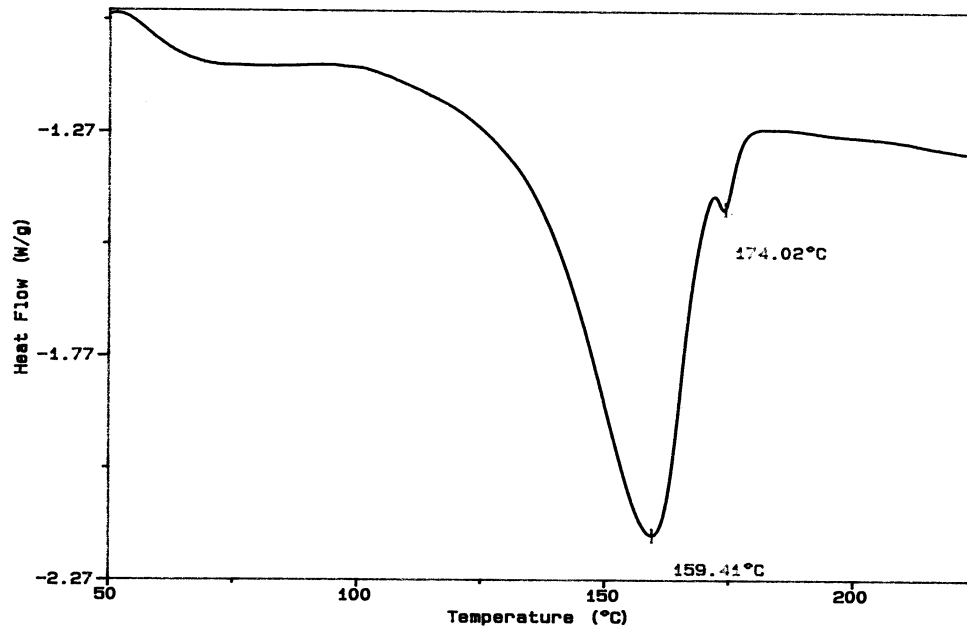


Figure 3.23.a) DSC thermogram of PABA-g-PP produced at 170°C containing 16.3% PABA

b)



c)

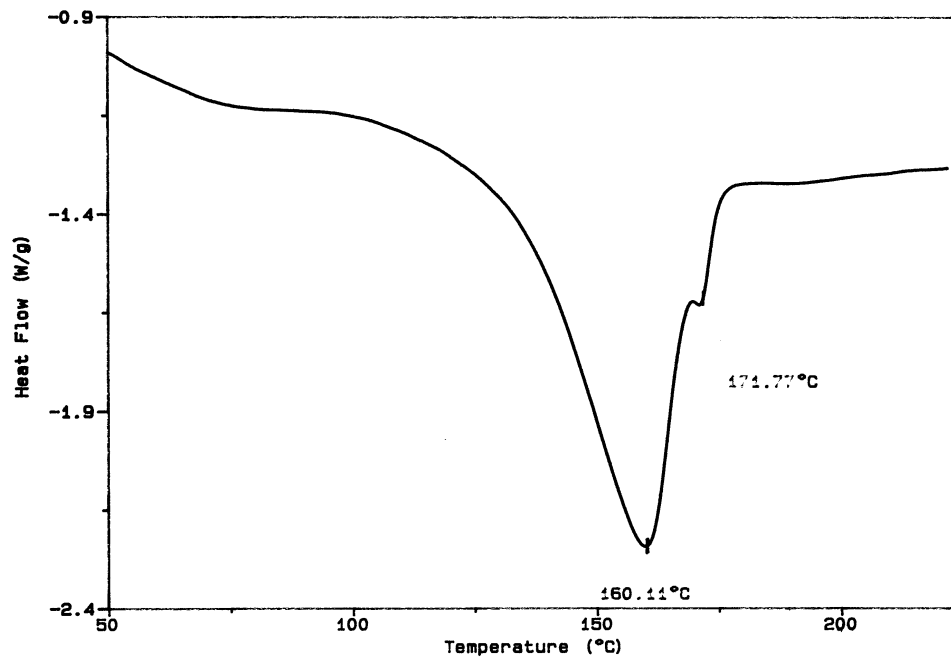


Figure 3.23. DSC thermograms of PABA-g-PP produced at 170°C containing b) 21.9% PABA, and c) 28.9% PABA

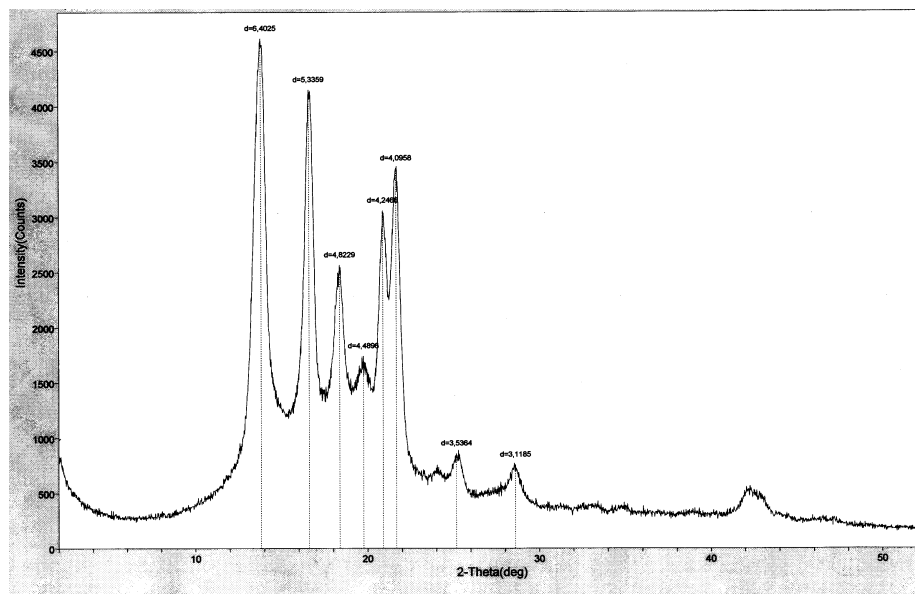


Figure 3.24. X-ray spectrum of PABA-g-PP (16.3% PABA)

On the other hand, formation of β form (hexagonal) has been shown through rapid quenching⁽⁷⁾, zone solidification^(14,15), crystallization in a temperature gradient^(16,17,82,83). It was reported that α form is thermodynamically more stable^(7,84), and β type crystals do transform into α form by a melting and recrystallization process⁽⁷⁾. The nucleation of β form occurs much more rarely in a bulk sample than that of the α form⁽¹⁴⁾, and in most cases, the β form can only be partially formed in samples mixed with other crystal forms⁽⁸⁵⁾. Padden and Keith⁽⁸⁴⁾ could observe β form only sporadically with the growth between 128°C and 132°C. Turner-Jones et al.⁽⁷⁾ produced β form by quenching the molten samples very rapidly to below 130°C, and investigated the efficiency of the quenching conditions. It was found that up to quench temperature of 90°C, the α form was formed predominantly, at 100-120°C β form was formed predominantly and above 130°C the α form only. They studied the effect of varying temperature of the melt by quenching the melts at 100°C and it was found that β form was formed when the polymer was quenched from the melt temperatures of 190 to 230°C. They proposed that in the polypropylenes, where β form was formed predominantly, the rate of nucleation and/or growth of the α form

was inherently slower than in the other polypropylenes examined, so that α -form nucleation did not have time to occur in the time required to pass through the temperature range from the melting point to below 130°C, and alternatively it is possible that the polymer has an inherently higher β form nucleation rate. The transformation of the β form into the α form can also be carried out by melt recrystallization at elevated temperature close to the melting temperature of bulk samples⁽¹⁴⁾. The conversion is very rapid at 150°C and at lower temperatures it proceeds more slowly reaching a limiting value at each temperature.

The formation of β form in PABA-g-PP samples was observed as a mixture with α form with the reflection of 5.59 Å from WAX studies in the products obtained above 170°C and in the second runs of DSC studies when fast cooling was performed with the rate of 20°C/min, Figure 3.25.a and b, 3.26.a and b, and 3.27. In slow cooling with the rate of 2°C/min, however, the β form disappeared giving only α form as crystalline phase, Figure 3.28.

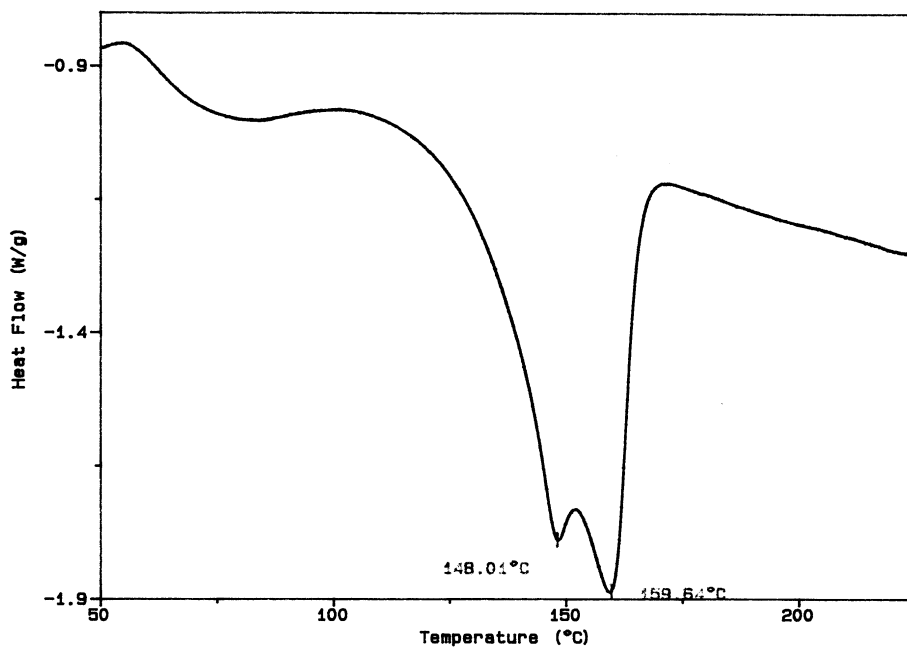


Figure 3.25.a) DSC thermogram of PABA-g-PP produced at 185°C with the reaction time of 40 minutes (31.9% PABA)

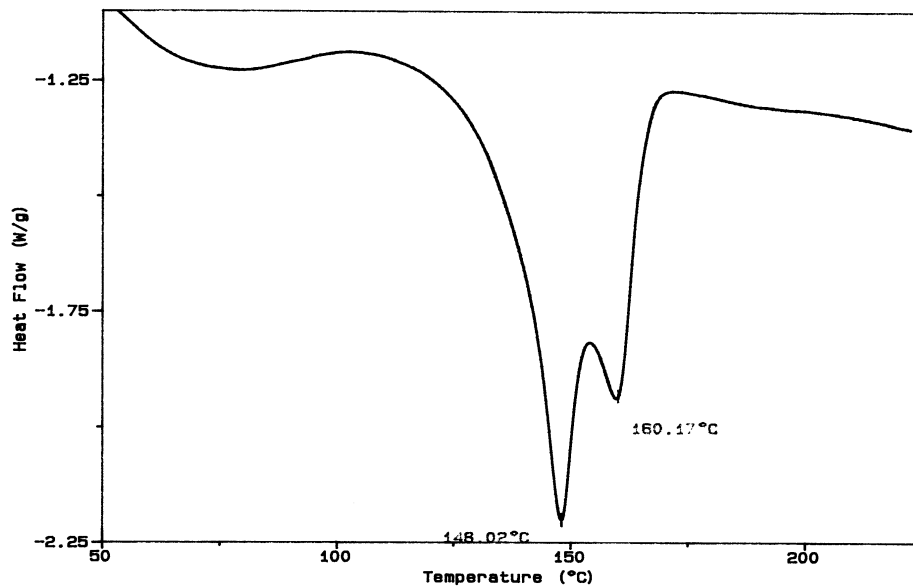


Figure 3.25.b) DSC thermogram of PABA-g-PP produced at 202°C with the reaction time of 40 minutes (31.5% PABA)

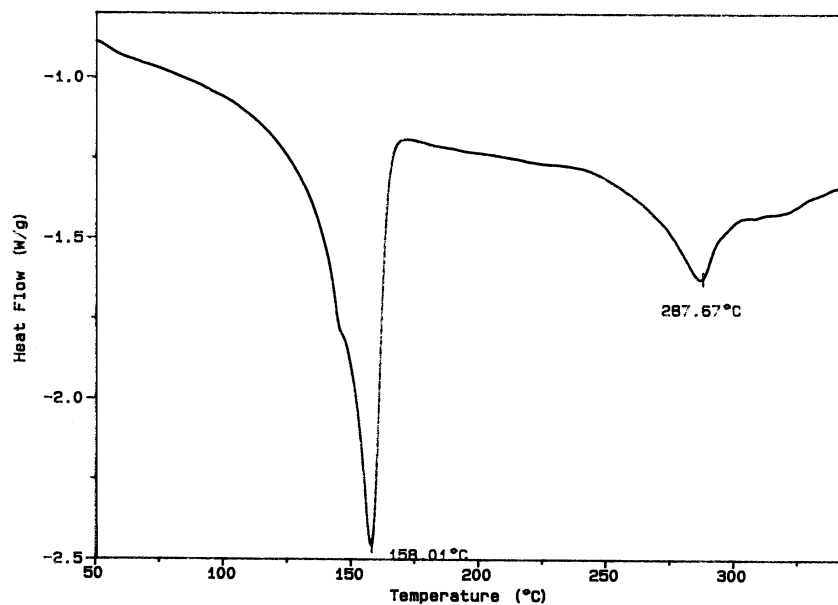


Figure 3.26.a) Second run DSC thermogram of PABA-g-PP produced at 170°C with the reaction time of 15 minutes (20.2% PABA) taken after cooling with the rate of 20°C/min

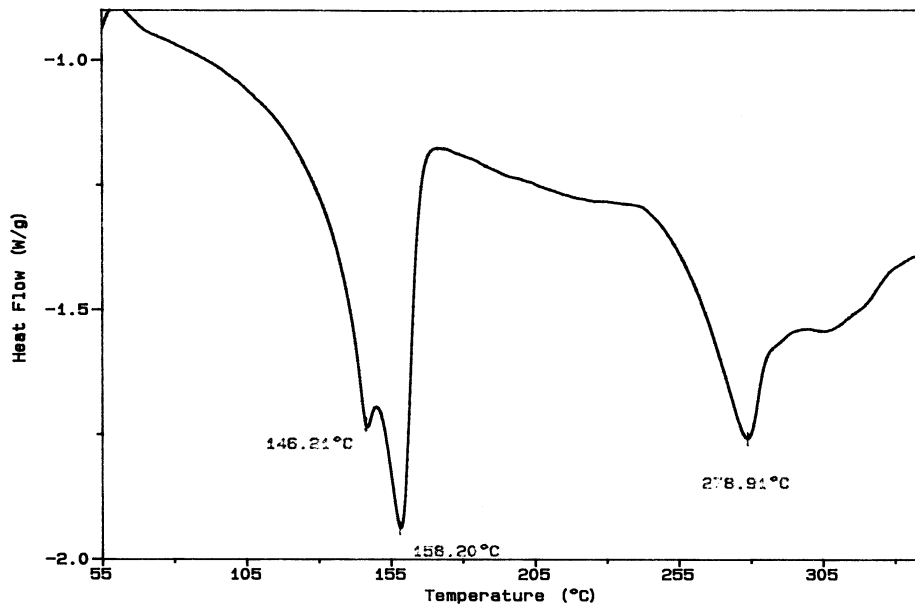


Figure 3.26.b) Second run DSC thermogram of PABA-g-PP produced at 185°C with the reaction time of 40 minutes (31.9% PABA) after cooling with the rate of 20°C/min

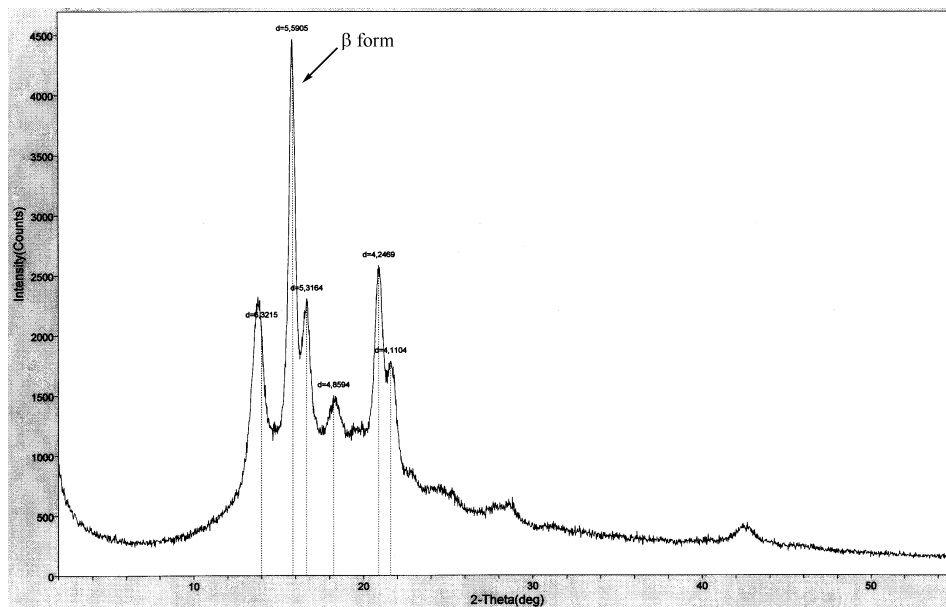


Figure 3.27. X-ray spectrum of PABA-g-PP produced at 202°C with the reaction time of 30 minutes (32.2% PABA)

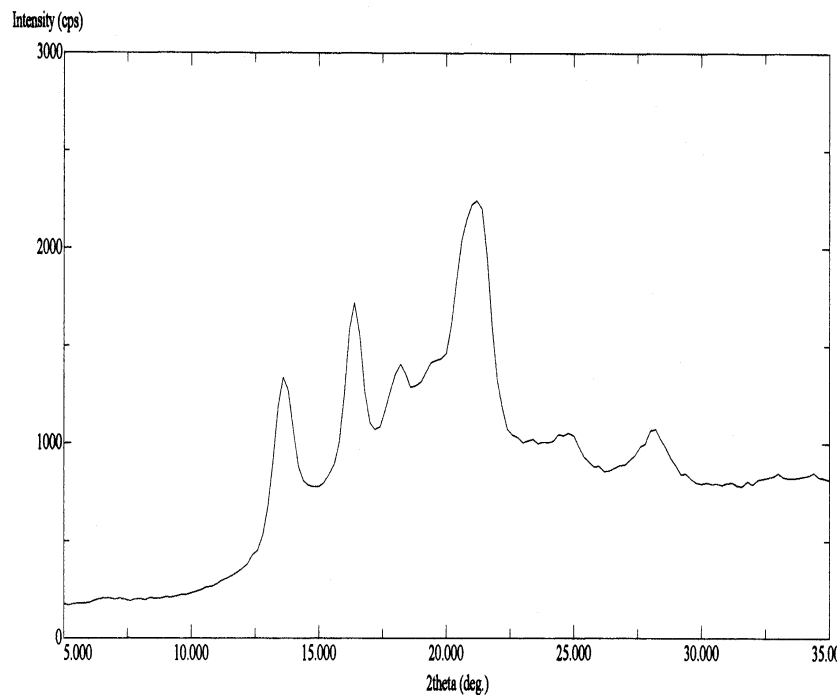


Figure 3.28. X-ray spectrum of PABA-g-PP produced at 185°C with the reaction time of 40 minutes (31.5% PABA) taken after heating the sample to 230°C and cooling to room temperature with the rate of 2°C/min

In the first run of DSC studies of the products obtained with the reaction time of 10 minutes at 170°C the melting point of PP (162.5°C) which includes very low amount of PABA (1.5%) is very close to the melting point of pure PP, and it is probably in α_1 form. The melting points, observed at 168.5 and 172.2 °C, of the products obtained with the reaction time of 15 and 20 minutes, containing 20.2 and 28.9 % of PABA, probably correspond to α_2 form. The other melting points observed between 160 and 157 °C are presumably in α_1 form, Table 3.6.

Table 3.6. DSC results with PABA percentages in products (1st run: 30-230°C with 20°C/min; cooling with 20°C/min; 2nd run: 30-350°C with 20°C/min) (italic numbers show % PABA in products, the stars with superscript, * and **, show melting points of PP in first and second runs)

	10 min	15 min	20 min	30 min	40 min	50 min
170°C	<i>1.5</i>	<i>20.2</i>	<i>28.9</i>	<i>32.9</i>	<i>33.3</i>	<i>33.3</i>
	162.5*	168.5*	160.0* 172.2*	157.8*	158.1*	157.9*
	158.45**	144.38** 158.01**	144.2** 156.1**	144.7** 156.9**	146.2** 158.2**	146.1** 157.9**
185°C	<i>2.3</i>	<i>31.7</i>	<i>31.5</i>	<i>32.6</i>	<i>31.9</i>	<i>32.5</i>
	151.1*	147.6*	147.7*	146.9*	148.0*	147.8*
	162.6*	159.2*	158.5*	158.8*	159.6*	159.6*
	158.9**	146.6** 159.1**	146.1** 158.8**	146.5** 158.6**	147.0** 159.2**	146.3** 158.5**
202°C	<i>5.1</i>	<i>30.9</i>	<i>30.2</i>	<i>32.2</i>	<i>31.5</i>	
	164.9*	148.0*	147.7*	146.9*	148.0*	
		160.0*	159.7*	159.6*	160.2*	
	158.2**	146.9** 159.2**	146.9** 159.5**	146.7** 159.0**	147.2** 160.2**	

In the second runs with fast cooling of 20°C/min in the products of the reaction time of 10 minutes, which contained very small amount of PABA grafted (1.5%), there was no change in the crystal form where only a single melting peak was observed at 158.4°C. In the other products α form was observed between 156.1 and 158.2°C, Table 3.6. β form started to form in the grafted polymers obtained in 15 minutes and was observed as a shoulder at 144°C on the endotherm of α form. This

formation of β form became more distinct and prominent as the reaction time increased and in the products of 40 and 50 minutes it was observed as a separate peak at about 146°C, Figure 3.26.a and 3.29, although there was no considerable difference in the PABA percents between 30 and 40 minutes, 32.9% and 33.3%, respectively.

Jacoby et al.⁽⁸⁶⁾ observed the melting of β form PP at 148°C and the melting of α form at 160°C, where the thermograms were obtained at a rate of 20°C/min. Lovinger et. al.⁽¹⁴⁾ reported the melting endotherms of various zone solidified samples of PP taken at a heating rate of 10°C/min that the lower endotherm around 152°C corresponds to the β phase while the higher ones in the region of 167°C are the melting curves for the α spherulites.

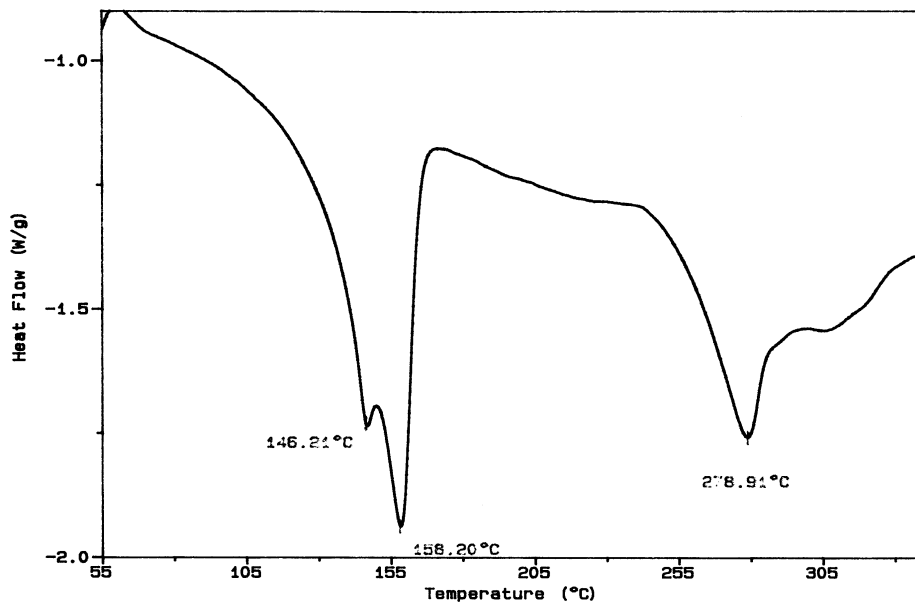


Figure 3.29. Second run DSC thermogram of PABA-g-PP produced at 170°C with the reaction time of 40 minutes (33.3% PABA) after cooling with the rate of 20°C/min

When cooling was performed with the rate of 2°C/min, in the second runs, there is no evidence corresponding to the formation of β form, Figure 3.30. On the other hand, the melting points which belong to the melting of α form are very improper and devious, and with respect to those of that when cooling was performed with the rate of 20°C/min they are lower with changing between 155.8 and 150.1°C, except for 161.1°C, T_m of the product of 10 minutes with the very low percent of PABA (1.5%) is very close to the melting point of pure IPP, Table 3.7. It may be concluded that when fast cooling was performed with the rate of 20°C/min formation of β form is observed since it grows with expedition with respect to α form, when it is nucleated, and the melting of α form is observed clearly within the narrow temperature range. In slow cooling with the rate of 2°C/min more stable α form is formed, however, in spite of this slow cooling the formed α form crystals are not developed perfectly and faultlessly, then very devious and improper meltings were observed.

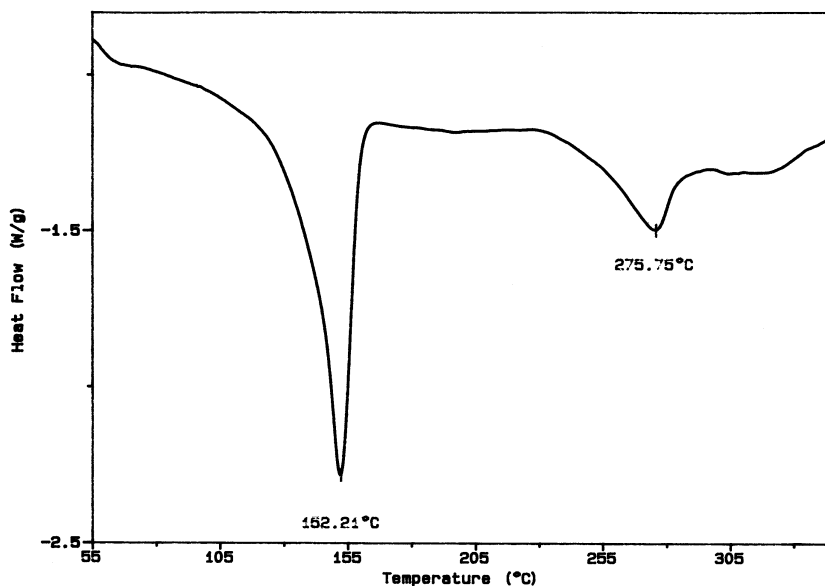


Figure 3.30. Second run DSC thermogram of PABA-g-PP produced at 170°C with the reaction time of 40 minutes (33.3% PABA) after cooling with the rate of 2°C/min)

Table 3.7. DSC results with PABA percentages in products (1st run: 30-230°C with 20°C/min; cooling with 2°C/min; 2nd run: 30-350°C with 20°C/min), (Italic numbers show % PABA in products, the stars with superscript, * and **, show melting points of PP in first and second runs)

	10 min	15 min	20 min	30 min	40 min	50 min
170°C	<i>1.5</i> 162.9* 161.1**	<i>20.2</i> 169.2* 154.9**	<i>28.9</i> 160.1* 171.8* 150.9**	<i>32.9</i> 158.7* 155.8**	<i>33.3</i> 156.8* 152.2**	<i>33.3</i> 158.9* 150.2**
185°C	<i>2.3</i> 151.1* 162.6* 161.2**	<i>31.7</i> 147.4* 159.6* 156.7**	<i>31.5</i> 147.7* 158.9* 153.5**	<i>32.6</i> 147.8* 159.2* 155.9**	<i>31.5</i> 147.3* 158.8* 150.5**	<i>32.5</i> 147.6* 159.3* 136.4**
202°C	<i>5.1</i> 164.6* 154.7**	<i>30.9</i> 148.5* 160.7* 138.1**	<i>30.2</i> 148.6* 160.0* 156.5**	<i>32.2</i> 147.0* 159.5* 140.1**	<i>31.5</i> 148.3* 160.5* 147.4**	
215°C				<i>31.7</i> 147.8* 160.9* 156.8**		

In 185°C grafting process the melting of α form is observed between 158.5 and 159.6°C. The observed disagreeing temperature of 162.6°C, which is very close to the melting point of pure IPP, belongs to the product involving very low percent of PABA (2.3%). In contrast to the products obtained at 170°C, the formation of β form which was seen in the first runs of DSC, Table 3.6 and Figure 3.25.a and 3.31 was observed in all products. The products obtained with the reaction time of 10 minutes containing very low percent of PABA (2.3%) showed the melting corresponding to the β form. However, there was a very weak shoulder at 151.1°C on the melting peak of α form. Increasing the reaction time between 15 and 30 minutes, the shoulder corresponding to the β form gets more distinctive and noticeable, where the meltings were observed between 146.9 and 147.7°C. The β form was observed as separate peaks in the reaction time of 40 and 50 minutes where the corresponding meltings were observed at 148.0 and 147.8°C, respectively, Figure 3.25.a and 3.32. As the reaction time increases through 40 and 50 minutes, it seemed that β form crystals got more regular and ordered. In the second runs of fast cooling with the rate of 20°C/min in DSC β form detected on the product of 10 minutes reaction time in the first run disappeared, probably due to the transformation to the α form. In the other products, as the reaction time increases starting from 15 minutes β form appeared between 146.1 and 147.0°C more sharply and distinctly with respect to those in the first runs. The melting points of α form, like in the first runs, were seen between 158.2 and 159.2°C. β form observed in the first runs and in the second runs taken with fast cooling disappeared in the second runs of slow cooling, Figure 3.28, due to the transformation to the more stable α form. The melting points of α form, however, are not uniform, changing between 150.5 and 156.7°C, Table 3.7. It may be concluded that in the second runs of slow cooling of 2°C/min β form transforms to α form, but, the formed α crystals are not ordered perfectly, since the divergence in the melting points was observed. The similar fashion was seen in the products obtained at 170°C.

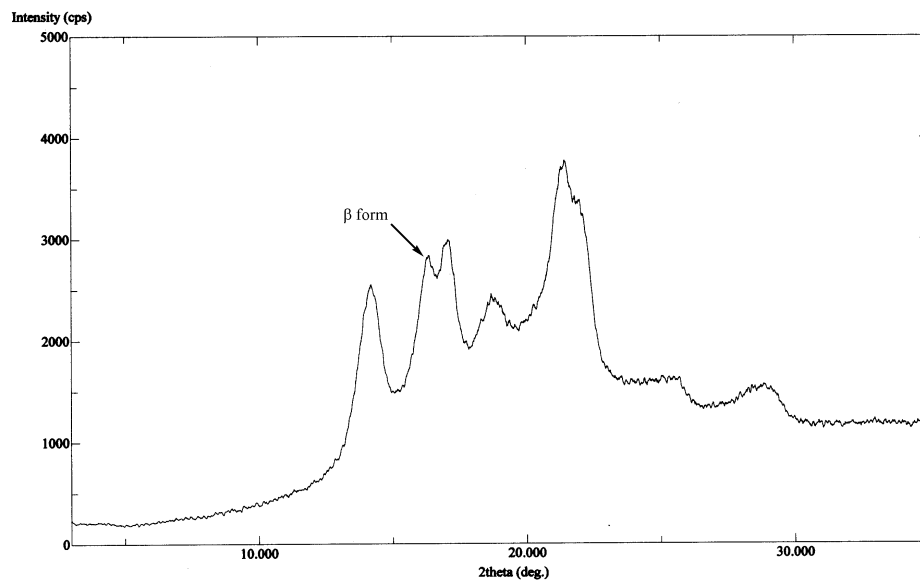


Figure 3.31. X-ray spectrum of PABA-g-PP produced at 185°C with the reaction time of 40 minutes (31.5% PABA)

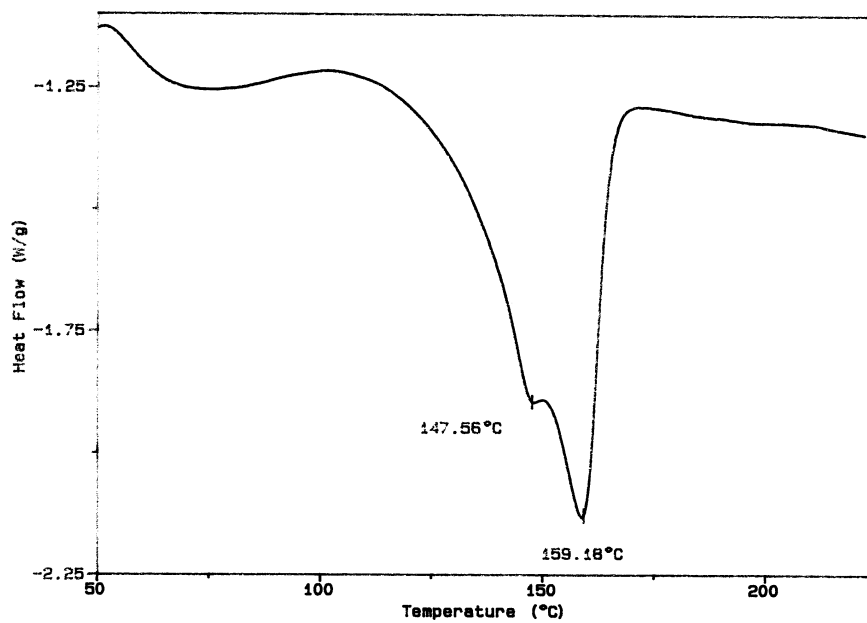


Figure 3.32. DSC thermogram of PABA-g-PP produced at 185°C with the reaction time of 15 minutes (31.7% PABA)

In the products obtained at 202°C similar to those obtained at 185°C in the first DSC runs β form was observed in all products except for the products of 10 minutes reaction time, where only α form was detected at 164.9°C, comprised of very low percent of PABA (5.1%) . In the other products the melting points of α form was between 159.6 and 160.1°C. The melting points which belong to β form was seen between 146.9 and 148.0°C, Table 3.6. The melting peaks corresponding to the β form are more distinct and prominent with respect to those of samples produced at 185°C. It may be concluded that as the reaction temperature increases from 185 to 202°C the formation of β form crystals increases, Figure 3.25.b and 3.32. This consequence was also evident from the x-ray spectra where the peak corresponding to β form at the spacing of 5.59 Å increased and became more distinct, Figure 3.27 and 3.31. In the second runs when cooling was performed quickly with the rate of 20°C/min, again β form was observed similar to the experience of the products of 185°C. However, in the second runs, the formation of β form was observed nearly as shoulder on the melting peak of α form, although they were detected as separate peaks in the first runs, Figure 3.33. Furthermore, β form was not detected in the slow cooled runs with the rate of 2°C/min in DSC due to the transformation to the α form, 3.34 and 3.35. The observed melting points corresponding to the melting of α form, however, varied between 138.1 and 156.5°C leading to a conclusion that the formed α form crystals are not ordered perfectly Table 3.6 and 3.7.

In the product obtained at 215°C the similar formation of β phase was observed, and the results almost were the same as 202°C reaction temperature.

In order to clarify the effect of graft copolymerization, i.e., the presence of PABA, on the formation of α and β form virgin IPP samples were heated to 170, 185 and 202°C keeping the temperature constant for 30 minutes as it was carried out in the graft copolymerization experiments. A double melting of 165.6 and 176.1°C was also observed in virgin PP which was kept in melt state at 170°C for 30 minutes. These melting points are apparently attributed to α_1 and α_2 crystalline forms. In the experiments at 185 and 202°C, the meltings were detected at 159.3 and 161.2°C, respectively, obviously due to melting of α_1 form, Figure 3.36 and 3.37

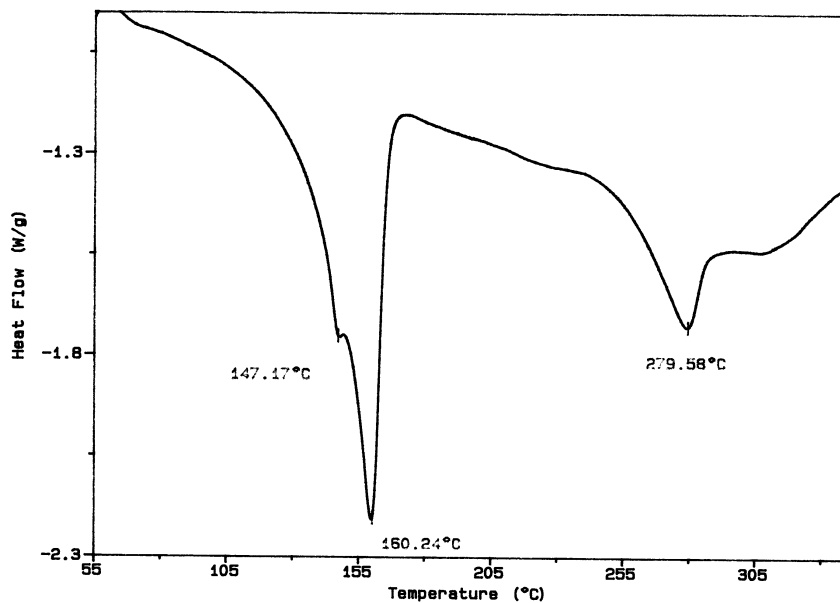


Figure 3.33. Second run DSC thermogram of PABA-g-PP produced at 202°C with the reaction time of 40 minutes (31.5% PABA) after cooling with the rate of 20°C/min)

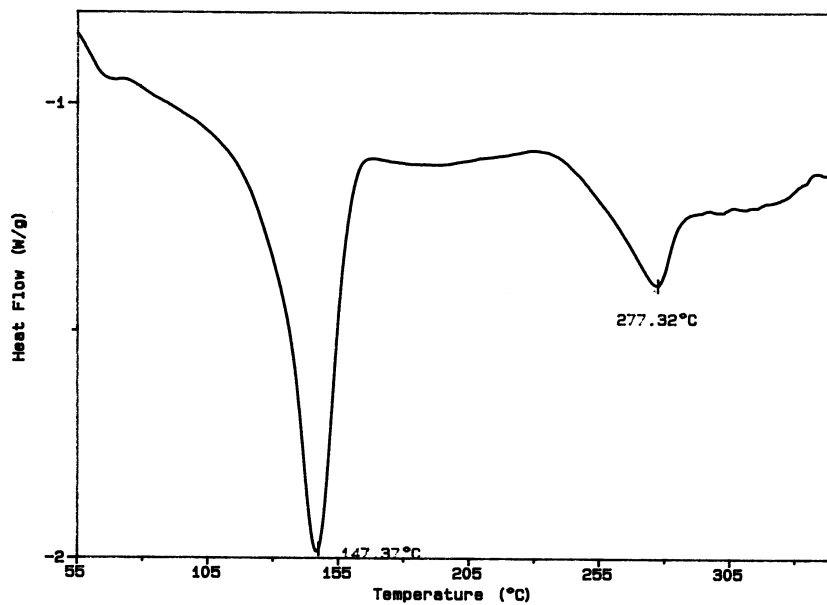


Figure 3.34. Second run DSC thermogram of PABA-g-PP produced at 202°C with the reaction time of 40 minutes (31.5% PABA) after cooling with the rate of 2°C/min)

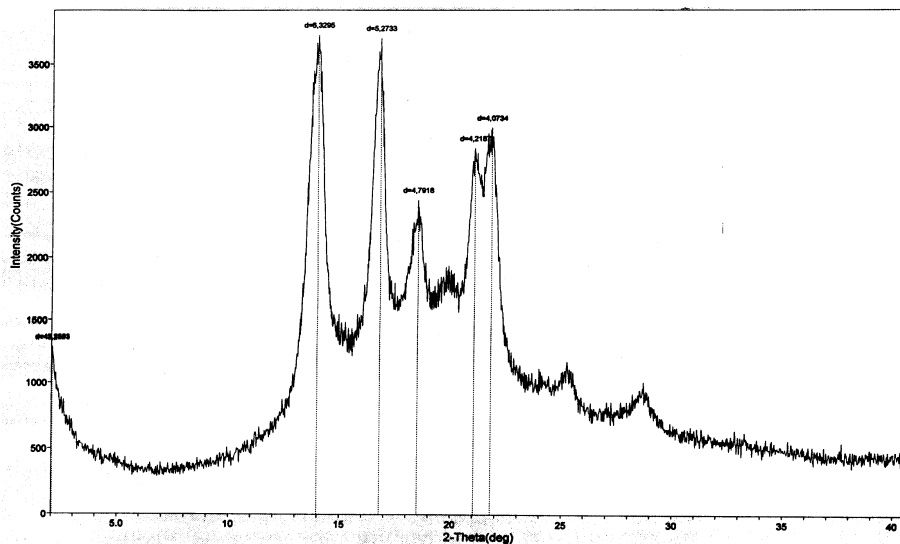


Figure 3.35. X-ray spectrum of PABA-g-PP produced at 202°C with the reaction time of 30 minutes (32.2% PABA) taken after heating the sample to 230°C and cooling to room temperature with the rate of 2°C/min

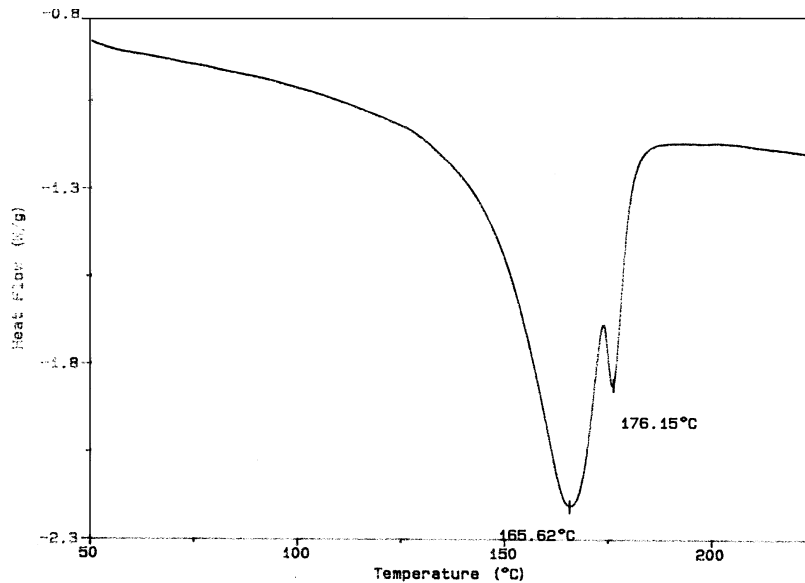


Figure 3.36. DSC thermogram of IPP (heated to 170°C keeping constant for 30 minutes)

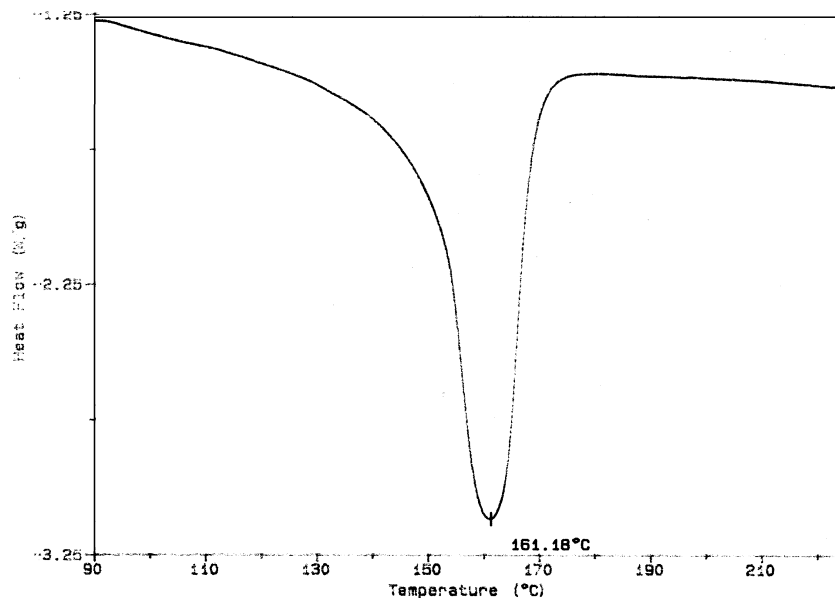


Figure 3.37. DSC thermogram of IPP (heated to 202°C keeping the temperature constant for 30 minutes)

Conclusively, we can state that the crystallization of PP units in both α_1 and α_2 modifications in the graft form were not affected with the presence of grafting units of PABA. On the other hand, the presence of PABA caused the formation of β form in the graft coproducts obtained at 185°C and at higher temperatures. PABA also leads to the formation of β form in the second run of DSC studies when fast cooling were performed with the rate of 20°C/min.

Finally, the crystalline melting of PABA was observed between 275 and 287°C in all graft coproducts, Figure 3.26.a and b, 3.29 and 3.33. PABA was indexed to monoclinic unit cell by Blumstein et. al⁽⁷⁰⁾. One of the reflections reported at the spacing of 4.47 Å corresponding to the monoclinic cell was also observed in the x-ray spectrum of the graft coproducts, Figure 3.24 and 3.35. However, the other diffraction peaks noted, 3.71 and 3.08 Å, overlapped with the peaks of IPP, and they could hardly state that these diffraction peaks arose from either of IPP or PABA units.

3.5. Characterization of PMBA-g-PP by DSC and X-Ray

The thermal properties and crystallization behavior of PMBA-g-PP samples were also studied by DSC and WAX in order to find out the effect of graft copolymerization of MBA onto PP. DSC analysis were also carried out as double runs, and all second runs performed after slow cooling of 2°C/min.

In the first run of DSC studies the double melting peak corresponding to the two crystalline forms of α form were observed in PMBA-g-PP samples produced at 170°C with the reaction time of 20, 30 and 40 minutes, comprised of 16.7, 18.8 and 19.8 % PMBA, respectively Table 3.8 and Figure 3.38 and 3.39. In addition, the samples containing 18.2, 19.8, and 30.7% PMBA, produced at 170°C with 40 minutes reaction time were shown in Table 3.9. The probable melting peaks of the α_1 form were observed between 161.4 and 163.8°C, and those melting points presumably corresponding to α_2 form were observed between 170.7 and 175.1°C. The α_2 form was observed either as a weak shoulder or small peak in thermograms of PABA-g-PP and in some of the PMBA-g-PP samples α_2 peak was detected as prominent and sharp peak next to the melting endotherm of α_1 form in 30 minutes reaction time, Figure 3.39. Furthermore, the single melting point of 50 minutes product, 170.7°C presumably belong to α_2 form, Figure 3.40. In the samples of 10 and 40 minutes reaction time products the melting points at 149.0 and 151.0°C which were observed as a very weak shoulder on the endotherm of α form may be attributed to the melting of β form. However, any characteristic peak of β form could not be detected on the x-ray spectra of that samples other than the diffraction peaks of α form probably owing to the overlapping of the peaks, Figure 3.41.

Table 3.8. DSC results with PMBA percentages in products (1st run:30-230°C with 20°C/min; cooling with 2°C/min; 2nd run: 30-350°C with 20°C/min), (italic numbers show % PMBA in products, superscript stars, * and ** show melting points of PP in the first and second runs).

	10 min	15 min	20 min	30 min	40 min	50 min
170°C	<i>3.8</i> 149.0* 163.8* 161.5**	<i>10.2</i> 163.1* 133.0** 152.8**	<i>16.7</i> 162.7* 174.4* 147.1**	<i>18.8</i> 161.4* 173.9* 150.7**	<i>19.8</i> 151.0* 162.0* 175.1* 149.5**	<i>17.9</i> 170.7* 143.6**
185°C	<i>12.3</i> 143.2* 162.8* 150.0**	<i>19.7</i> 161.2* 142.8**	<i>24.6</i> 161.6* 156.9**	<i>24.4</i> 149.0* 162.5* 154.1**	<i>24.6</i> 161.2* 156.5**	<i>24.2</i> 161.1* 157.7**
202°C	<i>22.6</i> 151.7* 161.6* 157.6**	<i>23.9</i> 161.1* 157.0**	<i>24.1</i> 160.5* 155.4**	<i>25.4</i> 161.5* 153.6**	<i>24.3</i> 161.2* 142.8**	<i>27.0</i> 159.9* 149.3**
215°C				<i>27.3</i> 160.8* 157.6**		
225°C				<i>33.9</i> 146.5* 161.0* 156.3**		

Table 3.9. DSC results with PMBA percentages in products (1st run:30-230°C with 20°C/min; cooling with 2°C/min; 2nd run: 30-350°C with 20°C/min), (*italic numbers show % PMBA in products, superscript stars, * and ** show melting points of PP in the first and second runs*).

% MBA in rxn. mixture	25	33	50	66	75
% PMBA in grafting at 170°C for 40 minutes rxn time	<i>14.6</i>	<i>18.2</i>	<i>19.8</i>	<i>29.6</i>	<i>30.7</i>
	162.5*	162.2*	151.0*	160.6*	160.3*
	153.8*	175.1*	162.0*	150.4**	174.8*
		153.2**	175.1*		150.7**
			149.5**		

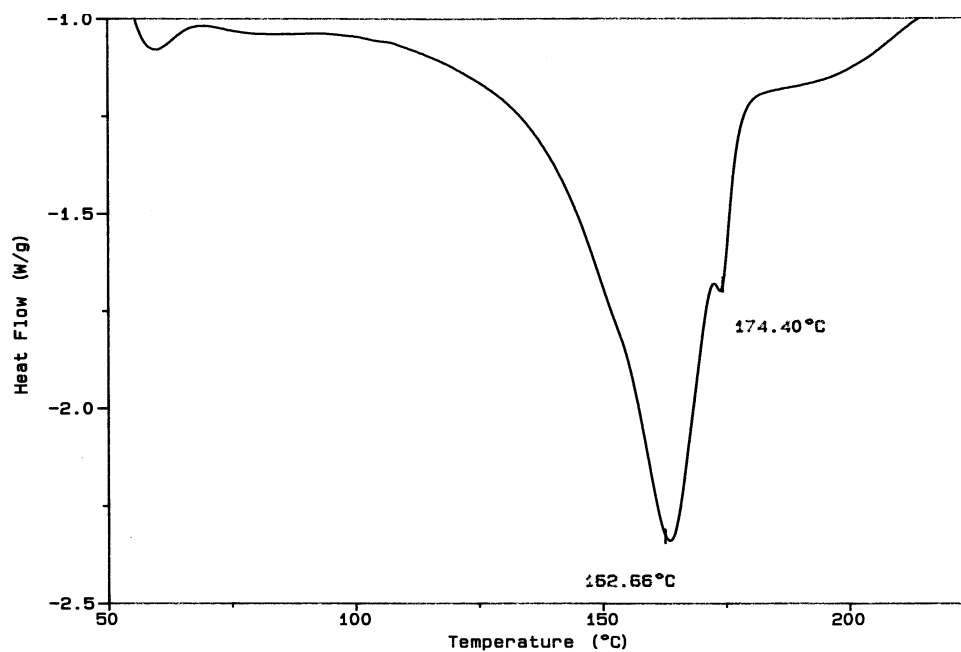


Figure 3.38. DSC thermogram of PMBA-g-PP produced at 170°C with the reaction time 20 minutes (16.7% PMBA)

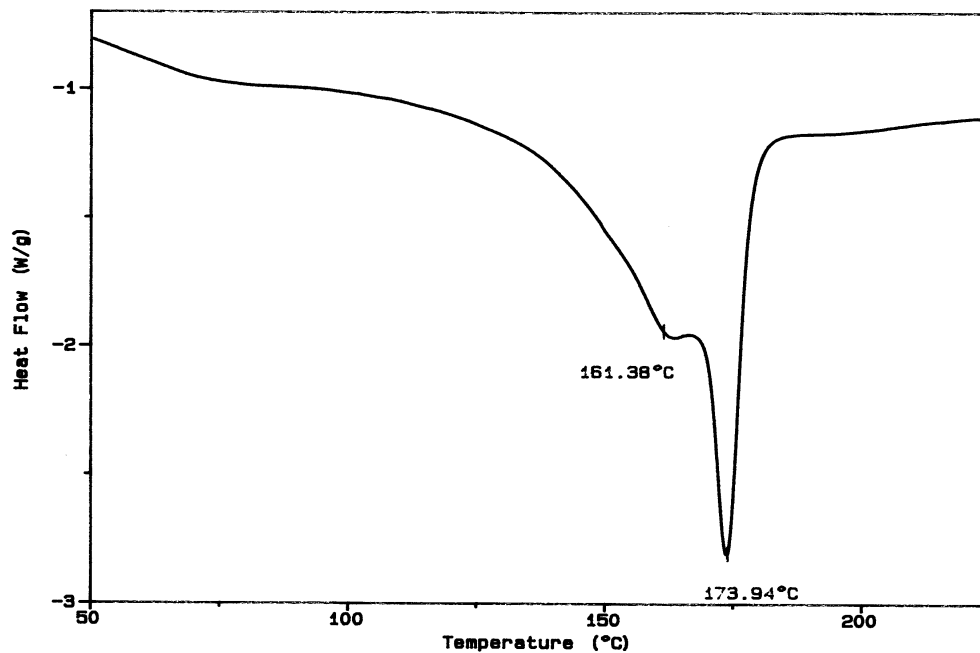


Figure 3.39. DSC thermogram of PMBA-g-PP produced at 170°C with the reaction time 30 minutes (18.8% PMBA)

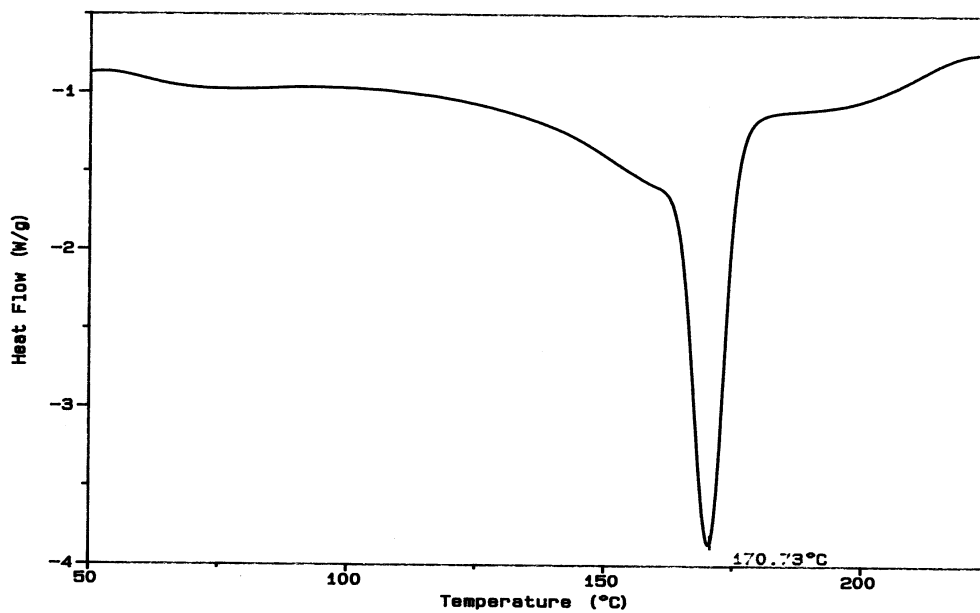


Figure 3.40. DSC thermogram of PMBA-g-PP produced at 170°C with the reaction time of 50 minutes (17.9% PMBA)

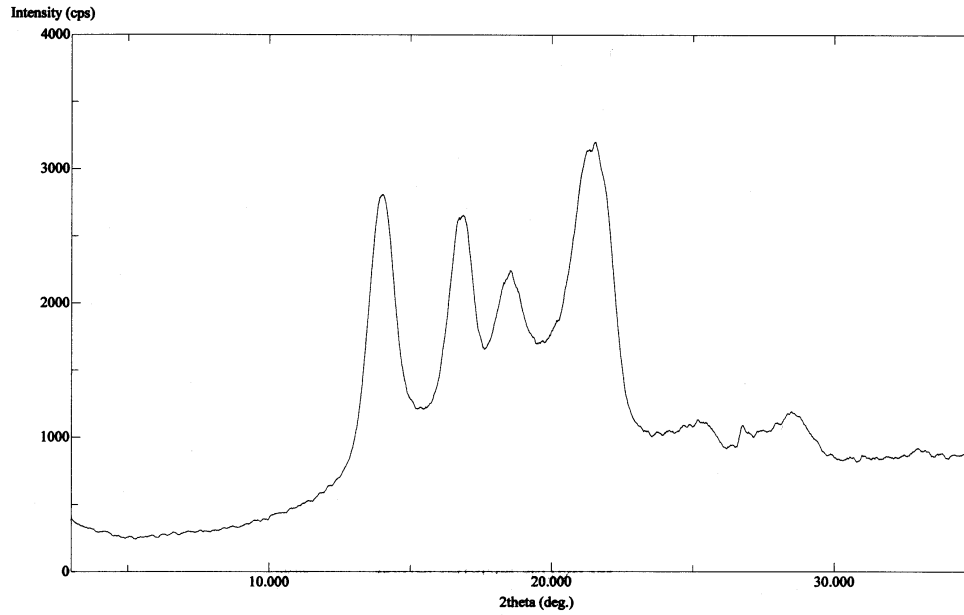


Figure 3.41. X-ray spectrum of PMBA-g-PP produced at 170°C with the reaction time of 40 minutes

In the second runs after slow cooling with the rate of 2°C/min there was no considerable difference in the melting point of the sample contained very low percent of PMBA (3.8%). In the other products large decreases were observed in the melting points with improper and devious constitution, and they were perceived between 133.0 and 152.8°C. The melting peak at 133.0°C of 15 minutes product was detected as a very weak shoulder on the melting endotherm of α form, Figure 3.42.

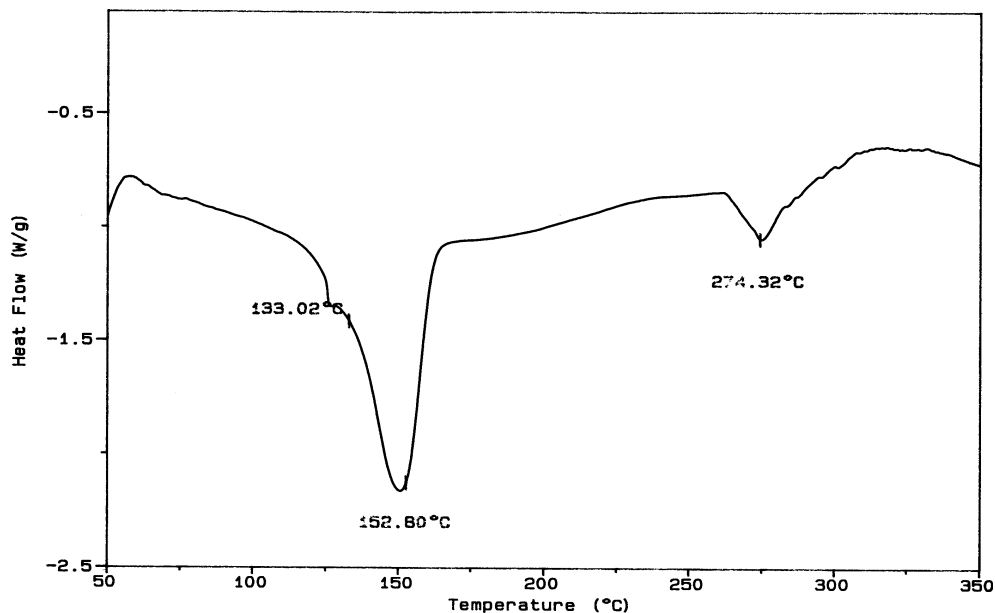


Figure 3.42. Second run DSC thermogram of PMBA-g-PP produced at 170°C with the reaction time of 15 minutes (10.2% PMBA)

In the products obtained at 185°C in the first run of DSC studies the double melting points were also observed. The first meltings at 143.2 and 149.0°C, of the products with 12.3 and 24.4% PMBA, were detected as very weak peak and shoulder on the melting endotherm of α form, respectively, Figure 3.43. They are, however, probably peculiar to β crystalline form, although any peak corresponding to β form in the x-ray spectrum was still not detected, since weak diffraction peaks of β form might be overlapped with the reflections of α form, Figure 3.44. The other melting points due to the melting of α crystalline form were observed between 161.1 and 162.8°C. In the second run of DSC studies the 185°C products had only single melting points ranged from 142.8 to 157.7°C with improper and devious character, which can be ascribed as the melting of α_1 modification.

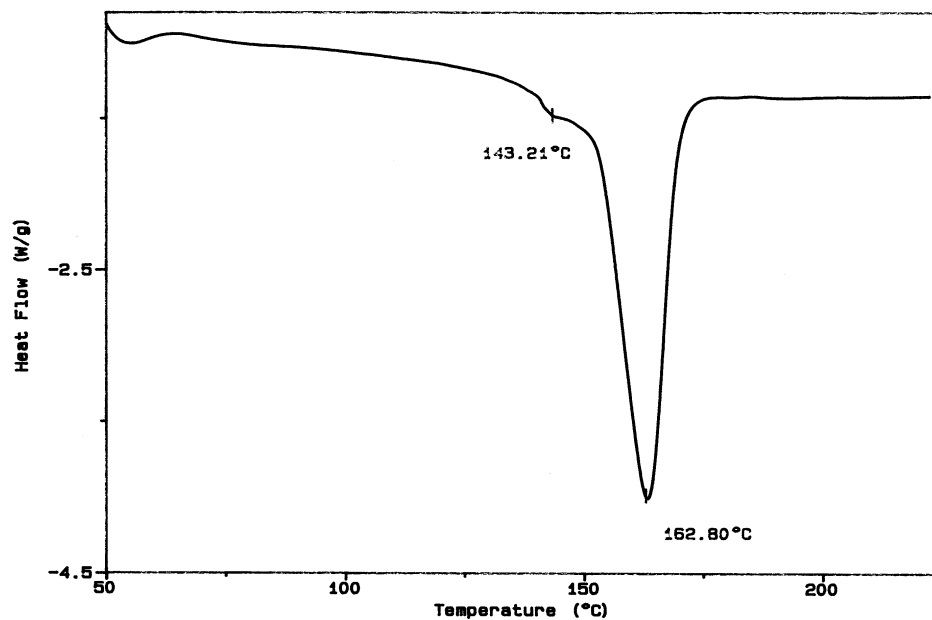


Figure 3.43. DSC thermogram of PMBA-g-PP produced at 185°C with the reaction time of 10 minutes (12.3% PMBA)

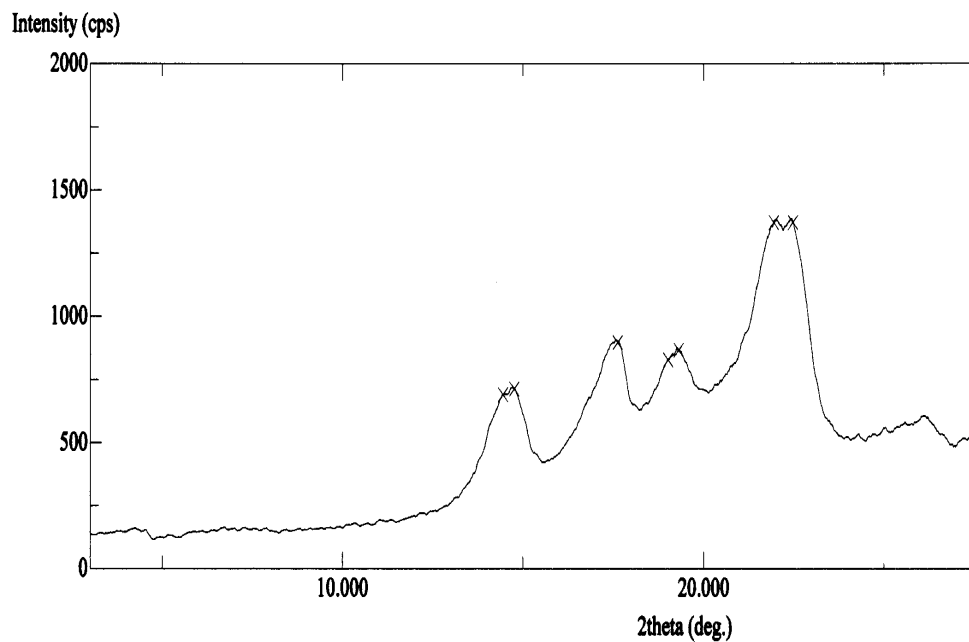


Figure 44. X-ray spectrum of PMBA-g-PP produced at 185°C with the reaction time of 30 minutes (24.4% PMBA)

The thermal properties of 202°C products are similar to those observed at 185°C. In the first run of DSC studies the double meltings were observed only in the product obtained with the reaction time of 10 minutes comprised of 22.6% PMBA. The first melting point at 151.7°C observed as a very weak shoulder on the melting endotherm of α form is possibly to be the melting of β form. No corresponding diffraction peak of β form again was detected as the reason explained above. The other melting points changing between 159.9 and 161.6°C obviously correspond to melting of α_1 form.

In the second run of DSC studies the melting points were observed between 142.8 and 157.6°C again. X-ray analysis showed that these melting points obviously also correspond to melting of α form, Figure 3.45.

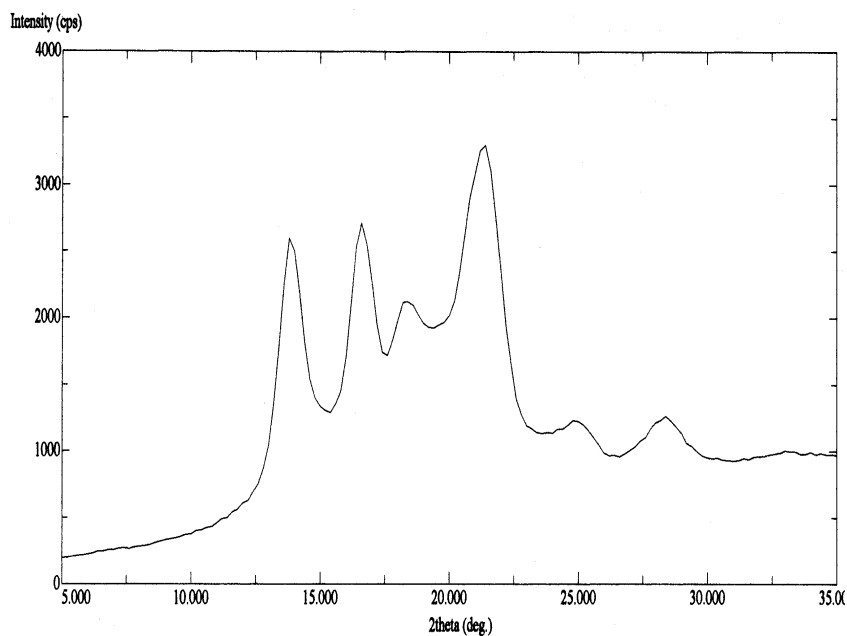


Figure 3.45. X-ray spectrum of PMBA-g-PP produced at 201°C with the reaction time of 40 minutes (23.08% PMBA), (heated to 230°C and cooled to room temperature with 2°C/min)

In the products obtained at 215 and 225°C with the reaction time of 30 minutes the similar melting behaviors were observed. Mostly α_1 was detected at 160.8°C in the first run of DSC study with β forms as shoulder around 147°C and only α_1 appeared at about 158°C in the second runs.

The effect of fast cooling (20°C/min) on the crystallization of PP after the first run of DSC did not show any reflection of β form in PMBA-g-PP in x-ray analysis. While we have observed β modification in case PABA-g-PP.

Conclusively, the presence of PMBA lead to the formation of α_2 form predominantly in some of the graft coproducts obtained at 170°C. In the products obtained at higher temperatures the crystallization of PP units in both α_1 and α_2 modification in the graft form were not affected with the presence of grafting units of PMBA. In addition, comparing the previous graft copolymer PABA-g-PP, PMBA did not produce any influence on the crystallization of PP during the high temperature grafting process leading to the formation of β form.

On the other hand, the melting point of PMBA was observed between 274 and 286°C in the graft coproducts, Figure 3.42. The smectic structure of PMBA was reported by Blumstein et al.⁽⁶⁹⁾ with the reflection at the spacing of 4.44 Å in the wide angle x-ray diffraction. No reflection peak was detected on the x-ray spectra corresponding to smectic structure in the graft coproducts, probably due to overlapping with the reflections of α form, Figure 3.41, 3.44 and 3.45.

3.6. Characterization of Polymers by MS and TG/IR

Beside the smectic form of PMBA^(69,70) and PABA⁽⁷⁰⁾, monoclinic and nematic phases were also reported for PABA^(70,71), where mobile nematic mesophase is produced by melting of the crystals. These works, however, state some conflicting results on the thermal behavior of both polymers. One of them⁽⁷²⁾ mentioned the fast decomposition of PABA without given any further information. There exists not any study on the decomposition mechanism of both PABA and PMBA. We detected that PABA started to decompose before completing the melting endotherm in grafted samples. In addition, the reported nematic mesophase of PABA was experienced by polarizing microscope with hot stage in vacuum. Yet, no mesomorphic behavior was seen in the melt state of PABA.

We tried the isothermal experiments of DSC studies. PABA-g-PP samples were heated to 200°C keeping the temperature constant for 15 minutes. Although there was not any heat flow when the experiments were carried out in nitrogen atmosphere, endothermic change was observed when it was performed in the presence of air, where the isotherm temperature was kept 200°C, was well below the melting point of PABA. A small amount of polymer, PABA, sample was put in glass tube, sealed under vacuum and heated to above the melting followed by fast cooling. We observed sublimation products as solid on the walls of the tube. These were possible decomposition products of PABA. It appears that thermal stability is also important for the processing of the graft coproducts, PABA-g-PP and PMBA-g-PP. Therefore it became necessary to clarify the thermal behavior of the polymers at the temperatures that the mesomorphic state was observed and to comprehend the optimum conditions at which the polymers are stable for processing. Decomposition mechanism and thermal behavior of PABA, PABA-g-PP, PMBA and PMBA-g-PP samples were studied by DSC, direct pyrolysis mass spectrometry and TG/IR system, which combined thermogravimetric analyzer and FTIR spectrometer.

3.6.1. MS Spectrometry

It appears that the thermal degradation of PABA produced by DCP initiator starts at early times of the heating, and takes place in a broad temperature range, Figure 3.46. The spectrum of the degradation products on the total ions current (TIC) were taken at 29.1 (291°C) and 41.5 minutes (415°C) with the heating rate of 10°C/min, Figure 3.47.a and b, respectively. The corresponding products were given in Table 3.10, and the possible degradation mechanism was shown in Figure 3.48. The peaks of degradation products observed were almost the same for both time scales.

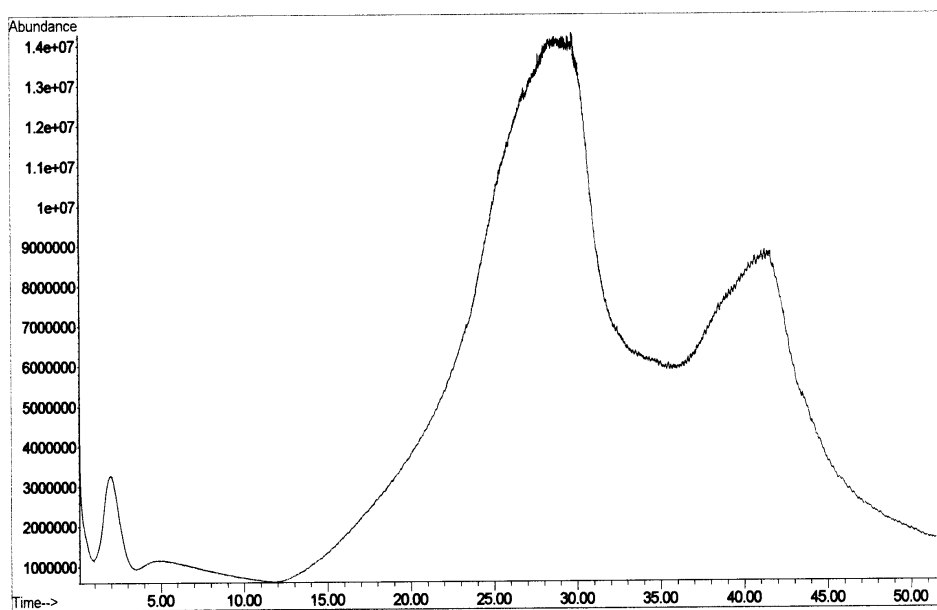
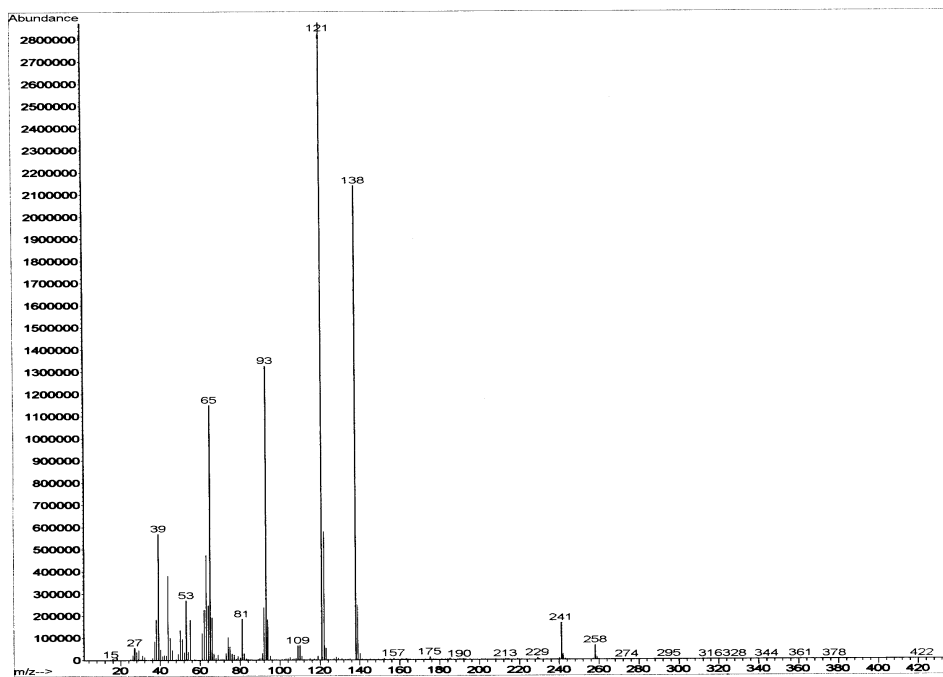


Figure 3.46. The total ion current of the pyrolysis of PABA produced by initiation of DCP at 202°C, with the heating rate of 10°C/min

a)



b)

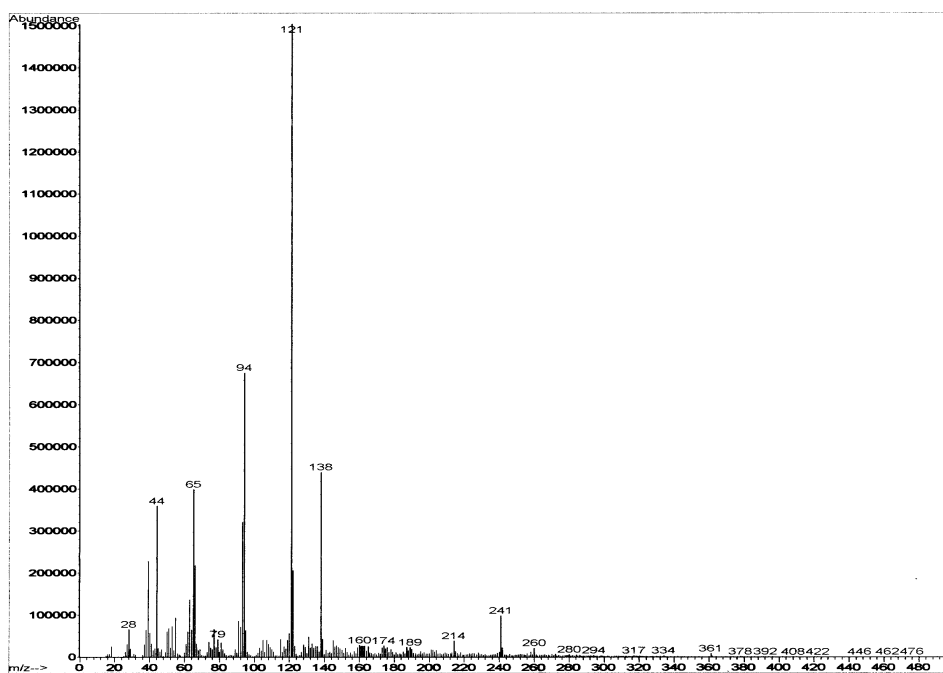


Figure 3.47. The mass spectra of PABA, produced by initiation of DCP at 202°C, taken at a) 29.1, and b) 41.5 minutes, with the heating rate of 10°C/min.

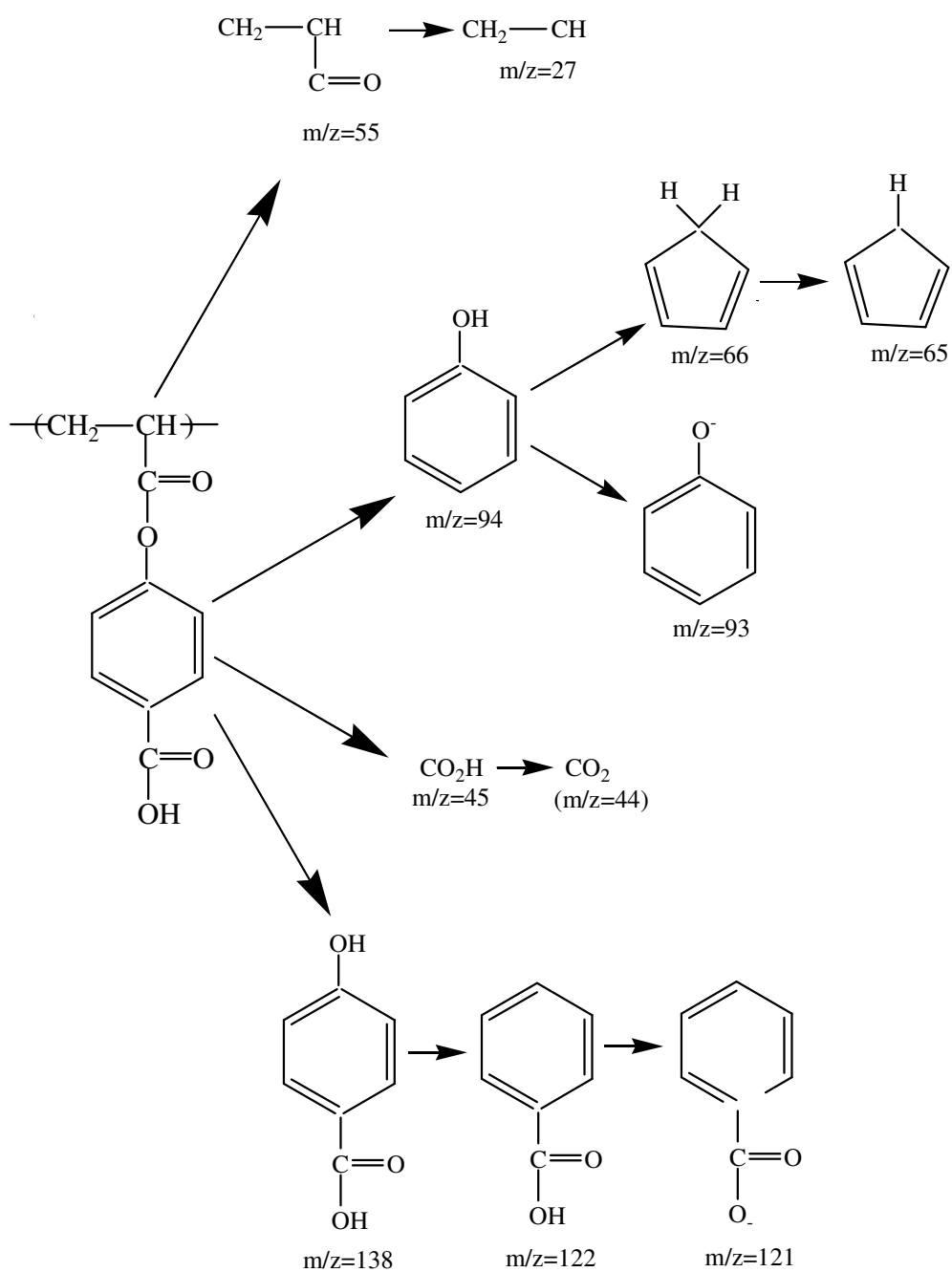


Figure 3.48. Degradation mechanism of PABA

Table 3.10. The characteristics of the peaks present in the pyrolysis mass spectra corresponding to the degradation products of PABA produced by initiation of DCP recorded at 29.1 minutes (291°C) with the heating rate of 10°C/min.

m/z	Assignment
27	C ₂ H ₃
38	C ₃ H ₂
39	C ₃ H ₃
44	CO ₂
45	CO ₂ H
53	C ₂ HCO
55	C ₂ H ₃ CO
63	C ₅ H ₃
64	C ₅ H ₄
65	C ₅ H ₅
66	C ₅ H ₆
81	C ₄ HO ₂ , C ₆ H ₉
92	C ₆ H ₅ O-H
93	C ₆ H ₅ O
94	C ₆ H ₅ OH
109	C ₂ H ₂ COC ₂ H ₃ CO, C ₂ H ₂ CO ₂ C ₃ H ₃
121	C ₆ H ₅ CO ₂
122	C ₆ H ₅ CO ₂ H
138	C ₆ H ₅ CO ₂ HOH
139	(C ₂ H ₃ CO ₂) ₂ CH, C ₂ HCO ₂ C ₂ H ₂ CO ₂
241	C ₂ HCO ₂ C ₆ H ₅ C ₂ HCO ₂ C ₂ H ₂
258	C ₂ HCO ₂ C ₆ H ₅ CO ₂ C ₂ HCO ₂

The decomposition mechanism of PABA produced by γ -radiation was found to be identical to PABA produced by initiation of DCP at 202°C in the first maximum of the total ion current giving almost the same degradation products, Figure 3.49 and Figure 3.50.a and b. However, as it was seen on the total ion current decomposition took place at earlier times. The peaks of the degradation products including the high m/z fragment structures beside the commonly observed ones on the total ion current taken at 35.5 minutes (355°C) with the heating rate of 10°C/min and the corresponding products were given in Table 3.11.

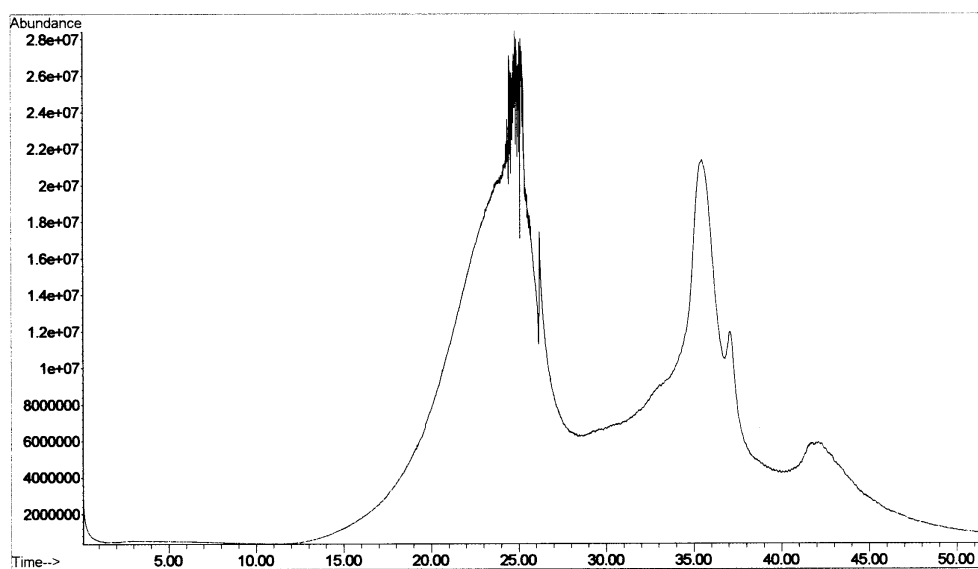
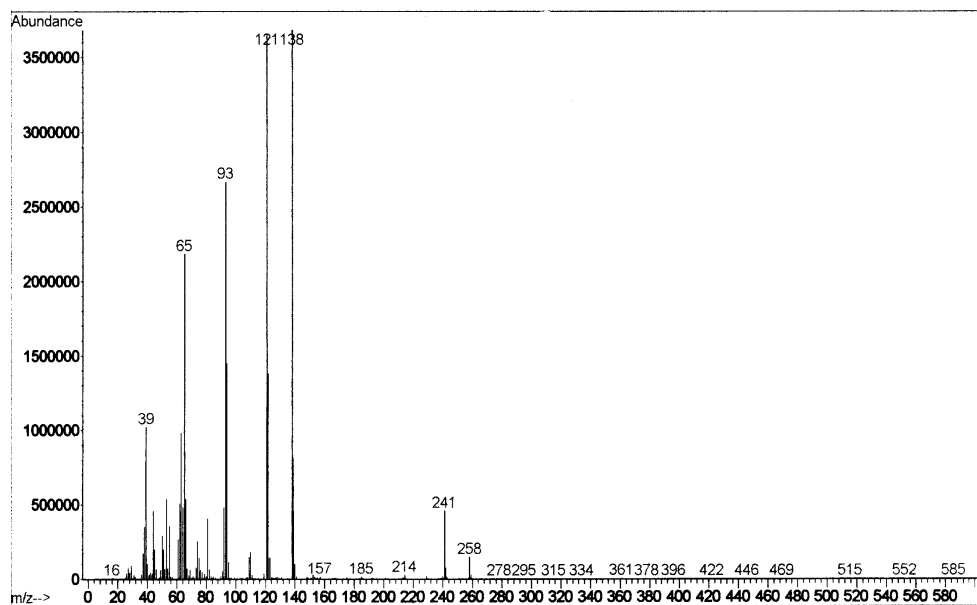


Figure 3.49. The total ion current of the pyrolysis of PABA produced by γ -radiation with the heating rate of 10°C/min.

a)



b)

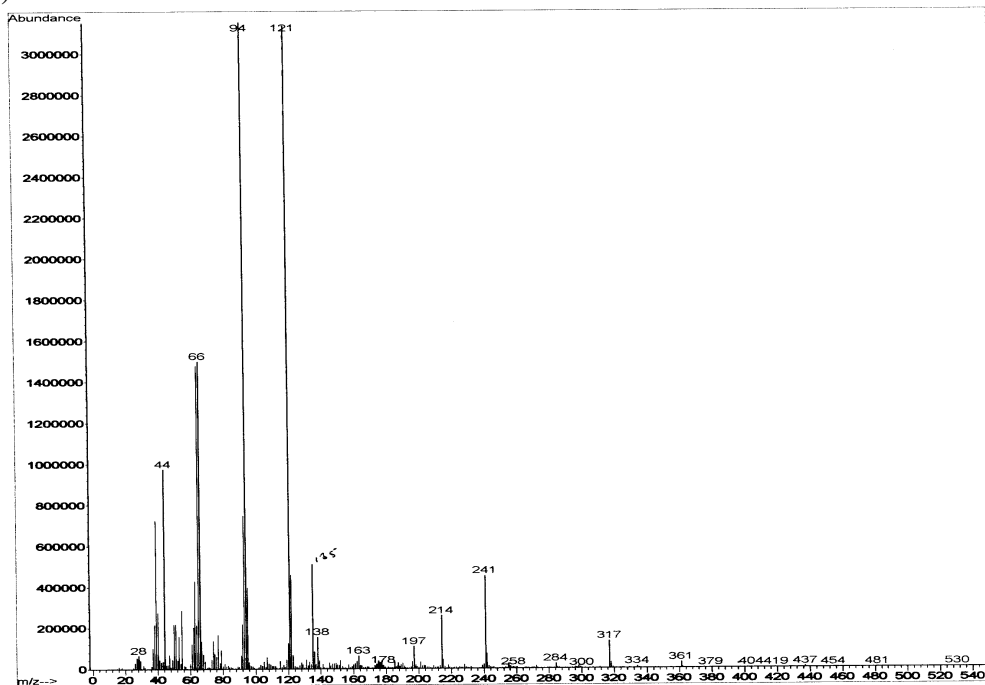


Figure 3.50. The mass spectrum of PABA produced by γ -radiation taken at a) 24.4 (244°C), and b) 35.5 minutes (355°C)

Table 3.11. The peaks present in the pyrolysis mass spectra corresponding to the degradation products of PABA produced by γ -radiation recorded at 35.5 minutes (355°C) with the heating rate of 10°C/min.

m/z	Assignment
28	CO
38	C ₃ H ₂
39	C ₃ H ₃
40	C ₃ H ₄
44	CO ₂
52	C ₄ H ₄
53	C ₂ HCO
55	C ₂ H ₃ CO
63	C ₅ H ₃
64	C ₅ H ₄
65	C ₅ H ₅
66	C ₅ H ₆
77	C ₆ H ₅
92	C ₂ HCOC ₃ H ₃
93	C ₆ H ₅ O
94	C ₆ H ₅ OH
95	C ₂ HCO ₂ C ₂ H ₂ , CHCOC ₂ H ₂ CO
121	C ₆ H ₅ CO ₂
122	C ₆ H ₅ CO ₂ H
135	C ₂ HCO ₂ C ₃ H ₂ CO, C ₂ H ₂ COC ₂ H ₂ COC ₂ H ₃
138	C ₆ H ₅ CO ₂ HOH
163	COC ₃ H ₃ COC ₂ H ₂ COCH ₂
197	C ₂ H ₃ CO ₂ C ₂ H ₃ CO ₂ C ₂ H ₃ CO
214	C ₂ H(CO ₂ C ₆ H ₅)C ₂ H ₂ (CO)CH ₂
241	C ₂ H(CO ₂ C ₆ H ₅)C ₂ H(CO ₂)C ₂ H ₂
317	C ₂ H ₃ (CO ₂ C ₆ H ₅)(C ₂ H ₃ (CO ₂)) ₂ C ₂ H ₃

There is no considerable difference in degradation products in the first maximum of the total ion current for PABA-g-PP samples in comparison to pure homopolymer PABA. This shows that at early stages the degradation proceeds predominantly by breaking up of grafting polymer PABA. Carboxylic, aromatic and carbonyl groups rather than that of the main chain of PP, and by decomposition of the phenol formed during degradation into cyclohexadiene were still observed clearly. The total ion current and the mass spectra taken at 25.4 minutes (254°C) and 41.8 minutes (418°C) with the heating rate of 10°C/min were given in Figure 3.50 and Figure 3.51.a and b, respectively. Furthermore, the mass spectra became more complicated at 41.8 minutes (418°C) due to the decomposition of PP main chain, compare Figure 3.47.b and Figure 3.51.b.

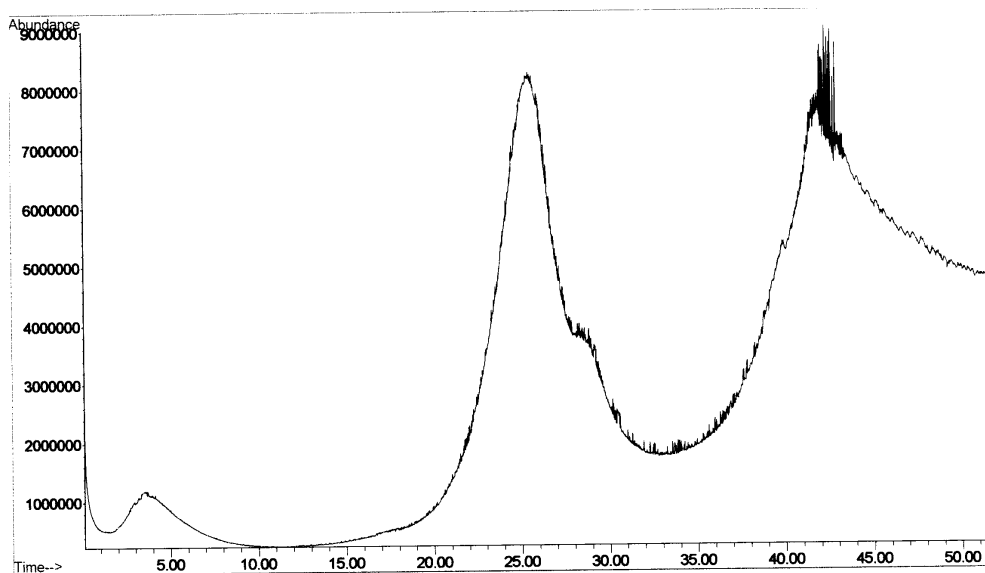


Figure 3.50. The total ion current during the pyrolysis of PABA-g-PP (47.5% PABA) with the heating rate of 10°C/min.

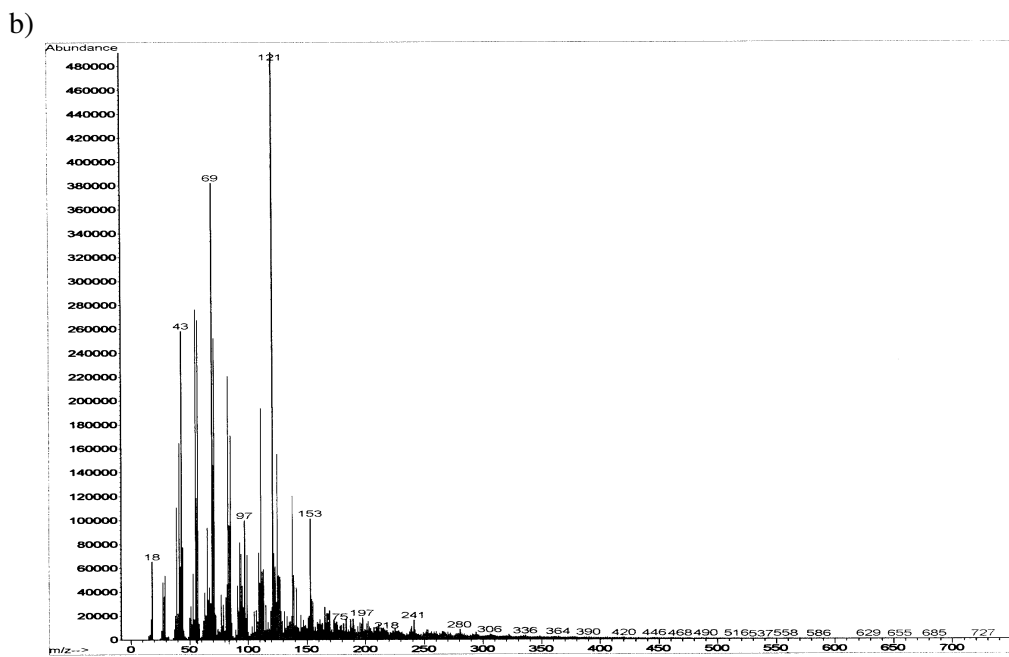
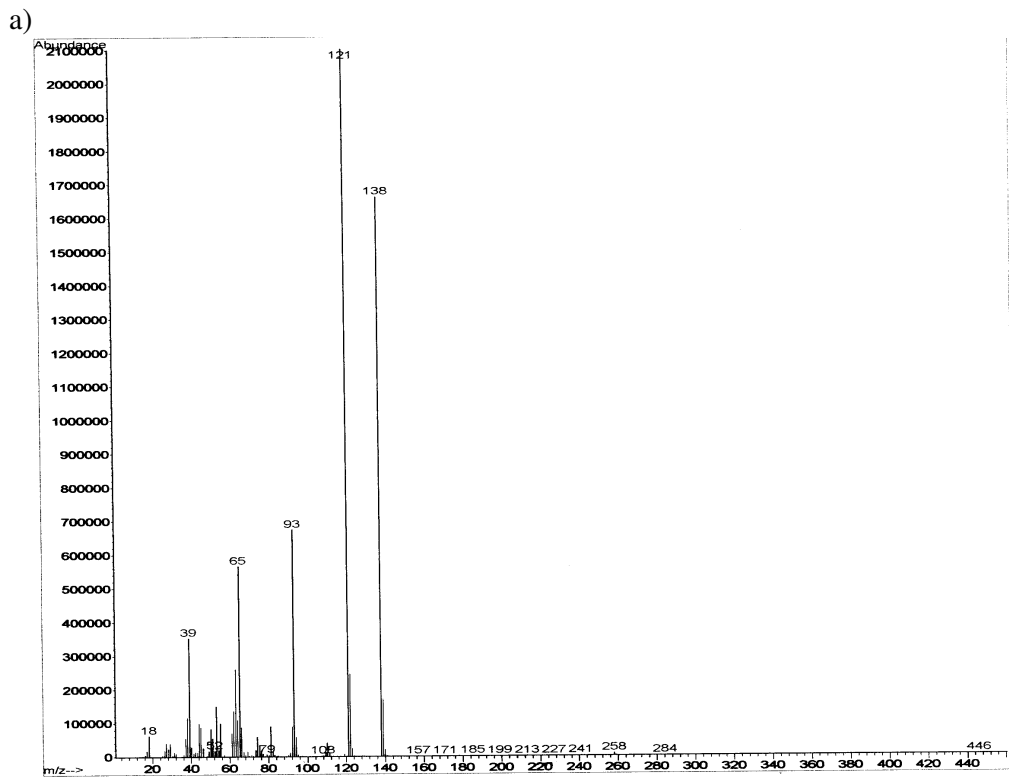


Figure 3.51. The mass spectra of PABA-g-PP (47.5% PABA) taken at a) 25.4 minutes (254°C), b) 41.8 minutes (418°C)

The degradation products of PMBA and PMBA-g-PP samples with the m/z values of 39, 53, 65, 66, 81, 93, 94, 121 and 138 were commonly observed in almost all mass spectra. This also indicates that the degradation occurs prevalingly by decomposition of side groups. At elevated temperature, however, it can be concluded that the samples start to burn out without giving any definite degradation mechanism. The total ion current of pyrolysis of PMBA, the peaks of the degradation products at 27.3 minutes (273°C) and 35.2 minutes (352°C) were given in Figure 3.52 and Figure 3.53.a and b, respectively. The total ion current of PMBA-g-PP and the mass spectra taken at 33.9 minutes (339°C) and 42.7 minutes (427°C), were also given in Figure 3.54, 3.55.a and b, respectively.

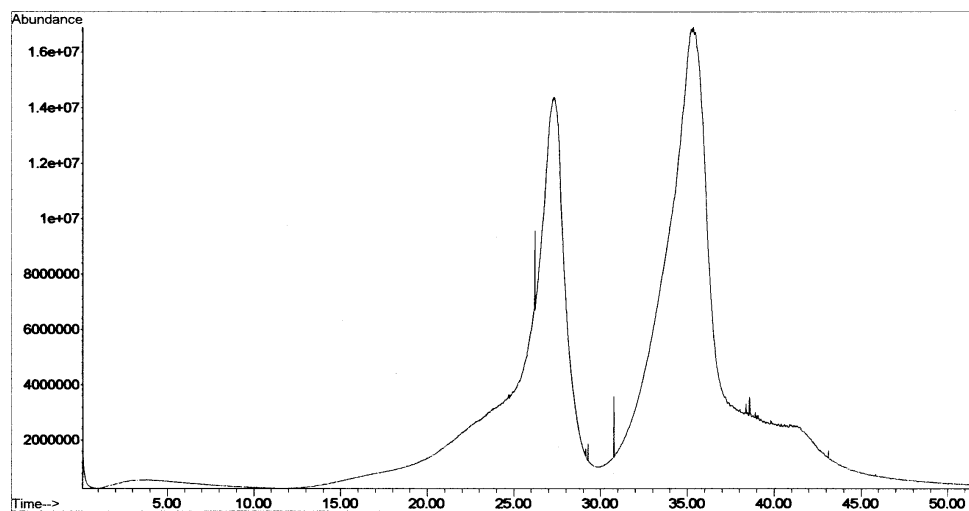


Figure 3.52. The total ion current of the pyrolysis of PMBA taken with the heating rate of 10°C/min

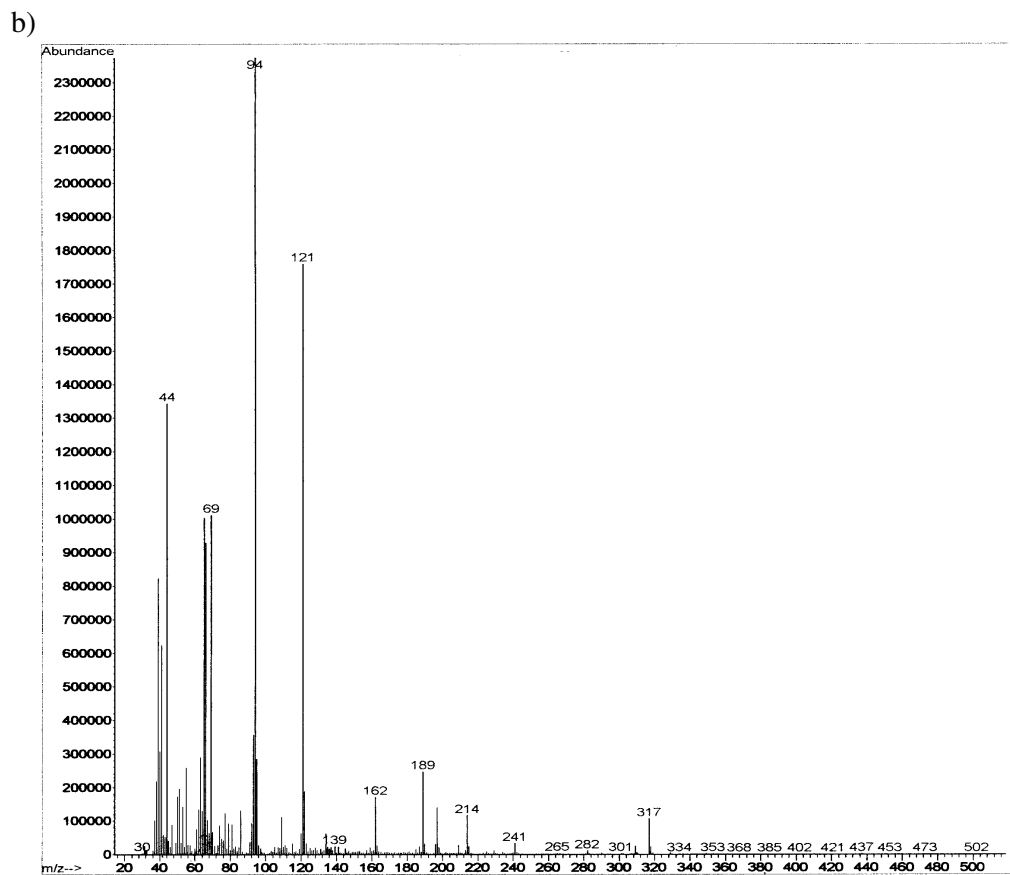
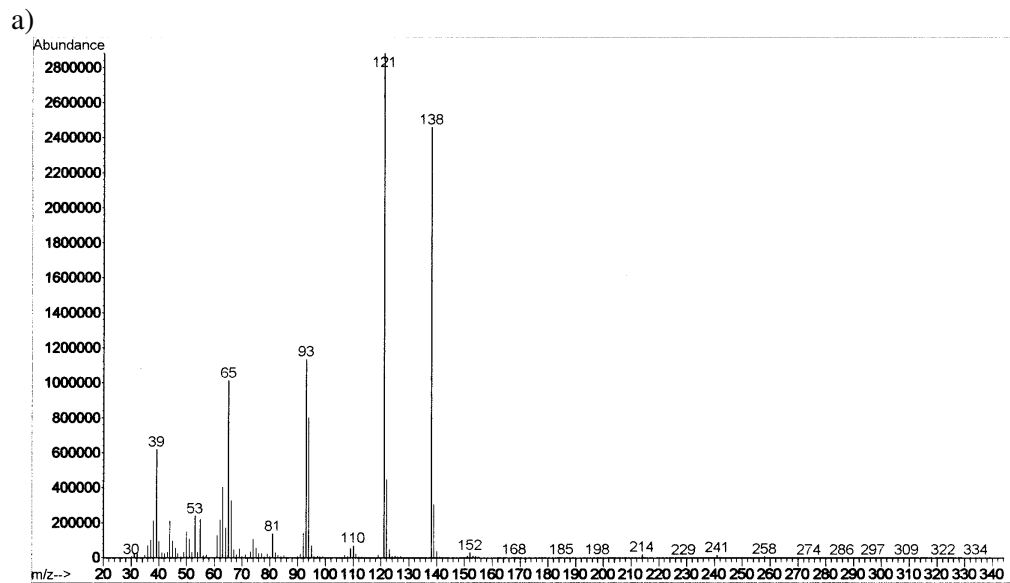


Figure 3.53. Mass spectra of PMBA taken at a) 27.3 minutes (273°C), and b) 35.2 minutes (352°C) with the heating rate of 10°C/min

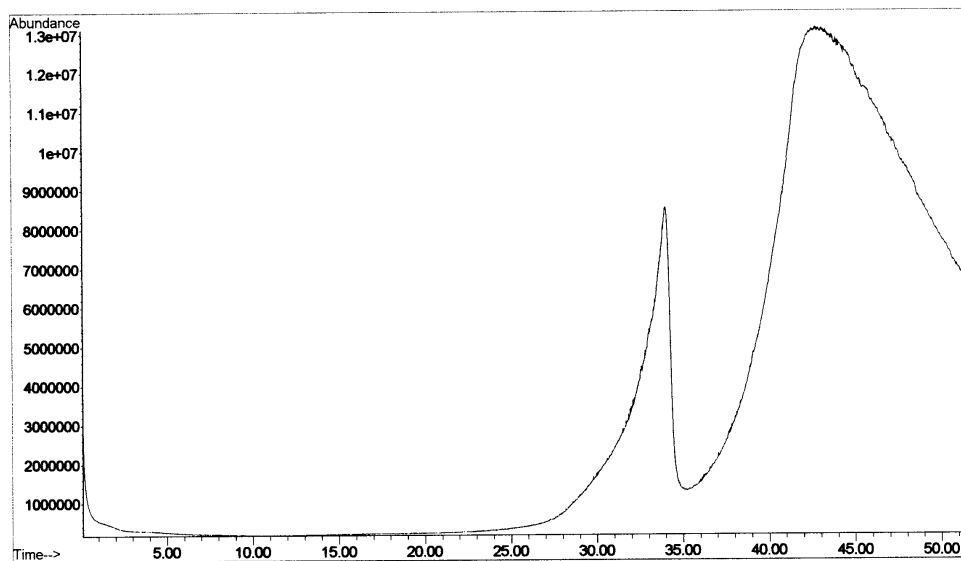


Figure 3.54. The total ion current of PMBA-g-PP (27.3% PMBA) taken with the heating rate of 10°C/min.

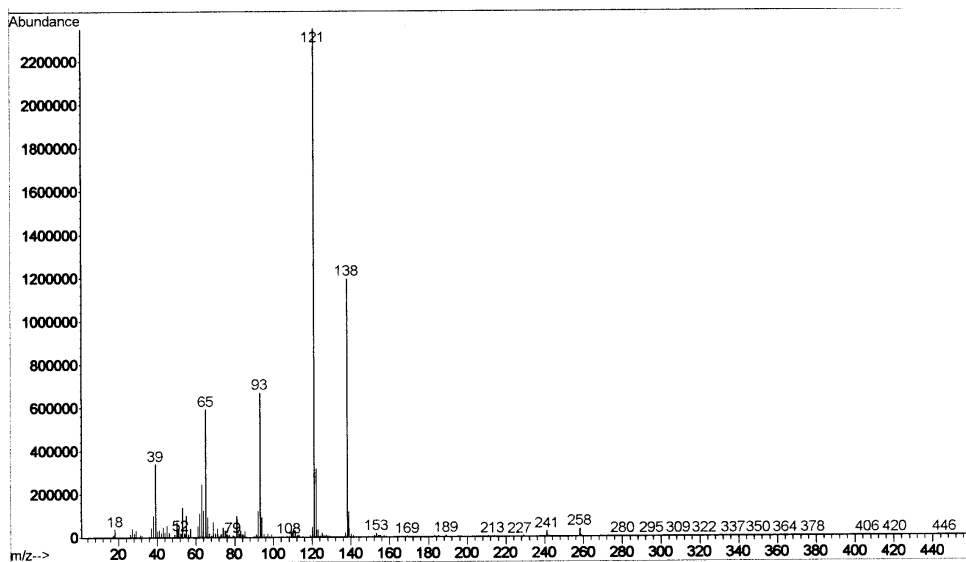


Figure 3.55.a) Mass spectrum of PMBA-g-PP (27.3% PMBA) taken at 33.9 minutes (339°C) with the heating rate of 10°C/min

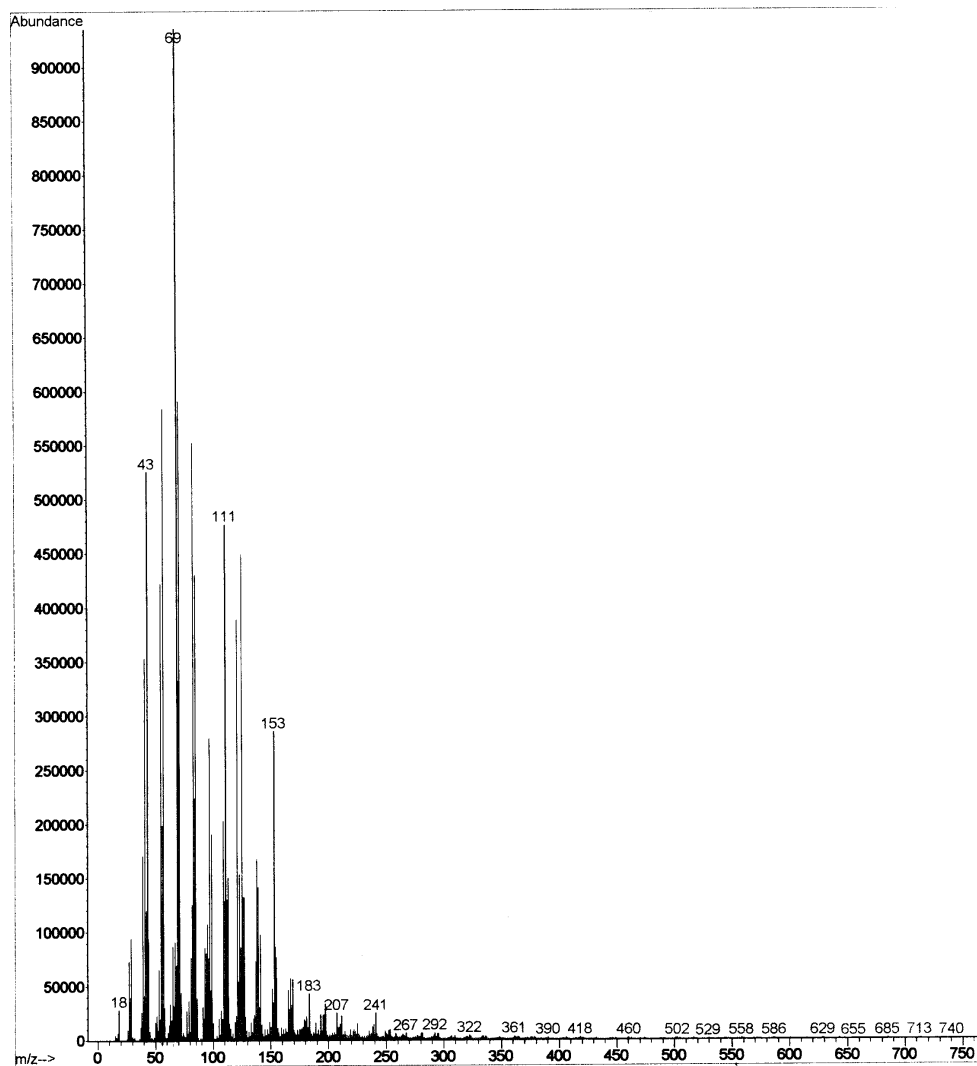


Figure 3.55.b. Mass spectrum of PMBA-g-PP (27.3% PMBA) taken at 42.7 minutes (427°C) with the heating rate of 10°C/min

Conclusively, at early stages degradation of the polymers proceeded by breaking up of the side groups into carbonly, carboxylic and aromatic groups, and decomposition of the phenol into cyclodiene. At high temperatures (prolong time of heating) smaller hydrocarbon peaks also started to appear in lower m/z regions due to PP of the PABA-g-PP or PMBA-g-PP decomposition.

3.6.2. TG-IR Analysis

Thermogravimetric analysis of PABA produced by DCP initiator carried out in N_2 showed that the weight loss due to decomposition started at about $200^\circ C$ and continued to $600^\circ C$, Figure 3.56. The decomposition products were also analyzed by FTIR spectrometer combined with the thermogravimetric analyzer, and the results supported the decomposition products observed in MS analysis. The formation of carbon dioxide was detected with the $C=O$ stretching bands at 2361 cm^{-1} at early times, and almost in all stages of heating. The other absorption bands observed due to the decomposition started at about $200^\circ C$. In the FTIR spectrum of PABA taken at $200^\circ C$ phenolic and carboxylic O-H stretching bands at 3643 and 3582 cm^{-1} , aromatic C-H stretching band at about 3050 cm^{-1} , carboxylic $C=O$ stretching band at 1756 cm^{-1} , aromatic $C=C$ stretching band at about 1606 and 1512 cm^{-1} , phenolic O-H in plane bending at about 1360 cm^{-1} , and C-O stretching bands at about 1264 , 1187 , 1163 and 1078 cm^{-1} correspond to phenol, benzoic acid and p-hydroxybenzoic acid, respectively. At all stages of heating the same decomposition products were observed with increasing absorption peaks in FTIR spectra, Figure 3.57.a, b, c and d.

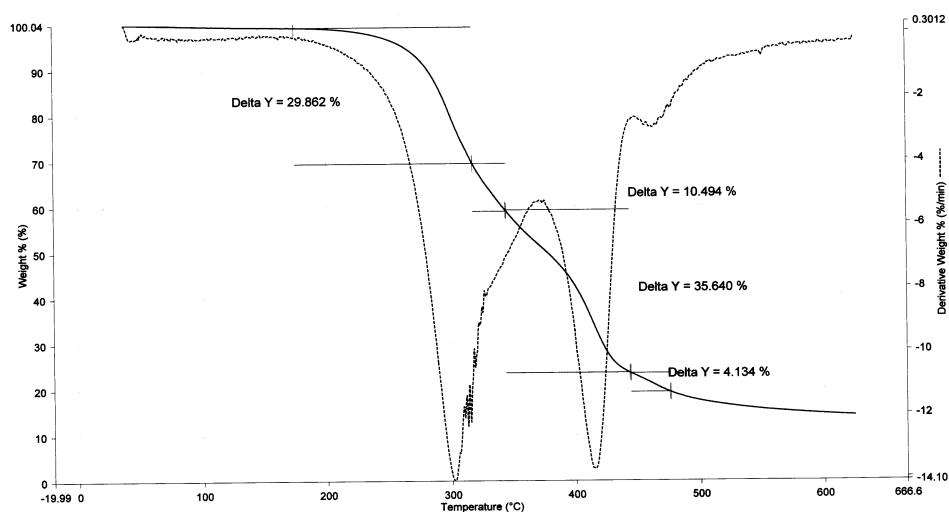


Figure 3.56. TGA thermogram of PABA produced by DCP initiator taken with the heating rate of $20^\circ C/min$ in N_2

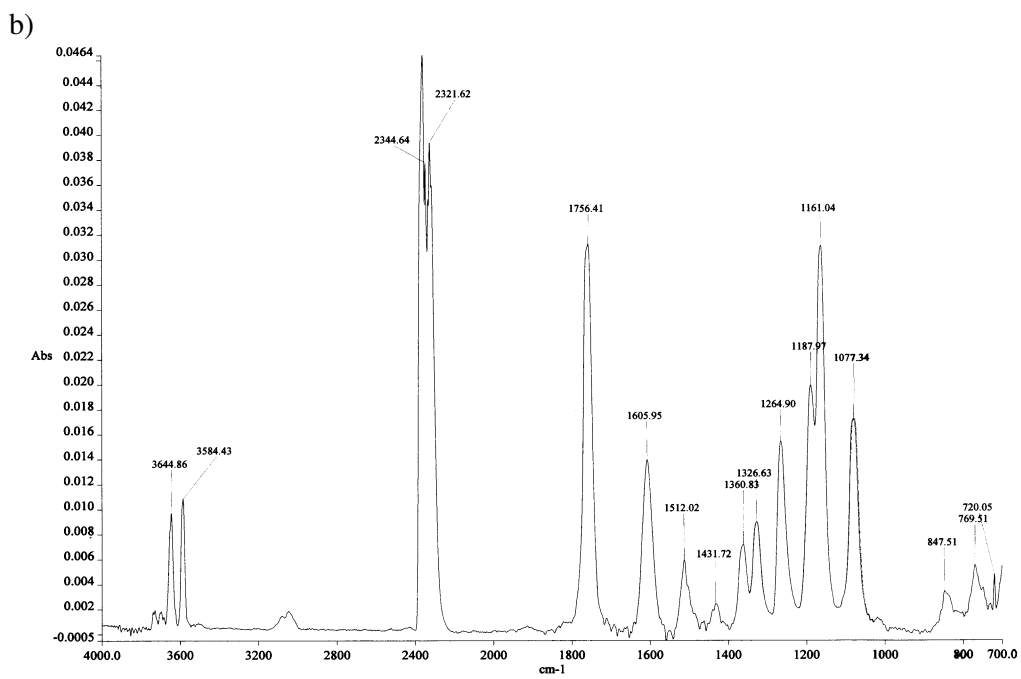
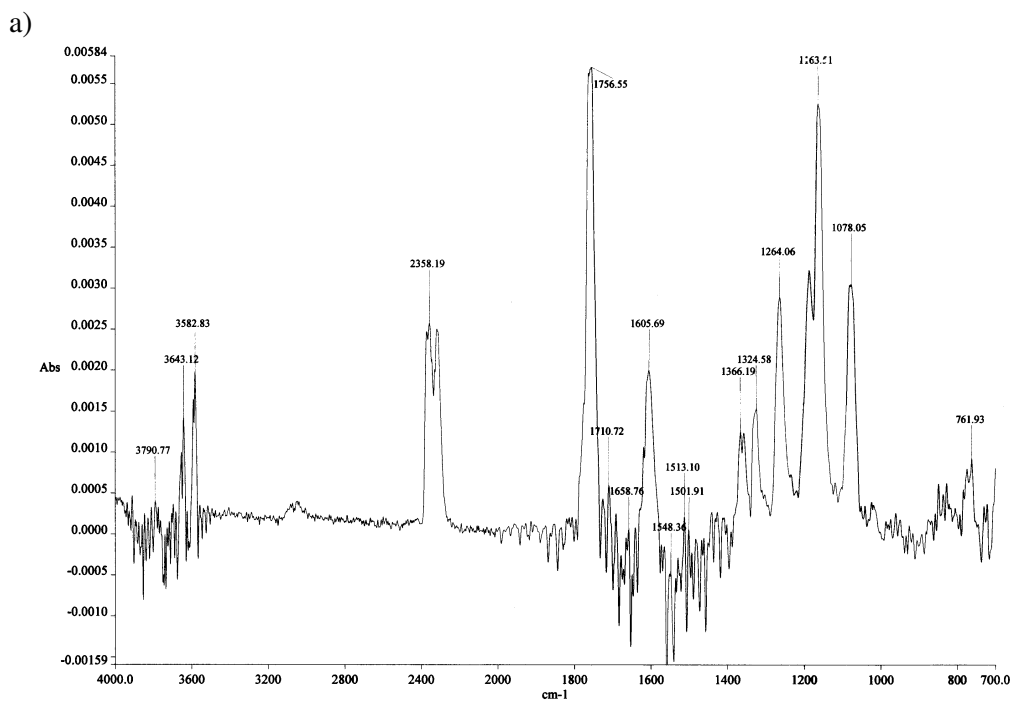


Figure 3.57. The FTIR spectra of the products formed at a) 12 minutes (240°C), and b) 14.4 minutes (288°C) during the heating of PABA with the rate of 20°C/min in nitrogen

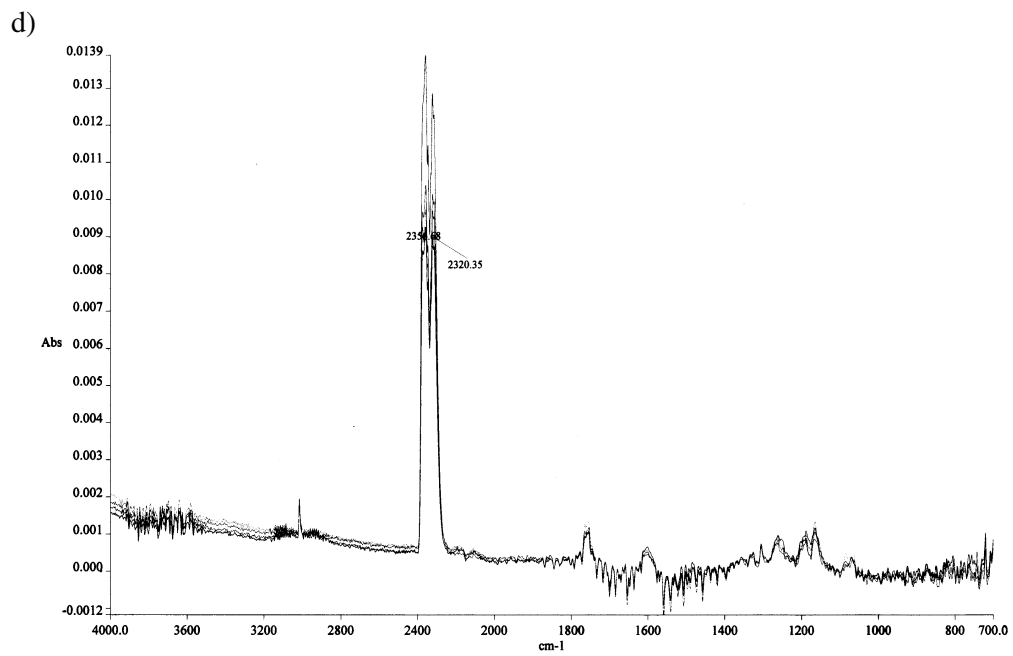
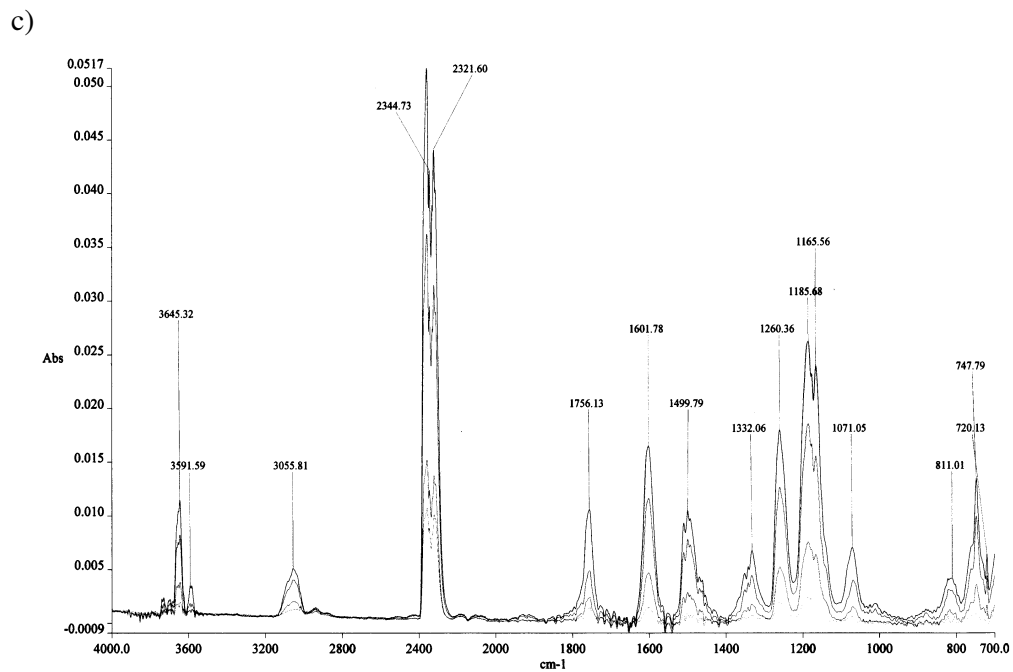


Figure 3.57. The FTIR spectra of the products formed during the heating of PABA between c) 19.7-22.7 minutes (394-454°C), and d) 24.9-29.5 minutes (498-590°C) with the rate of 20°C/min in nitrogen

PABA was also tested in air. We found the same decomposition mechanism and trend, however, with starting at earlier temperatures, again around 200°C, with respect to that observed in nitrogen, Figure 3.58 and 3.59.a, b and c.

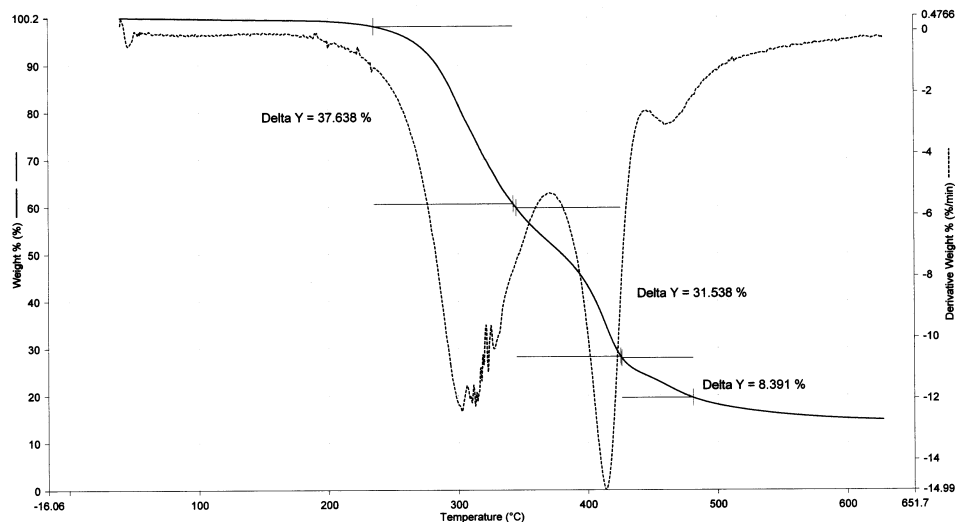


Figure 3.58. TGA thermogram of PABA produced by DCP initiator taken with the heating rate of 20°C/min in air

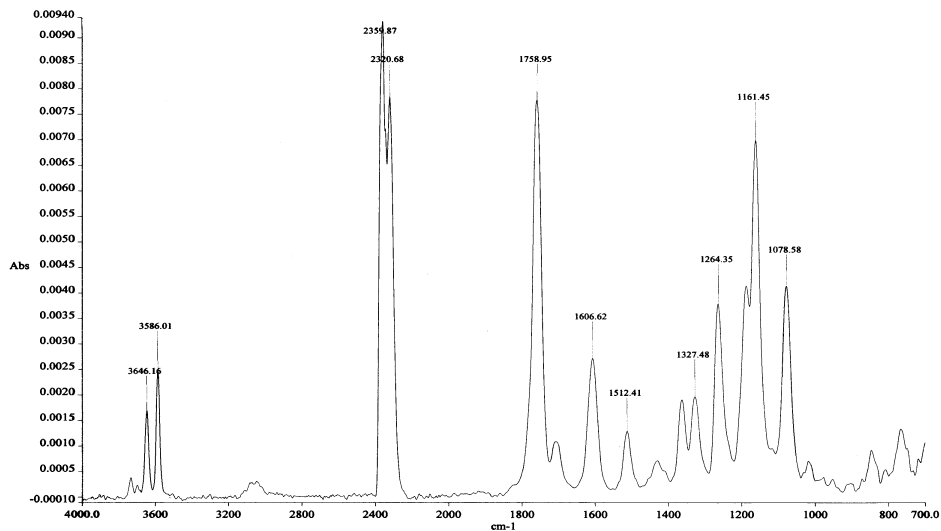


Figure 3.59.a) The FTIR spectrum of the products formed during the heating of PABA at 12 minutes (240°C) with the rate of 20°C/min in air

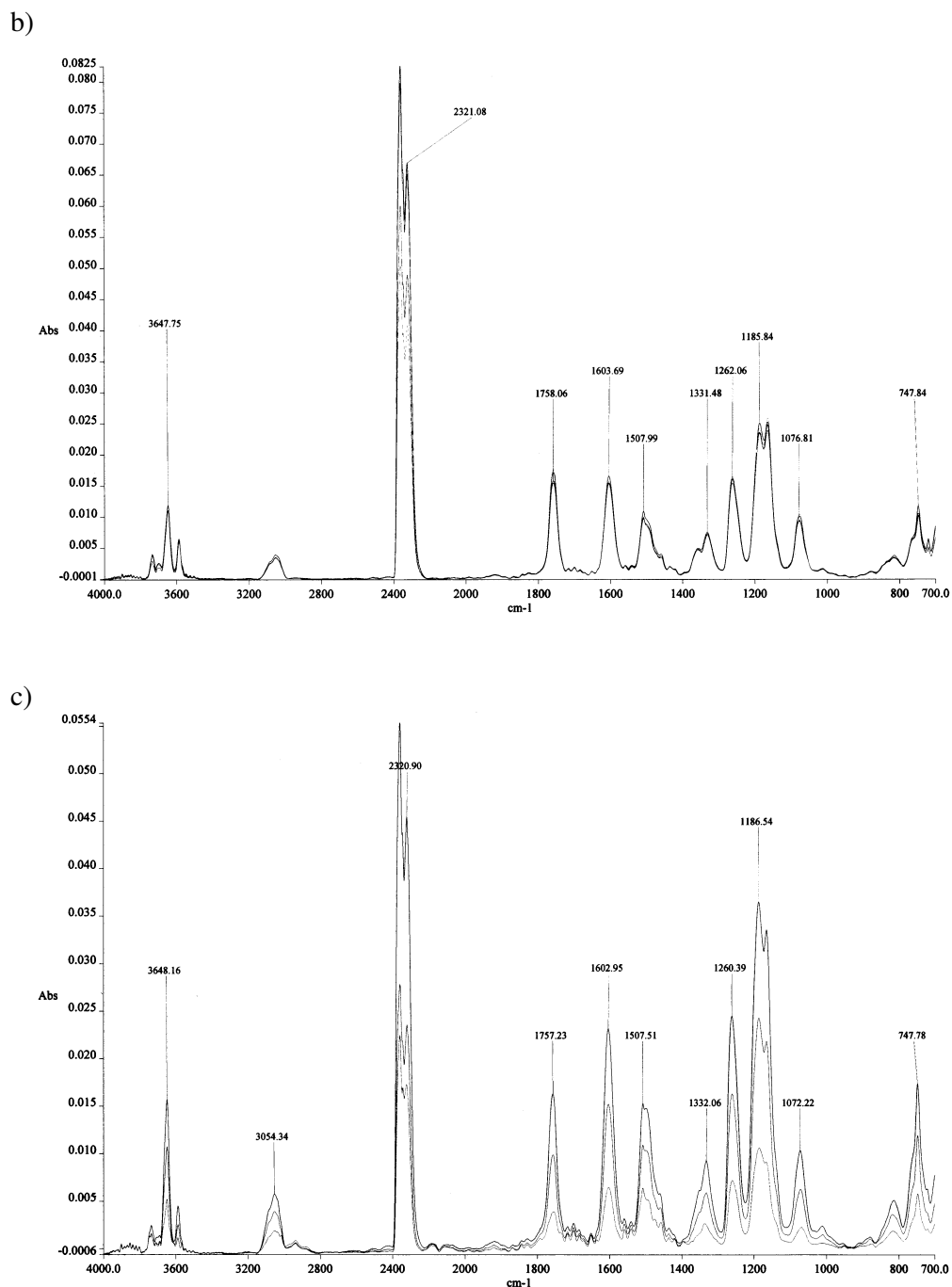


Figure 3.59 The FTIR spectra of the products formed during the heating of PABA between b) 15.4-17.5 minutes (308-350°C), and c) 20.0-21.3 minutes (400-426°C) with the rate of 20°C/min in air

Thermogravimetric analysis of PMBA-g-PP carried out in N₂ atmosphere displayed that the first weight loss started at about 225°C and continued to 600°C. The weight loss was 8% at about 306°C and 17.5% at about 360°C, which was followed by rapid weight loss with respect to earlier ones, Figure 3.60. FTIR analysis of the decomposition products indicated that at initial stage of decomposition the products similar to those observed in PABA were formed, which were verified by the absorption bands corresponding to phenol, benzoic acid, hydroxybenzoic acid and carbondioxide in the FTIR spectra. Furthermore, the decomposition products observed in MS spectra were also supported by FTIR spectra of the products formed in termogravimetry. In addition to the bands observed above, C-H stretching bands of CH₂ and CH₃ were detected at about 2966 and 2925 cm⁻¹. The alkenyl C=C stretching band at 1649 cm⁻¹ and C-H out of plane bending band at 890 cm⁻¹ corresponding to cyclodiene observed in MS spectra with the molecular weight of 65 were detected above 340°C. As the temperature increased above 340°C, however, undefined peaks started to form beside the observed peaks. It seemed that at higher temperatures the phenol and carboxylic acid formed by decomposition diminished, and then after 400°C almost only the groups of CO₂, CH₂ and CH₃ were detected indicating that the polymer completely burned out, Figure 3.61.a and b.

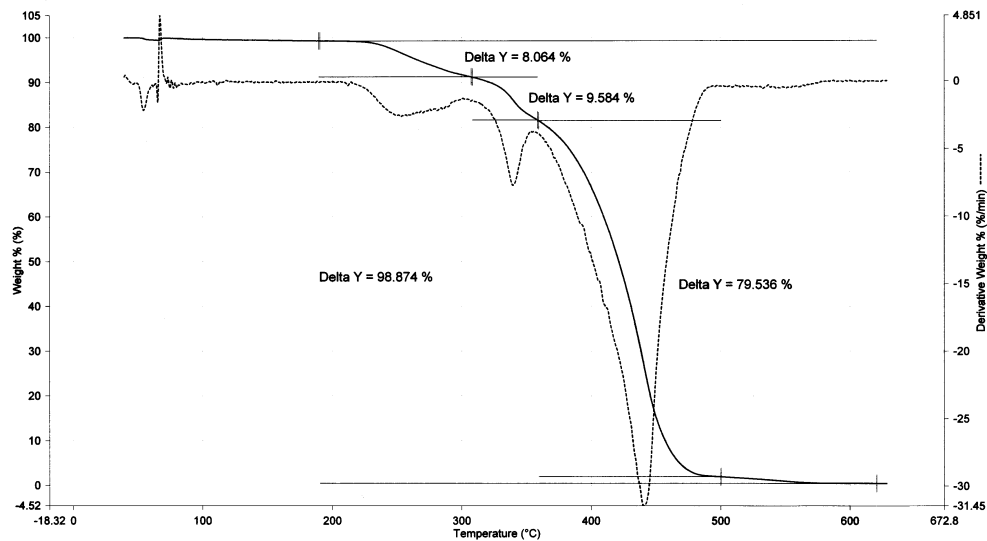


Figure 3.60. TGA thermogram of PMBA-g-PP (30.68% PMBA) taken with the heating rate of 20°C/min in nitrogen

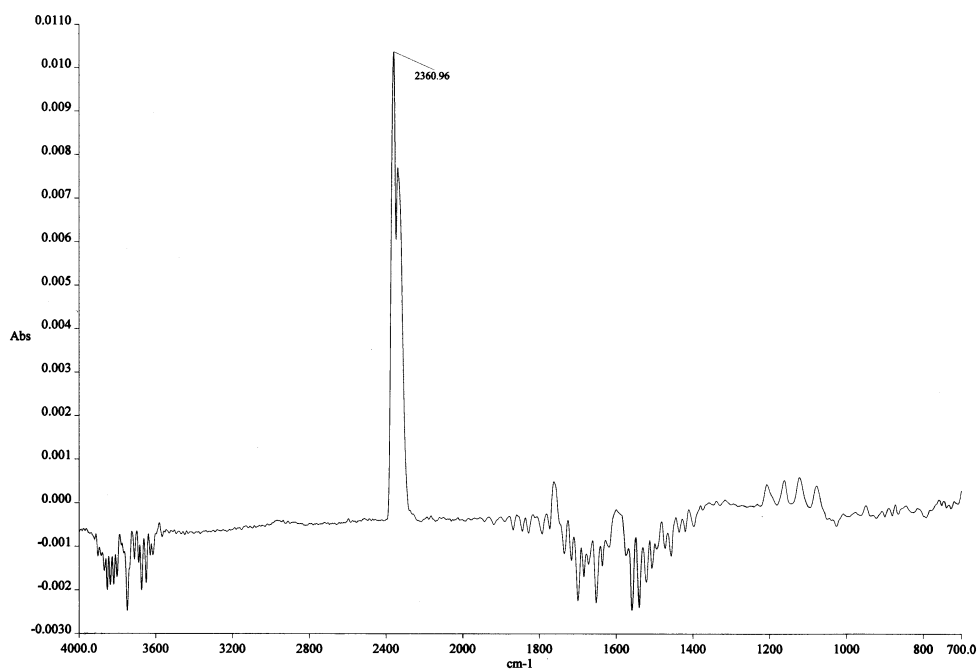


Figure 3.61.a) FTIR spectrum of the products taken at 9.6 minutes (192°C) formed during the heating of PMBA-g-PP (30.68% PMBA) with the rate of 20°C/min in nitrogen

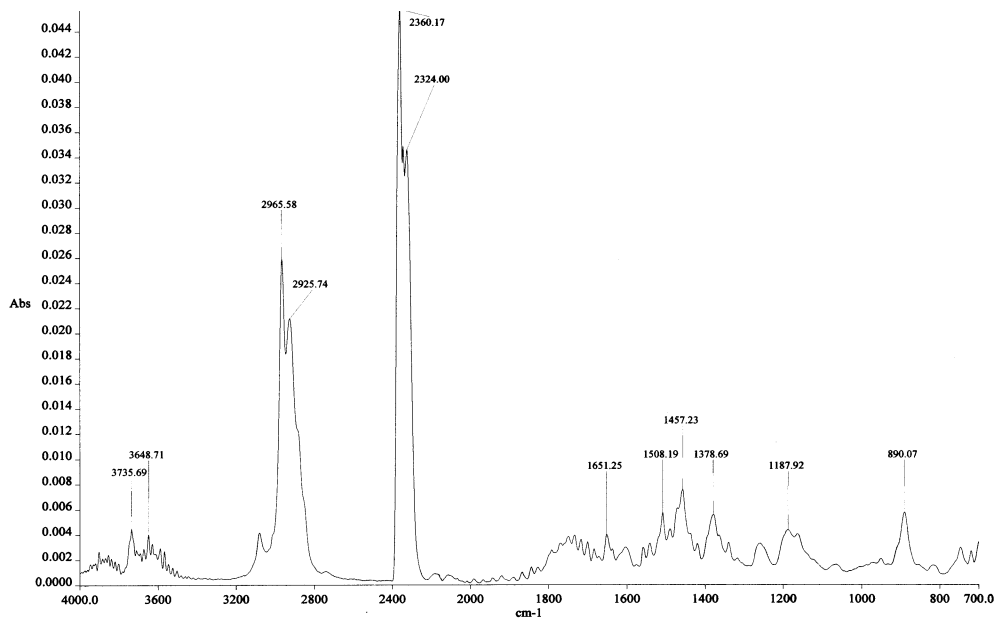


Figure 3.61.b) FTIR spectrum of the products formed during the heating of PMBA-g-PP (30.68% PMBA) taken at 19.8 minutes (396°C) with the rate of 20°C/min in nitrogen

The PMBA-g-PP was also tested in air. The results indicated that the decomposition took place a little faster but almost with the same mechanism and trend in air, Figure 3.62 and 3.63.a and b.

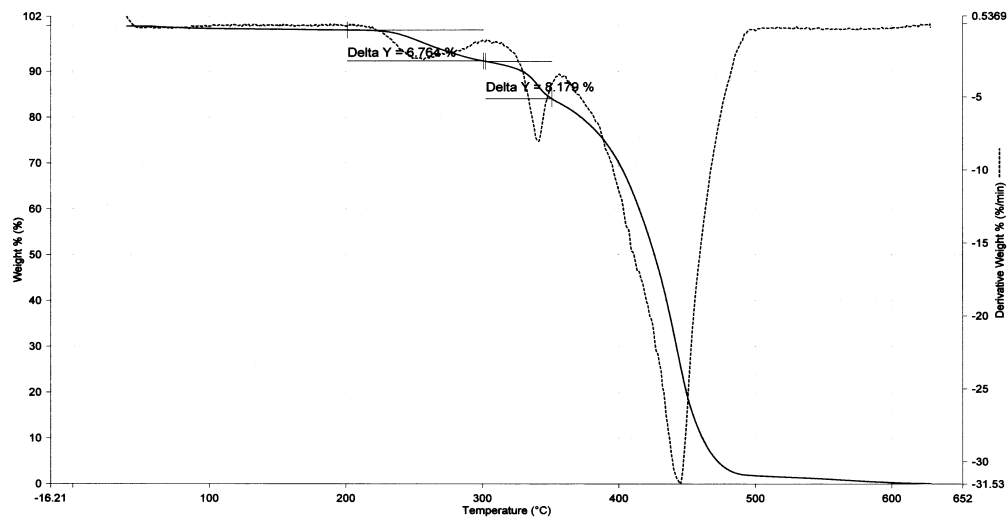


Figure 3.62. TGA thermogram of PMBA-g-PP (30.7% PMBA) taken with the heating rate of 20°C/min in air

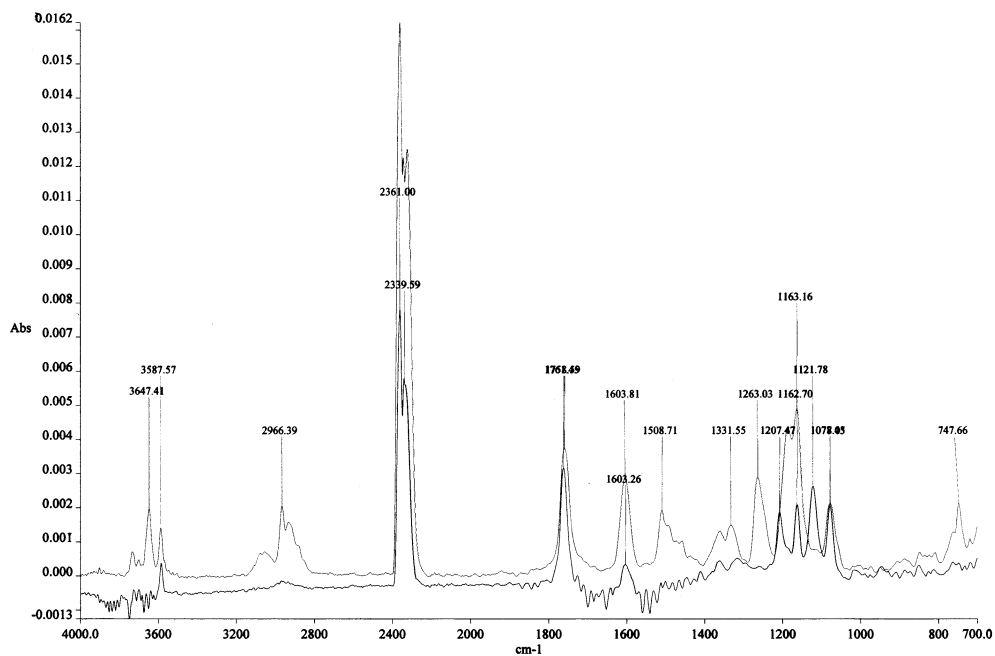


Figure 3.63.a) FTIR spectrum of the products formed during the heating of PMBA-g-PP (30.7% PMBA) taken at 11.6 minutes (232°C) and 14.9 minutes (298°C) with the rate of 20°C/min in air

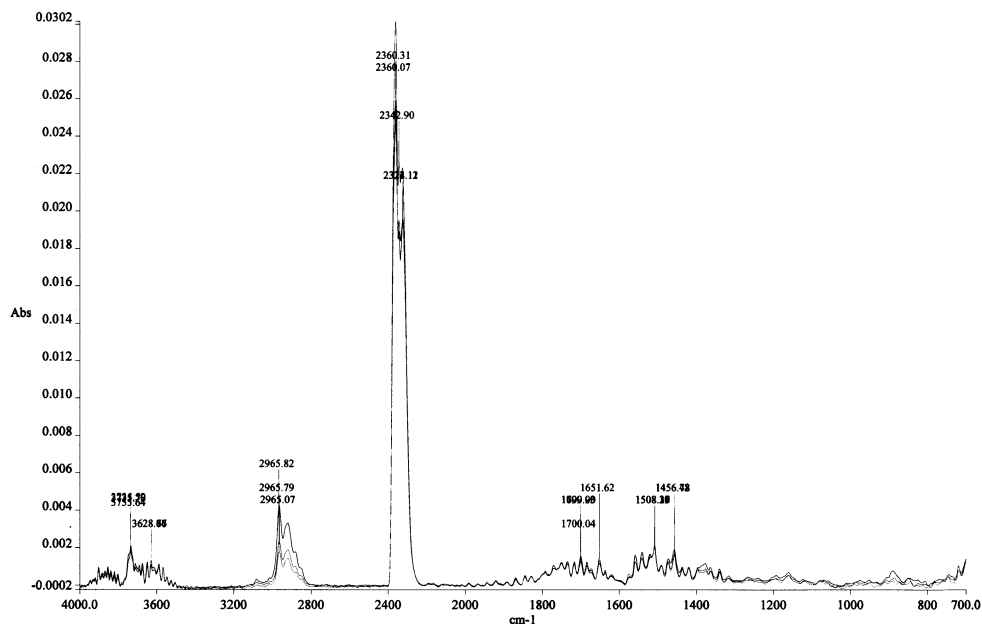


Figure 3.63.b) FTIR spectrum of the products formed during the heating of PMBA-g-PP (30.7% PMBA) taken at 21.9 minutes (438°C) and 24.2 minutes (484°C) with the rate of 20°C/min in air

In conclusion, what we have found in MS and TG/IR characterization is that PABA and PMBA graft coproducts of PP are very sensitive to thermal degradation. The thermal degradation occurs predominantly by breaking up of the side groups at early stages. This is particularly important because a high temperature processing may inevitably cause an extensive degradation of the grafted polymers of PABA and PMBA. Indeed, both grafted polymers when heated in air showed sudden color change close to their melting point. Also, in the second run of DSC studies we did not observe any indication of T_m of grafted polymers when the temperature was increased over the melting point of PABA or PMBA in the first run. The decomposition of aliphatic groups, i.e., PP backbone might act as a protective material during melt processing, took place at elevated temperatures.

3.7. Mechanical Properties of the Polymers

The mechanical properties of the graft coproducts, PABA-g-PP and PMBA-g-PP were studied in order to find out the effect of graft copolymerization of ABA and MBA onto IPP. The samples were prepared by microinjection molding at 200°C because the PABA and PMBA units of the graft coproducts started to decompose above this temperature. Although this processing was well below the melting of both PABA and PMBA it became highly compulsory to process the injection mould samples at 200°C. The degradation mechanism and conditions of the polymers were stated in previous section, 3.6. In fact, the processing at this temperature was not ideal that the perfect dispersion and orientation of PABA and PMBA could not be achieved since processing temperature was well below the melting point of the grafting polymers. However, even in this processing condition beyond our expectations, considerable and important improvements were observed in the mechanical properties. Particularly, improvement in ultimate tensile strength and modulus were observed, but with loss of yield stress and loss in percent elongation, therefore the samples were mostly broken in brittle nature.

Stress-Strain curve of PABA-g-PP was given in Figure 3.64. We did not observe any yield stress in any of the grafted polymers. Although non-irradiated PP showed a great extent of cold drawing or orientation, the irradiated PP broke just after yield stress and there existed no yield stress in grafted PP. Table 3.12 given below showed the ultimate tensile strength, modulus and impact strength of virgin and γ -irradiated IPP for comparison with grafted IPP.

Table 3.12. Ultimate tensile strength, Young's modulus and impact strength of irradiated and non-irradiated PP.

	Ultimate Str. (Mpa)	Modulus (Mpa)	Impact Str. (kJ/m ²)
PP	33.93 ± 1.35	632 ± 22	39.68 ± 1.42
Irrad. PP	28.14 ± 1.14	486 ± 13	19.95 ± 1.24

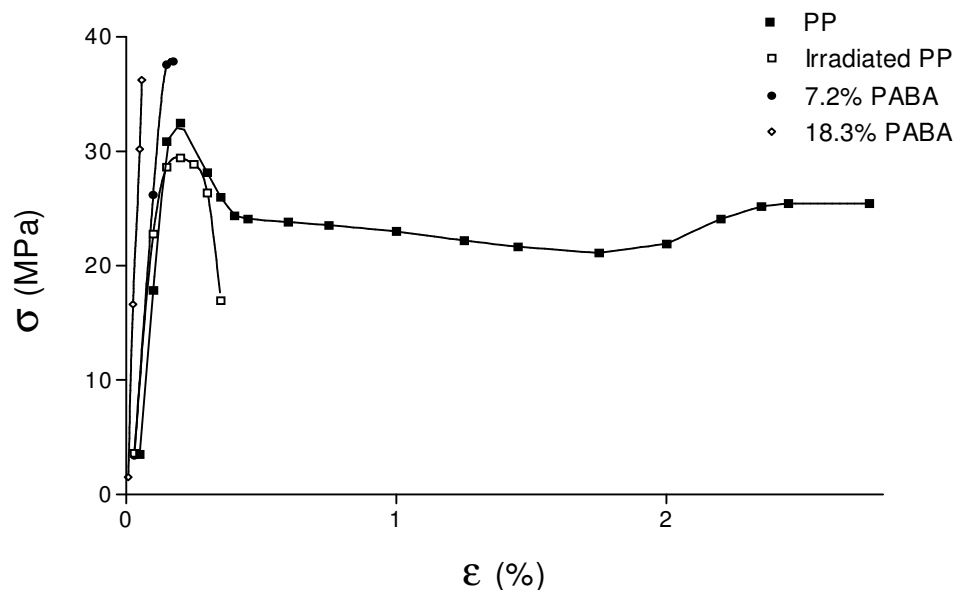


Figure 3.64. Stress-strain curves of PP, irradiated PP and PABA-g-PP with the content of 7.2 and 18.3% PABA

The results of tensile strengths of PABA-g-PP were tabulated in Table 3.13 and drawn in Figure 3.65, which were determined with the elongation speed of 5 cm/min. The strength of PABA-g-PP samples increased with the increase of PABA percentage in the graft coproducts. The maximum strength of 41.1 MPa which was well above those of irradiated and virgin PP, 28.14 and 33.93 MPa, respectively, was achieved with 12.8% PABA. A similar trend was also observed in modulus, measured with the speed of elongation, 0.32 cm/min. Modulus increased with PABA content in the products. The maximum, 881 MPa was reached at 13.4% PABA, which was very high comparing to the modulus of irradiated and virgin PP, 486 and 632 MPa, respectively, and then followed by a decrease, Table 3.14 and Figure 3.66.

Table 3.13. Ultimate tensile strength of PABA-g-PP with % PABA in samples.

% PABA	7.2	9.2	12.8	13.4	18.3	33.3
Ult. Strength (MPa)	37.13 ± 0.63	38.51 ± 0.23	41.12 ± 0.54	36.97 ± 0.97	35.22 ± 0.98	13.11

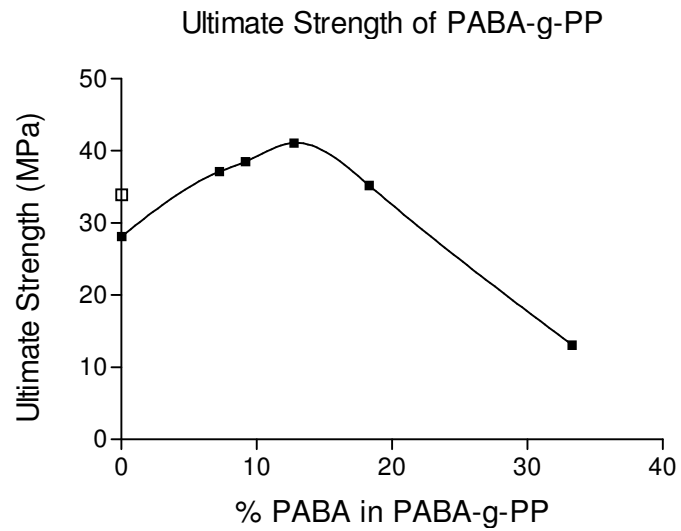


Figure 3.65. The dependence of ultimate strength of PABA-g-PP on content of PABA (□ shows the ultimate strength of virgin PP)

Table 3.14. Young's modulus of PABA-g-PP with % PABA

% PABA	7.2	9.2	13.4	18.3
Modulus (MPa)	734	772	881	853

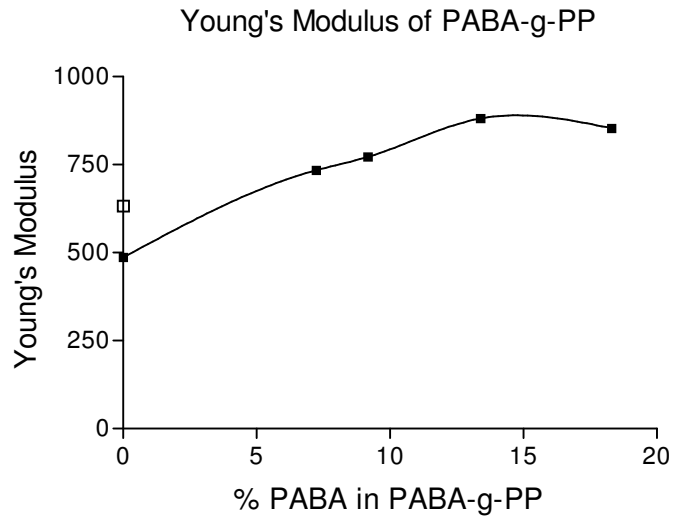


Figure 3.66. The dependence of Young's modulus of PABA-g-PP on content of PABA (\square shows the modulus of virgin PP)

The samples were processed at 200°C at which, however, PABA units of the graft coproducts are in solid state but this temperature is well above T_g of PABA. At this temperature, although the samples with low percentages of PABA could be processed, the processing became very difficult as the content of PABA increased in the graft coproducts particularly after the concentration of the maximum tensile strength. Usually unsuccessful test samples were seen in the graft copolymer containing 33.3% PABA, and although they were processed we could not achieve good quality test samples. These samples usually contained brown tints of degradation. The decreases detected in the tensile strengths after attainment of the maximum was presumably due to the problem of processing at the temperature, 200°C. It should be rementioned that the grafting polymers start to degrade at a very close temperature just above the processing.

The variation of impact strength with respect to PABA content in the graft was given in Table 3.15 and Figure 3.67. It appears that there exists almost no change in the impact strength of the material (note that base material is an irradiated PP). The impact strength compared to non-irradiated PP was found to be lower. Indeed, the increased brittleness and the missing yield stress in grafted samples show that the samples are in brittle nature. Yet, the variation in impact strength also shows

that there is no observable change with the increased grafting. Therefore the grafting did not alter the impact properties of the material.

Table 3.15. Impact strength of PABA-g-PP with % PABA

% PABA	6.6	12.8	13.4	18.3
Impact Strength (kJ/m ²)	17.35 ± 7.28	18.57 ± 1.25	22.21 ± 2.01	21.45 ± 1.59

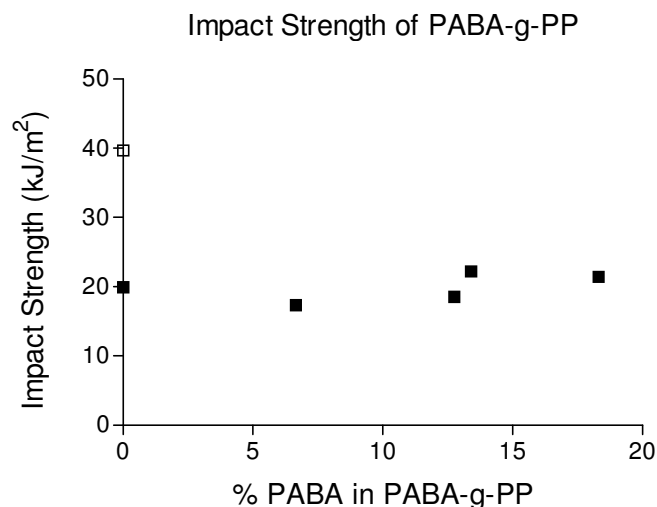


Figure 3.67. The dependence of impact strength of PABA-g-PP on content of PABA (□ shows the impact strength of virgin PP)

The results of tensile strengths of PMBA-g-PP were given in Table 3.16 and drawn in Figure 3.68. The improvement in tensile strength was also observed in PMBA-g-PP samples. The maximum tensile strength was observed in the sample contained 4.8% PMBA, with 35.95 MPa. Then, it started to decrease to the value of 26.04 MPa at the content of 14.2% PMBA. The enhancement in modulus was also achieved. However, in contrast to the trend of tensile strength, modulus of PMBA-g-PP samples increased with PMBA content reaching the maximum 721 MPa at 14.1% PMBA, Table 3.17 and Figure 3.69.

Table 3.16. Ultimate tensile strength of PMBA-g-PP with % PMBA

% PMBA	4.8	11.2	14.2
Ult. Strength (MPa)	35.95 ± 0.58	32.92 ± 0.62	26.04 ± 1.74

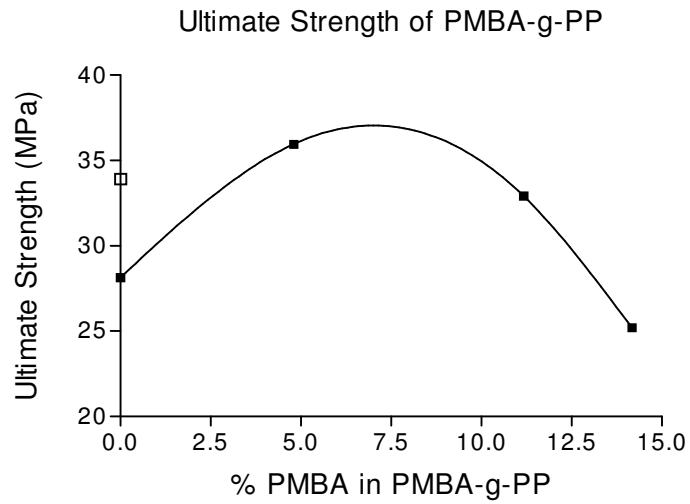


Figure 3.68. The dependence of ultimate strength of PMBA-g-PP on content of PMBA (□ shows the ultimate strength of virgin PP)

Table 3.17. Young's modulus of PMBA -g-PP with % PMBA

% PMBA	4.8	11.2	14.2
Modulus (MPa)	555	579	721

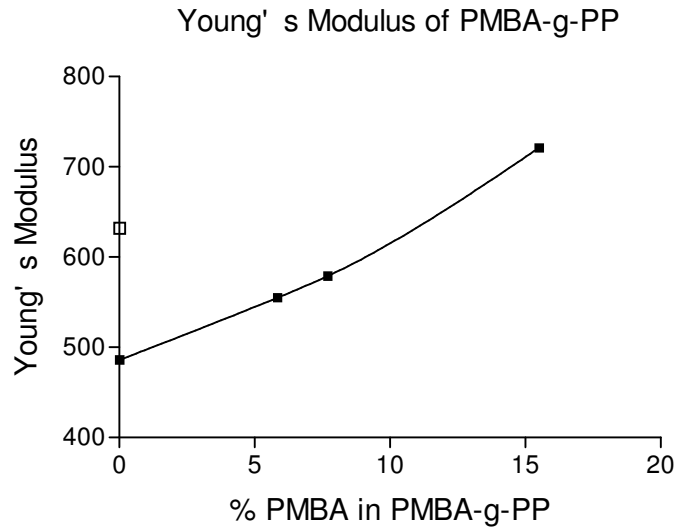


Figure 3.69. The dependence of Young's modulus of PMBA-g-PP on content of PMBA (□ shows the modulus of virgin PP)

The variation of impact strength of PMBA-g-PP with respect to PMBA content was given in Table 3.18 and Figure 3.70. A slight improvement was observed in low content of PMBA comparing impact strength of the irradiated PP (19.95 kJ/m²). The maximum impact strength was achieved at 5.8% PMBA with the value of 24.03 kJ/m² which was, however, still well below the impact strength of virgin PP, 39.68 kJ/m². Although the slight enhancement was observed it was followed by a dramatic decrease with the increase of PMBA content reducing to 10.23 kJ/m² at 15.5% PMBA leading to conclusion that the PMBA-g-PP samples are in brittle nature and brittleness increases with the increase of PMBA content.

Table 3.18. Impact strength of PMBA-g-PP with % PMBA

% PMBA	5.8	7.7	11.0	15.5
Impact Strength (kJ/m ²)	24.03 ± 5.86	22.14 ± 1.97	14.50 ± 1.49	10.23 ± 0.49

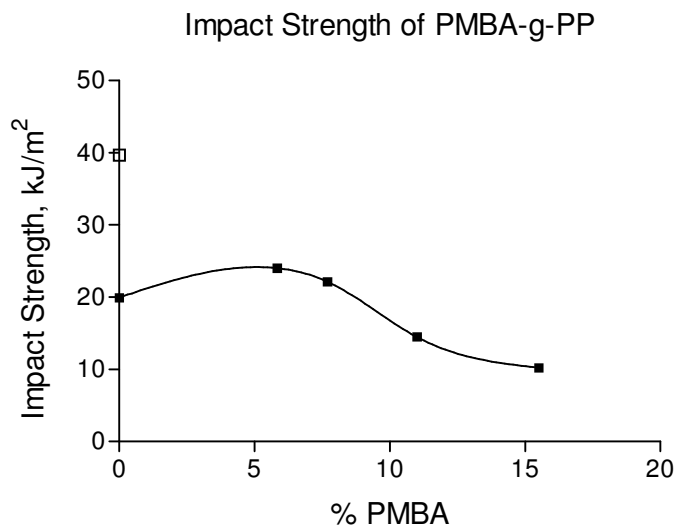


Figure 3.70. The dependence of impact strength of PMBA-g-PP on content of PABA (□ shows the impact strength of virgin PP)

Since the PMBA-g-PP samples were also prepared at 200°C where the PMBA units were not in melt state, in similar condition of PABA-g-PP the desired quality in the test samples could not be achieved. The processing got more difficult as the concentration of PMBA increased in graft copolymers. That's why although some improvements were observed in mechanical properties they showed the decreasing trend after certain content of PMBA.

3.8. SEM Analysis of the Polymers

The tensile and impact fractured surfaces of PABA-g-PP and PMBA-g-PP samples were shown in Figure 3.71-3.84. The SEM photographs showed that the graft copolymers of both PABA and PMBA displayed no phase separation although the graft units of PABA and PMBA were different from IPP in nature. This result confirmed the graft copolymerization of the monomers ABA and MBA onto IPP homogeneously.

In general, brittle fracture was observed in the samples. Some extent of ductility was also detected in tensile tests particularly if tensile testing was carried

out at low speed of elongation (0.32 cm/min) which allows an orientation of crystalline IPP, but no extensive fibrillation was seen.

Tensile fractographs of PABA-g-PP with increasing PABA content were given in Figure 3.71-76. As the extent of grafting increases, the morphology of fracture greatly altered, but they were basically in brittle nature. We observed a short fibrillar structure broken in ductile but also microcracks and openings between layers indicating the major fracture goes through brittle fracture, Figure 3.71 and 72 where Figure 3.72 is the magnified version of the same sample. In 13.4 % PABA-g-PP these extensions (like fibrillar structure) were smaller and the morphology was changed. Figure 3.73, 74 and 75 showed the most important change in the morphology. The fractographs showed the cracks and holes with brittle fracture, but the material did not show any phase separation at all. At the highest grafting in PABA onto IPP we observed some nodular structures, actually it was first seen in Figure 3.76, with greater size holes, in turn the tensile strength was found to be the smallest in this sample.

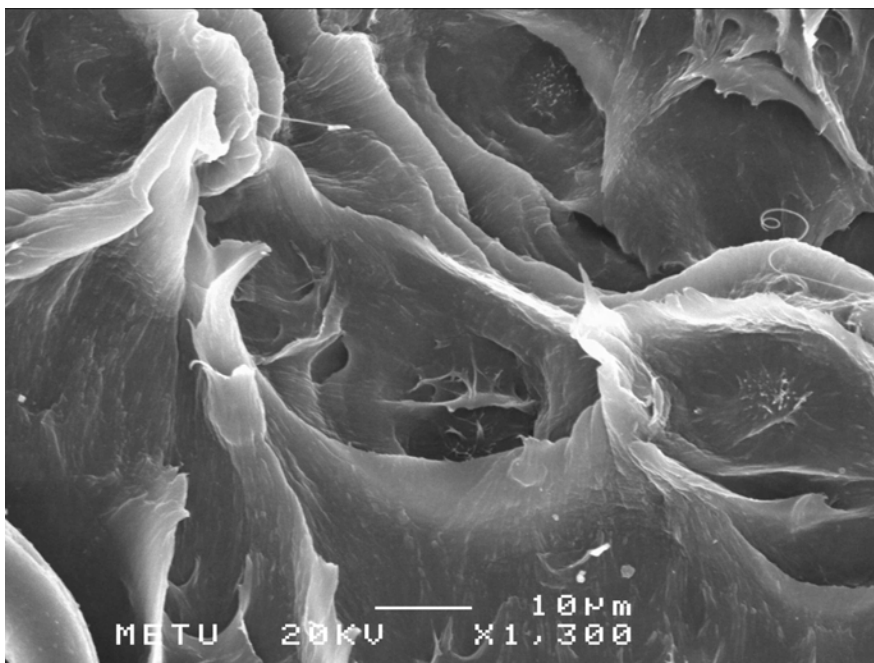


Figure 3.71. SEM photograph of PABA-g-PP (9.2% PABA), Tensile Test

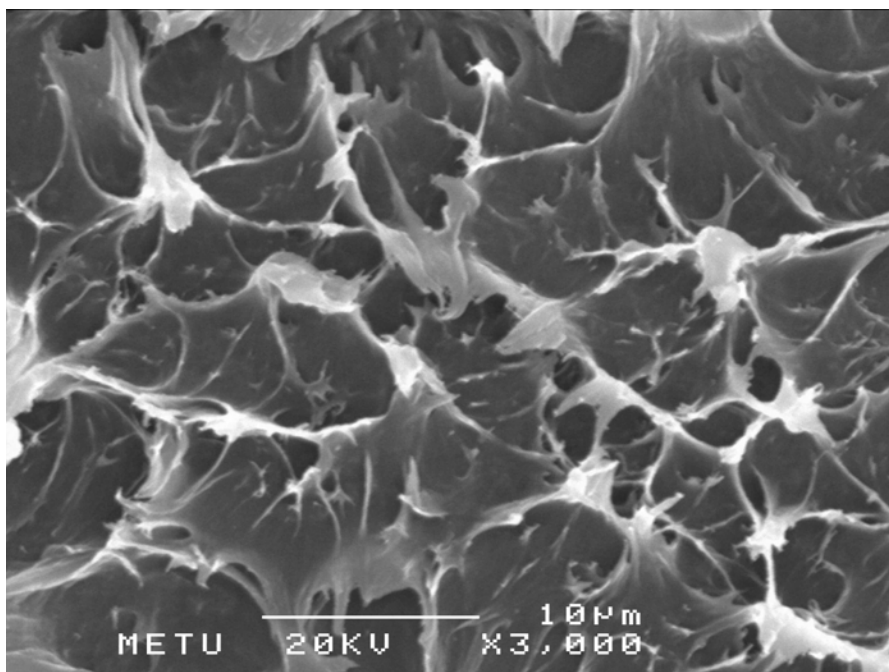


Figure 3.72. SEM photograph of PABA-g-PP (9.2% PABA), Tensile Test

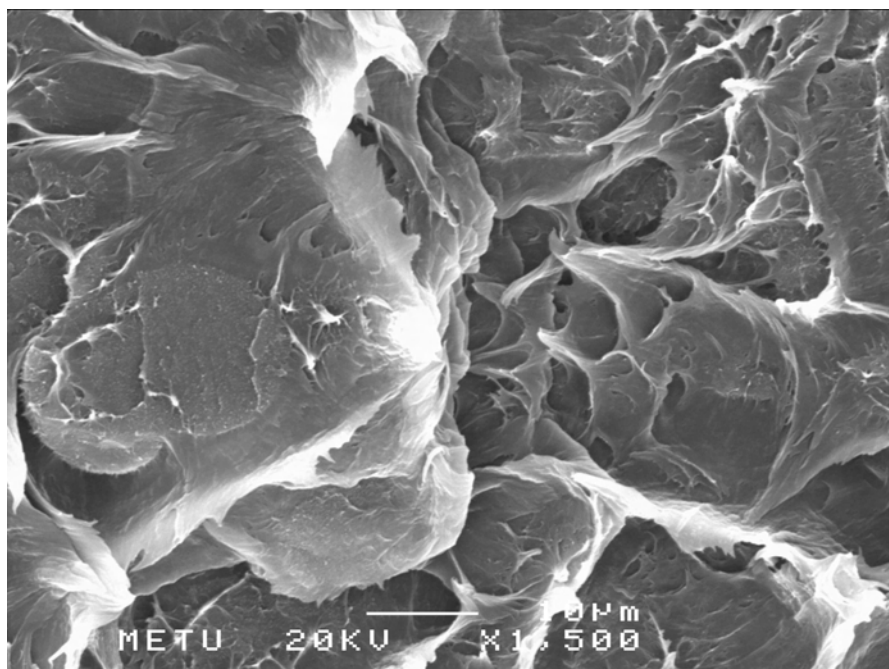


Figure 3.73. SEM photograph of PABA-g-PP (13.4% PABA), Tensile Test

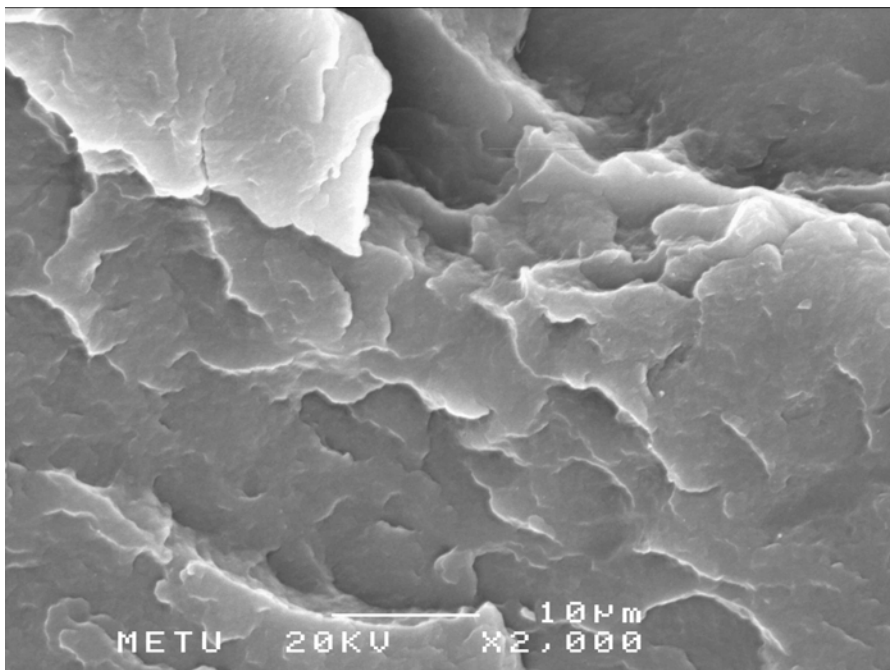


Figure 3.74. SEM photograph of PABA-g-PP (18.3% PABA), Tensile Test

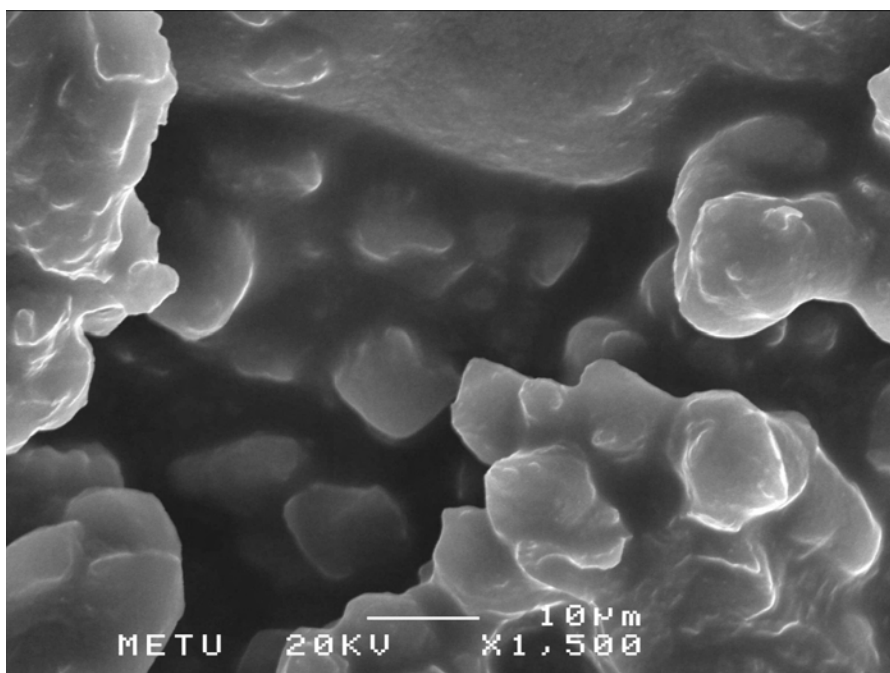


Figure 3.75. SEM photograph of PABA-g-PP (20.2% PABA), Tensile Test

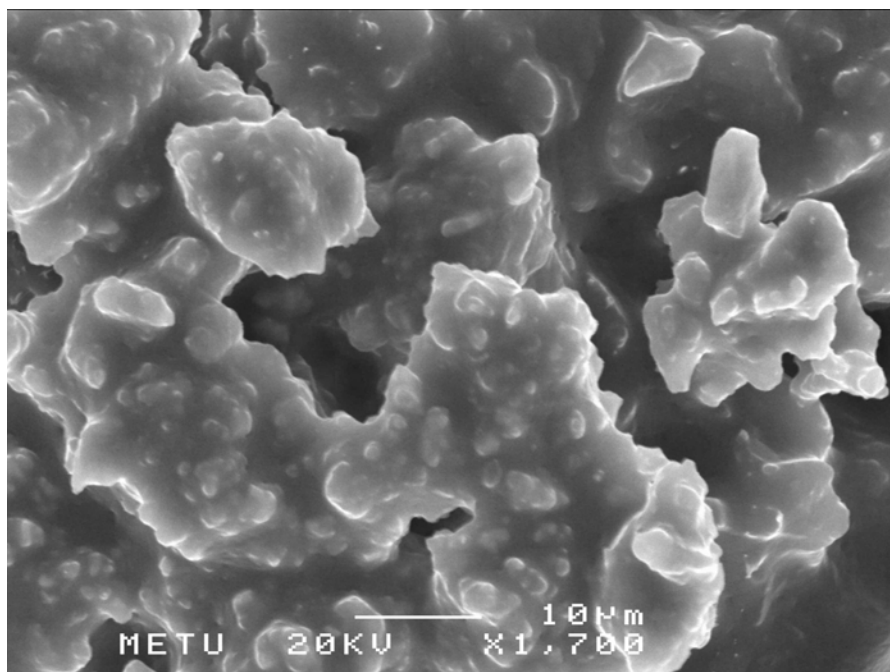


Figure 3.76. SEM photograph of PABA-g-PP (32.1% PABA), Tensile Test

It is well known that the rate extension in material testing may affect the fracture nature. Slow tensile testing allows ease of orientation of macromolecules along the extension direction. Indeed, slow tensile testing (0.32 cm/min) in 18.3 % PABA showed a different morphology. Though we still observed brittle nature cracks, voids, holes, but at the back ground (left bottom of the picture) we observed some ductile extensions, Figure 3.77. This Figure, 3.77, shows how the fracture nature varies with rate of drawing when compared to Figure 3.74. Indeed, we observed the same type of fractures in PMBA-g-PP. Figure 3.78 showed that in slow testing we have some certain extent of orientation, but still the sample was broken without giving a yield, i.e. brittle.

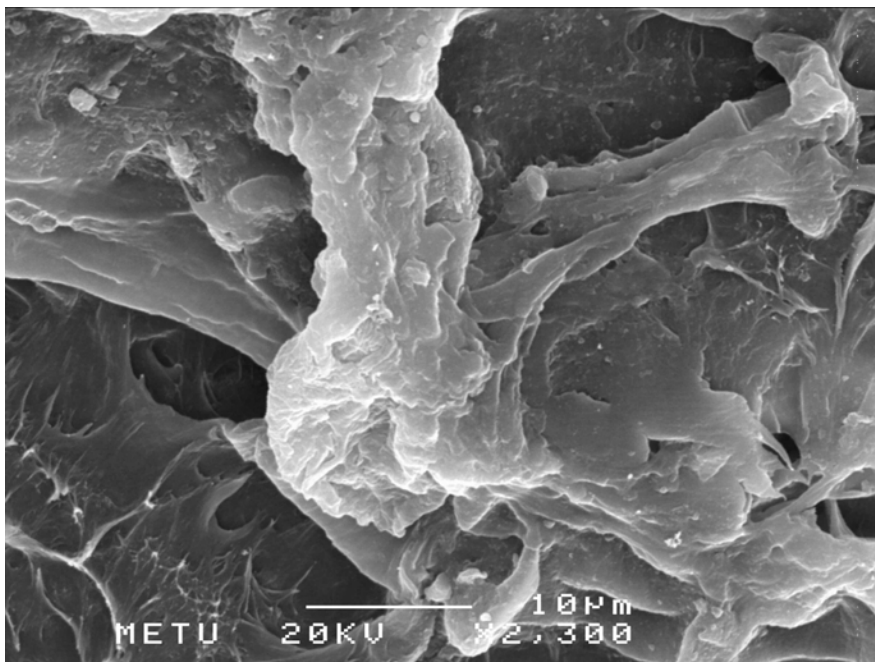


Figure 3.77. SEM photograph of PABA-g-PP (18.3% PABA), Slow Tensile Test

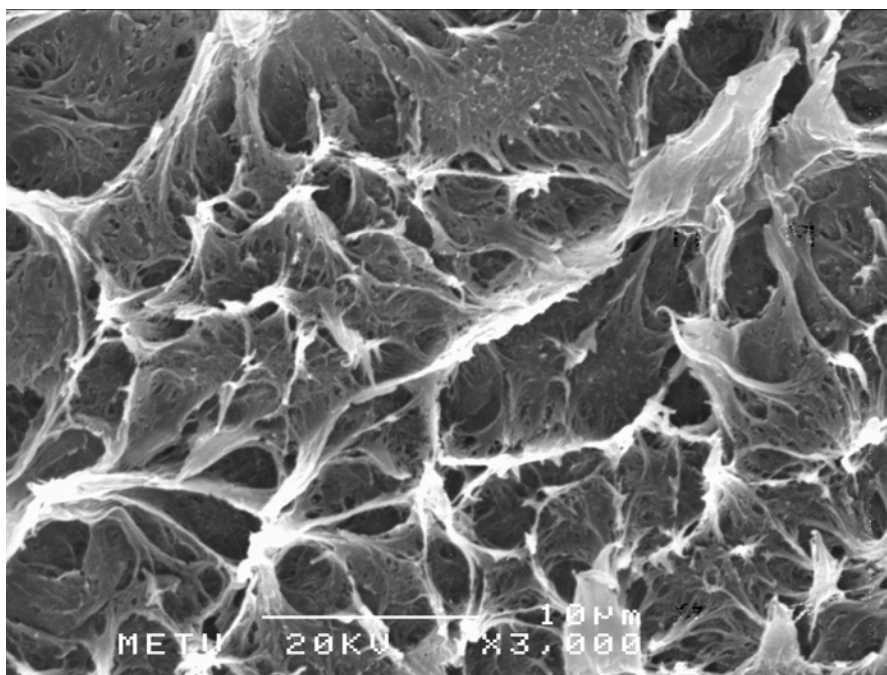


Figure 3.78. SEM photograph of PABA-g-PP (15.5% PABA), Slow Tensile Test

All the impact fractographs of the samples revealed that the fracture is brittle. The impact testing showed that, if any, there existed almost a slight improvement within the graft samples but worse than that of virgin IPP. Impact fractographs were given through Figure 3.79-3.84. Since impact testing is loading a force in a small time scale onto the certain area of the test samples, the time allowed for any orientation of polymer chains is very restricted, i.e. impact energy delocalization is prohibited. Therefore, energy is localized in the weak regions of the structure of material to form cracks and voids at the molecular level. Layered structure, Figure 3.79, 80 and also 3.81 revealed how the straight but zigzagged propagation lines produced the crack to failure of the material. A nice SEM photograph was given in Figure 3.83, 5.8% PMBA zigzagged-tortuous crack formation. A similar observation on a layered morphology 10.5% PMBA-g-PP was given in Figure 3.84.

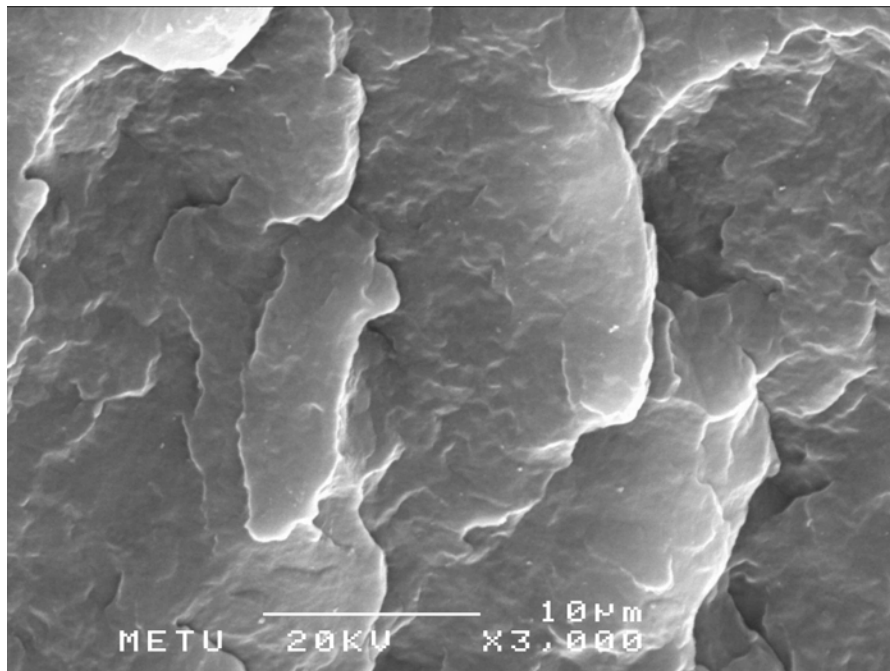


Figure 3.79. SEM photograph of PABA-g-PP (6.6% PABA), Impact Test

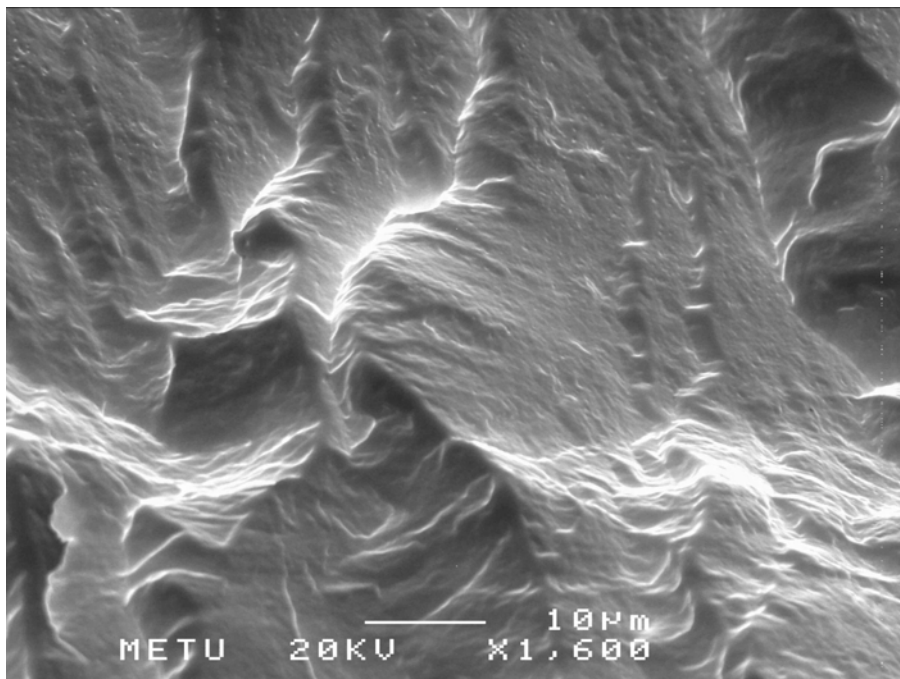


Figure 3.80. SEM photograph of PABA-g-PP (12.7% PABA), Impact Test

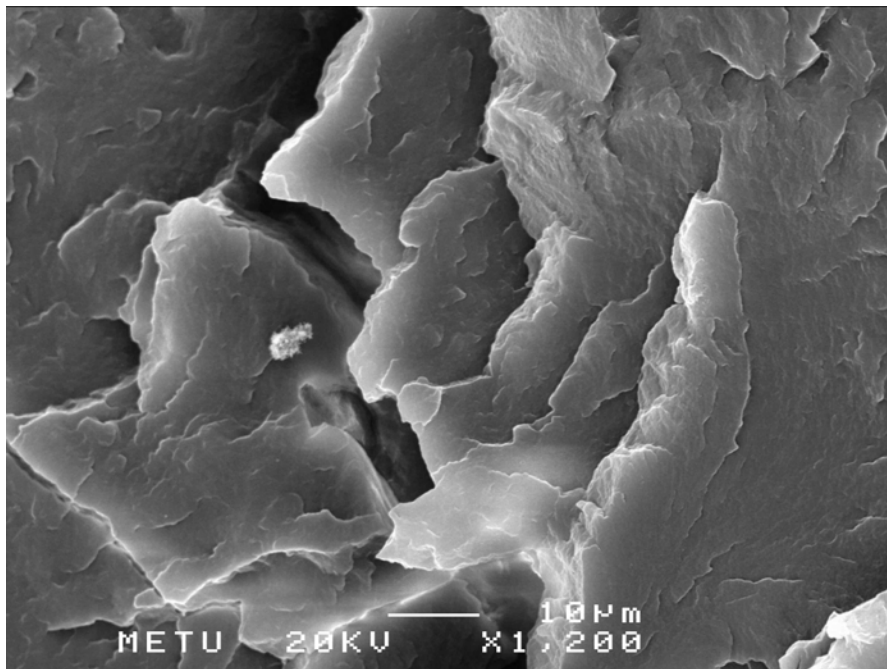


Figure 3.81. SEM photograph of PABA-g-PP (18.3% PABA), Impact Test

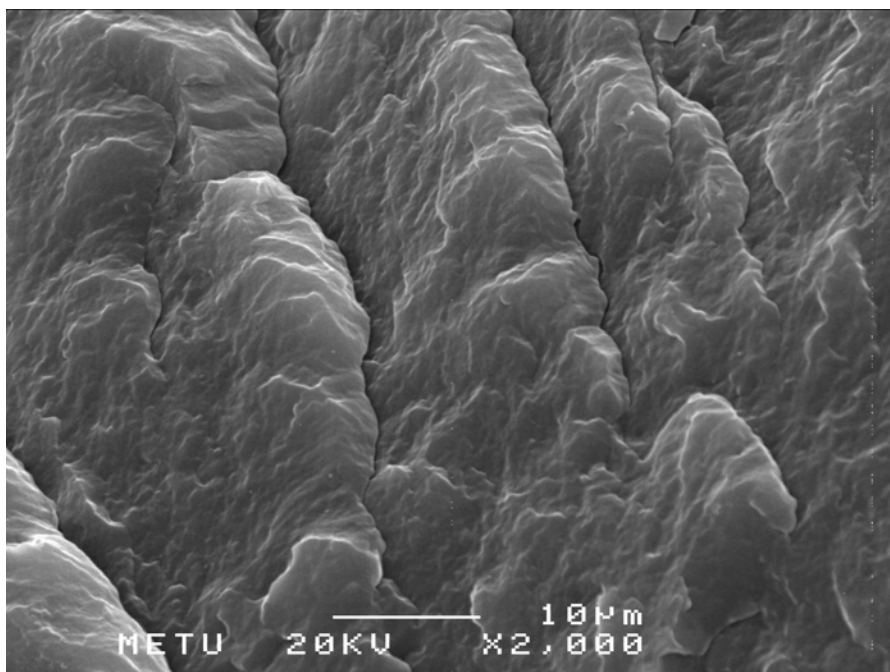


Figure 3.82. SEM photograph of PMBA-g-PP (5.8% PMBA), Impact Test

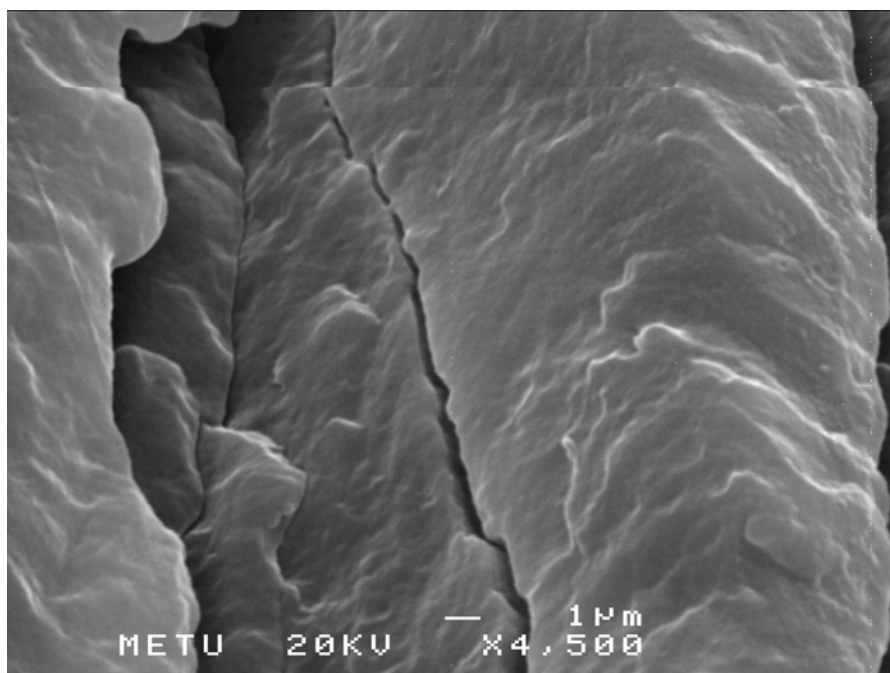


Figure 3.83. SEM photograph of PMBA-g-PP (5.8% PMBA), Impact Test

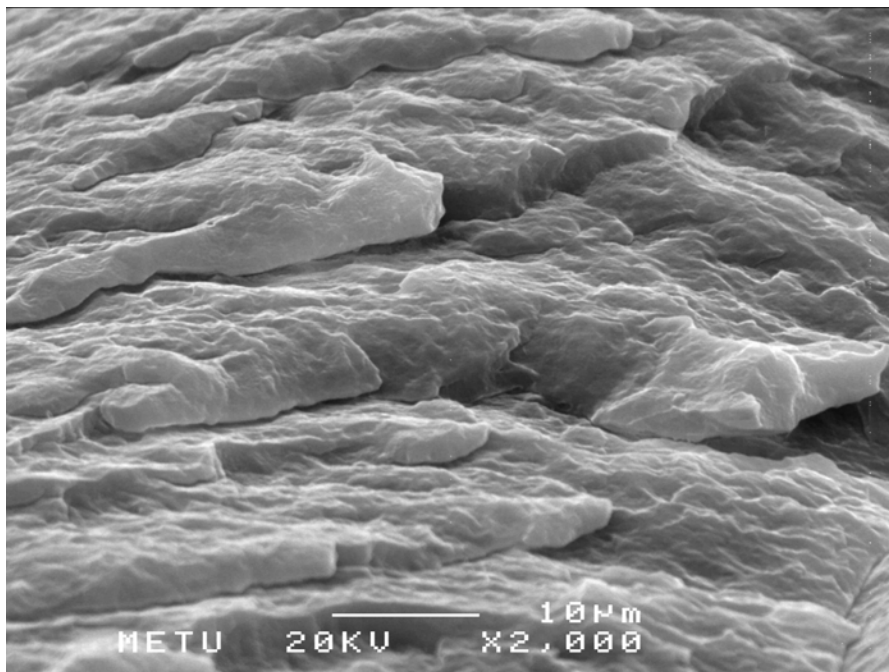


Figure 3.84. SEM photograph of PMBA-g-PP (10.5% PMBA), Impact Test

Morphological study reveals that the grafted samples are completely homogeneous as far as seen at these magnifications and the material breaks in brittle nature in standard testing speeds. But it also shows some extent of micro ductility at low grafting in slow rate testing.

CHAPTER 4

CONCLUSION

PABA was obtained by γ -radiation induced polymerization, bulk melt polymerization and solution polymerization of ABA. The maximum conversion, 95% was obtained by bulk melt polymerization with initiation of DCP at 202°C.

PMBA was obtained only by bulk melt polymerization with the conversion of 45%. The polymerization of MBA by γ -radiation induced polymerization, bulk melt polymerization and solution polymerization was failure.

Thermally induced graft copolymerization of monomers ABA and MBA onto peroxidized PP were carried out at 170, 185, 202, 215 and 225°C at constant concentration of the monomers in the reaction mixture (50%). The maximum content of PABA and PMBA were 33.3% and 33.9% in the graft copolymers. The extent of grafting reached the maximum at earlier times in the experiments carried out at higher temperatures. The amount of grafting increased with the increase of concentration of monomers in the reaction medium.

When initiator was used in the graft copolymerizations the amount of grafting decreased due to homopolymerization of the monomers and the direct reactions between peroxides formed by dissociation of initiator and peroxides on the PP formed by γ -radiation.

The formation of both crystalline forms (α_1 and α_2) of α form was observed in the samples studied at 170°C. The graft copolymerization ABA onto IPP did not produce any influence on the formation of both forms of α form, while, MBA lead to increase in α_2 form in the graft copolymers.

The β crystalline modification formed in PABA-g-PP products obtained at 185°C and at higher temperatures and in the second run of DSC studies carried out with fast cooling. In graft copolymers of PMBA β form was not observed.

The graft coproducts degrades predominantly by decomposition of side groups giving phenol, benzoic acid, hydroxybenzoic acid, carbon dioxide and cyclodiene

mainly.

The improvement in the mechanical properties was obtained particularly in strength and modulus. Graft copolymerization of ABA did not alter the impact properties of the graft copolymer, while decreases were observed in PMBA-g-PP samples

All the graft coproducts showed homogeneous structure. The copolymers of both PABA and PMBA showed brittle nature with some ductility.

This is the first study on the graft copolymerization of monomers which have mesomorphic behavior when polymerized onto isotactic polypropylene.

A further study leading an improved stability of grafting copolymers, PABA or PMBA, would provide better processing and higher mechanical property measures by some advanced modifications in future.

REFERENCES

1. G. XU and S. Lin, *Polym. Materials Sci. and Eng.*, 70, 151 (1993)
2. G. XU and S. Lin, *J.M.S.-Rev. Macromol. Chem. Phys.*, C39(4), 555 (1994)
3. K. Mukherjee and B. D. Gupta, *J. Macromol. Sci.-Chem.*, 19(7), 1069 (1983)
4. G. Natta and P. Corradini, *Nuovo Cimento Suppl.*, 15, 40 (1960)
5. Z. Mencik, *J. Macromol. Sci., Phys.*, B(6), 101 (1972)
6. M. Hikosaka and T. Seto, *Polym. J.*, 5, 111 (1973)
7. A. Turner Jones, J. M. Aizlewood, and D. R. Beckett, *Makromol. Chem.*, 75, 134 (1964)
8. D. R. Morrow and B. A. Newman, *J. Appl. Phys.*, 39, 4944 (1968)
9. J. L. Kardos, A. W. Christiansen and E. J. Baer, *J. Polym. Sci., Part A2*, 4, 777 (1966)
10. E. Baer and J. L. Kardos, *J. Polym. Sci., Part A*, 3, 2827 (1965)
11. U. Leute, W. Dollhopf and E. Liska, *Colloid and Polym. Sci.*, 256, 914 (1978)
12. C. Nakafuku, *Polymer*, 22,1673 (1981)
13. M. Kojima, *J. Polym. Sci., Part A2*, 6, 1255 (1968)
14. A. J. Lovinger, O. J. Chua and C. C. Gryte, *J. Polym. Sci., Polym. Phys. Edn.*, 15, 641 (1977)
15. J. M. Crissman, *J. Polym. Sci., Polym. Phys. Edn.*, 7, 389 (1969)
16. Y. Fujiwara, *Colloid and Polym. Sci.*, 253, 273 (1975)
17. T. Asano and Y. Fujiwara, *Polymer*, 19, 99 (1978)
18. T. Yoshida, Y. Fujiwara and T. Asano, *Polymer*, 24, 925 (1983)

19. H. I. Leugering, *Makromolekulare Chemie*, 109, 204 (1967)
20. Y. Onagi, J. L. White and J. F. Fellers, *J. Non-Newt. Fluid Mech.*, 7, 121 (1980)
21. S. Suto, K. Shimamura, J. L. White and J. F. Fellers, *SPE ANTEC Tech. Papers*, 28, 42 (1982)
22. S. Kenig, *Polym. Eng. Sci.*, 27, 887 (1987)
23. M. Jaffe, *Polym. Prepr. Am. Chem. Soc. Div. Poly. Chem.*, 19, 355 (1977)
24. D. L. Lewis and J. F. Fellers, *High Modulus Polymers*, (A. E. Zachariades and R. S. Porter, eds.), Marcel Dekker Inc. (1988)
25. P. J. Barham, and A. J. Keller, *J. Mater. Sci.*, 20, 2281 (1985)
26. D. Done and D. G. Baird, *Polym. Eng. Sci.*, 27(11), 816 (1987)
27. D. Done and D. G. Baird, *Polym. Eng. Sci.*, 30(16), 989 (1990)
28. H. J. O'Donnel and D. G. Baird, *Polymer*, 36, 3113 (1995)
29. Y. Ide and Z. Ophir, *Polym. Eng. Sci.*, 23(5), 261 (1983)
30. T. -S. Chung, *J. Polym. Sci. (C) Polym. Lett.*, 24, 299 (1986)
31. T. -S. Chung, *J. Polym. Sci. (B) Polym. Phys.*, 26, 1549 (1988)
32. S. Kenig, *Polym. Eng. Sci.*, 29(16), 1136 (1989)
33. A. Kohli, N. Chung and R. A. Weiss, *Polym. Eng. Sci.*, 29(9), 573 (1989)
34. A. Siegmann, A. Dagan and S. Kenig, *Polymer*, 26, 1325 (1985)
35. M. R. Nobile, E. Amendola and L. Nicolais, *Polym. Eng. Sci.*, 29(4), 244 (1989)
36. K. G. Blizard and D. G. Baird, *Polym. Eng. Sci.*, 27(9), 653 (1987)
37. F. P. La Mantia, M. Saiu, A. Valenza, M. Paci and L. P. Magagnini, *Eur. Polym. J.*, 26(3), 323 (1990)

38. G. I. Taylor, *Prog. R. Soc. (A)*, 146, 501 (1934)
39. S. Tomotika, *Prog. R. Soc.*, 150, 322 (1935)
40. S. S. Daglı and K. M. Kamdar, *Polym. Eng. Sci.*, 34, 1709 (1994)
41. P. Zhuang, T. Kyu and J. L. White, *Polym. Eng. Sci.*, 29(17), 1095 (1988)
42. J. He and J. Liu, *J. Appl. Polym. Sci.*, 67, 22141 (1998)
43. A. Eisenberg, P. Smith and Z. Zahou, *Polym. Eng. Sci.*, 22, 1127 (1982)
44. E. M. Woo, J. W. Barlow and D. R. Paul, *J. Appl. Polym. Sci.*, 28, 1347 (1983)
45. A. Eisenberg and M. Hara, *Polym. Eng. Sci.*, 22, 1306 (1984)
46. X. Zhang and A. Eisenberg, *J. Polym. Sci., Polym. Phys. Edn.*, 28, 1841 (1990)
47. O. Olabisi, *Macromolecules*, 8, 316 (1975)
48. N. G. Gaylord, *J. Macromol. Sci., Chem. (A)*, 26(8), 1211 (1989)
49. A. Y. Goran and R. Patel, *Rubber Chem. Technol.*, 56, 1045 (1983)
50. X. Jin and W. Li, *Macromol. Sci., Rev. Macromol. Chem. Phys.*, C35, 1 (1995)
51. D. Done, A. M. Sukhadia, A. Datta and D. G. Baird, *SPE Tech. Pap.*, 48, 1857 (1990)
52. A. Datta, A. M. Sukhadia, J. P. Desouza and D. G. Baird, *SPE Tech. Pap.*, 49, 913 (1991)
53. C. Federici, G. Attalla and L. Chapoy, *Eur. Pat.*, 0,340,655 A2 (1989)
54. Y. Yongcheng, F. P. La Mantia, A. Valenza, V. Citta, U. Pedretti and A. Roggero, *Eur. Polym. J.*, 27, 723 (1991)
55. S. C. Tjong, S. L. Liu and R. K. Y. Li, *J. Mater. Sci.*, 31, 479 (1996)

56. A. Datta, H. H. Chen and D. G. Baird, *Polymer*, 34, 759 (1993)
57. A. Datta and D. G. Baird, *Polymer*, 36, 505 (1995)
58. M. Kozłowski, F. P. La Mantia, *J. Appl. Polym. Sci.*, 66, 969 (1997)
59. M. M. Miller, D. L. Brydon, J. M. G. Cowie and R. R. Mather, *Macromol. Rapid. Commun.*, 15, 857 (1994)
60. M. M. Miller, J. M. G. Cowie, J. G. Tait, R. R. Mather and D. L. Brydon, *Polymer*, 36, 3107 (1995)
61. Y. Qin, M. M. Miller, J. M. G. Cowie, R. R. Mather and D. L. Brydon and R. H. Wardman, in *Liquid Crystalline Polymer Systems, Technological Advances*, (A. I. Isayev, T. Kyu, and S. Z. D. Cheng Eds.), American Chemical Society, Washington, DC., 98 (1996)
62. R. M. H. Miettinen, M. T. Heino and J. V. Seppala, *J. Appl. Polym. Sci.*, 57, 573 (1995)
63. Y. P. Chiou, K. C. Chiou and F. C. Chang, *Polym. Eng. Sci.*, 37, 4099 (1996)
64. G. Friedel, *Ann. Phys.*, 19, 273-281 (1972)
65. N. A. Plate and V. P. Shibaev, *Comb-Shaped Polymers and Liq. Crystals*, Plenum Press, New York (1987)
66. A. M. Donald and A. H. Windle, *Liq. Cryst. Polymers*, Cambridge University Press, Cambridge (1992)
67. A. Blumstein and N. Kitagawa, *Mol. Cryst. Liq. Cryst.*, 12, 215 (1971)
68. A. Blumstein, J. Billard and R. Blumstein, *Mol. Cryst. Liq. Cryst.*, 25, 83 (1974)

69. A. Blumstein, R. B. Blumstein, S. B. Clough and E. C. Hsu, *Macromolecules*, 8, 73 (1975)
70. A. Blumstein, R.B. Blumstein, S. B. Clough, L. Patel and E. C. Hsu, *Macromolecules* 9, 243 (1976)
71. J. Menczel and B. Wunderlich, *Polymer*, 22, 778 (1981)
72. J. Menczel, J. P. Walsh and B. Wunderlich, *J. Polym. Sci., Polym. Phys. Edn.*,19, 837 (1981)
73. A. V. Sessa Sainath, T. Inoue, K. Yonetaka and K. Koyama, *Polymer*, 24, 9859 (2001)
74. I. Ishigaki, T. Sugo, K. Senoo, T. Takayama, S. Machi, J. Okamoto and T. Okada, *Radiat. Phys. Chem.*, 18, 5, 899 (1981)
75. I. Ishigaki, T. Sugo, K. Senoo, S. Machi, J. Okamoto and T. Okada, *J. Appl. Polym. Sci.*, 27, 1033 (1982)
76. D. W. Clegg and A. A. Collyer, *Irrad. Effects on Polym.*, Elsevier Appl Sci., London and New York, (1991)
77. A. Chapiro, *Rad. Chem. Polym. Syst.*, John Wiley & Sons, Inc. (1962)
78. R. Napolitano, B. Prozzi and V. Varriale, *J. Polym. Sci., Part B: Polym. Phys.*, 28, 139 (1990)
79. G. Guerra, V. Petraccone, P. Corradini, C. De Rosa, R. Napolitano, and B. Pirazzi, *J. Polym. Sci., Polym. Phys. Edn.* 22, 1029-1039 (1984)
80. *International Tables for X-Ray Crystallography*, Kynoch, Birmingham, 1952, V. I.
81. K. D. Pae and J. A. Sauer, *J. Appl. Polym. Sci.*, 12, 1901 (1968)
82. Y. Fujiwara, T. Asano and T. Yoshida, *Polym. J.*, 11, 383 (1979)

83. Y. Fujiwara, *Colloid and Polym. Sci.*, 265, 1027 (1987)
84. F. J. Padden, Jr. and H. D. Keith, *J. Appl. Phys.*, 30, 1479 (1959)
85. J. Karger-Kocsis, *Polypropylene, Structure and Morphology*, 37,38 (1995)
86. P. Jacoby, B. H. Bersted, W. J. Kissel, and C. E. Smith, *J. Polym. Sci., Part B. Poly. Phys.*, 24, 461-491 (1986)

VITA

Sedat Çetin was born in İnegöl/Bursa on July 27, 1970. He received his B.Sc. degree in Department of Chemistry from Middle East Technical University in June 1995, and M.Sc. degree in Department of Chemistry from Abant İzzet Baysal University in September 1998. The subject of his M.Sc. study was Functionalization of Atactic Polypropylene under the supervision of Assoc. Prof. Dr. Gülsu Akın Öktem and Assoc. Prof. Dr. Zeki Öktem. He has been a research assistant in the same department since 1995 and in the Department of Chemistry at METU since 2000 (35. Madde). He worked in General Chemistry, Analytical Chemistry, Industrial Chemistry and Physical Chemistry Laboratories. His main area of interest is the preparation and characterization of graft copolymers. He has two publications.

Papers

1. Zeki Öktem, Sedat Çetin, Gülsu Akın Öktem, Functionalization of Low Molecular Weight Atactic Polypropylene. Part I. Spectroscopic Studies, Polymer Bulletin, 43, 239-246, 1999.
2. Gülsu Akın Öktem, Sedat Çetin, Zeki Öktem, Functionalization of Low Molecular Weight Atactic Polypropylene. Part II. Thermal and Molecular Weight Studies, Polymer Bulletin, 45, 245-252 (2000).